

Imperial College London  
Department of Physics

# A privileged quantum state from causal structure

Michel Buck

October 2014

Supervised by Prof. H. F. Dowker

Submitted in part fulfilment of the requirements for the degree of  
Doctor of Philosophy in Physics of Imperial College London  
and the Diploma of Imperial College London

# Abstract

This thesis investigates a new proposal for a privileged ground state of a free scalar quantum field in arbitrary regions of spacetime. This Sorkin-Johnston (SJ) state, implicit in work by S. Johnston on quantum field theory on causal sets, is defined solely in terms of the spacetime causal structure and is unique in any globally hyperbolic spacetime region.

The first part of the thesis contains an analysis of the simplest possible setting: a flat two-dimensional causal interval. The simplicity of the setup makes analytic calculations tractable and allows for some general features of the state to be better understood.

The second part deals with an investigation of the SJ state in de Sitter space. It turns out to be possible to construct the state explicitly using limiting procedures, which provides further interesting insights. In particular, the state is found to depend on the spacetime dimension, field mass, and on the choice of subregion, differing in many cases from the usual “Bunch-Davies” vacuum.

The formalism does not select a unique state in spacetimes that are not globally hyperbolic, which include, among others, spacetimes exhibiting spatial topology-change. These are relevant in the context of quantum gravity and in relation to the old question as to whether violent spacetime curvature fluctuations at Planckian scales can lead to changes in spatial topology, or whether such transitions are unphysical. Some efforts to understand the SJ state in the topology-changing two-dimensional “trousers” spacetime are discussed in the final part of the thesis.

# Acknowledgements

There are many people who have helped me through the completion of this thesis. I thank all of them: Fay Dowker, for her dedication as a supervisor, for her time explaining and discussing physics and everything else, and for introducing me to a beautiful set of ideas. Her approach to physics and her breadth of interest have made research meaningful and fun. Rafael Sorkin, who has been the source of inspiration for many of the ideas in this thesis, for sharing his exceptional depth of knowledge and his boundless creativity with everyone around him. The chance to learn from him and to work with him has been a great privilege. Dionigi Benincasa for sharing most of the PhD experience with me and for innumerable useful discussions about physics and other things. Siavash Aslanbeigi, Leron Borsten, Ian Jubb and David Rideout for numerous discussions on various topics and for having made research as enjoyable as it has been. Special thanks to Ian and Dion, as well as to Jamie Moller-Nielsen, for reading and commenting on parts of this text. I would also like to thank Niayesh Afshordi and Yasaman Yazdi for fruitful exchanges in the course of our collaboration. I thank Laure, my love, for supporting me and bringing me joy throughout the last two years. Finally, I thank my parents, Helga and Charlie, for their unlimited encouragement, love and support. This thesis is dedicated to you.

## **Declaration of Originality**

I herewith certify that all material in this dissertation which is not my own work has been properly acknowledged. The results of Chapters 3 and 4 have been published in [1] and [2].

Michel Buck

July 2014

## **Copyright Declaration**

The copyright of this thesis rests with the author and is made available under a Creative Commons Attribution Non-Commercial No Derivatives licence. Researchers are free to copy, distribute or transmit the thesis on the condition that they attribute it, that they do not use it for commercial purposes and that they do not alter, transform or build upon it. For any reuse or redistribution, researchers must make clear to others the licence terms of this work.

# Contents

<b>1. Introduction</b>	<b>12</b>
<b>2. Background</b>	<b>15</b>
2.1. Quantum fields in curved spacetime . . . . .	15
2.1.1. Canonical quantisation . . . . .	16
2.1.2. Non-uniqueness of the quantum state . . . . .	17
2.1.3. Propagators . . . . .	18
2.2. The discrete SJ state . . . . .	19
2.2.1. Background on causal sets . . . . .	20
2.2.2. Definition . . . . .	22
2.2.3. Alternative definition . . . . .	25
2.3. The continuum SJ state . . . . .	26
2.3.1. Definition . . . . .	27
2.3.2. Explicit construction . . . . .	30
2.3.3. Alternative Definition . . . . .	31
2.3.4. The Hadamard property . . . . .	33
<b>3. The SJ state in the flat causal diamond in two dimensions</b>	<b>34</b>
3.1. The massless scalar field in two-dimensional flat spacetimes . . . . .	35
3.1.1. The SJ state in Rindler space . . . . .	39
3.2. The massless SJ two-point function in the flat causal diamond . . . . .	41
3.2.1. The SJ state in the centre and corner . . . . .	45
3.3. Comparison with the discrete SJ state . . . . .	49
3.3.1. Causal sets and discrete propagators . . . . .	50
3.3.2. The SJ state in the centre . . . . .	50
3.3.3. The SJ state in the corner and in the full diamond . . . . .	51
3.4. Conclusions . . . . .	54

---

<b>4. The SJ state in de Sitter space</b>	<b>57</b>
4.1. Geometry of de Sitter Space . . . . .	58
4.1.1. The global patch of de Sitter space, $dS^D$ . . . . .	60
4.1.2. The Poincaré patch of de Sitter space, $dS_P^D$ . . . . .	60
4.2. Vacuum states in de Sitter space . . . . .	61
4.2.1. BD modes . . . . .	62
4.2.2. Euclidean modes . . . . .	62
4.2.3. Two-point functions and $\alpha$ -vacua . . . . .	63
4.3. The SJ state in de Sitter space . . . . .	66
4.3.1. The SJ state in the Poincaré patch . . . . .	67
4.3.2. The SJ state in the global patch . . . . .	70
4.3.3. The critical mass $m_*$ . . . . .	75
4.4. The discrete SJ state on a sprinkling into $dS^2$ . . . . .	76
4.4.1. Sprinkling into a causal diamond in $dS^2$ . . . . .	76
4.4.2. Simulation results . . . . .	77
4.5. Conclusions . . . . .	81
<b>5. Remarks on the SJ state in the trousers spacetime</b>	<b>84</b>
5.1. Quantum Fields in the trousers spacetime . . . . .	87
5.2. The pair of diamonds . . . . .	89
5.3. Propagators in the trousers . . . . .	91
5.3.1. Integral form of Green's equation . . . . .	92
5.3.2. The field equations near the singularity . . . . .	94
5.3.3. A one-parameter family of propagators . . . . .	95
5.4. Propagation of plane waves past the singularity . . . . .	98
5.5. Eigenmodes of the Pauli-Jordan function . . . . .	99
5.5.1. Counting eigenmodes . . . . .	100
5.5.2. Ordinary plane waves . . . . .	101
5.5.3. Restricted plane waves . . . . .	102
5.5.4. Ordinary plane waves revisited . . . . .	104
5.5.5. Restricted constant functions . . . . .	104
5.6. Outlook . . . . .	105
<b>6. For Future Investigation</b>	<b>107</b>
<b>A. Corrections to the SJ two-point function</b>	<b>109</b>

<b>B. Modes in <math>dS^D</math> and <math>dS_P^D</math></b>	<b>112</b>
B.1. Bunch-Davies modes on $dS_P^D$ . . . . .	112
B.2. Euclidean modes on $dS^D$ . . . . .	114

# List of Tables

- 4.1. The SJ state in the global and Poincaré patches of de Sitter space. Depending on the mass  $m$  of the field, the SJ state corresponds to different  $\alpha$ -vacua (the Euclidean, in- and out- vacua are all special cases of  $\alpha$ -vacua and in odd spacetime dimensions the in- and out- vacua coincide). The critical mass that marks these transitions is  $m_* = \frac{d}{2\ell}$ , where  $d$  is the spatial dimension and  $\ell$  is the de Sitter radius. 81
- 5.1. Some subregions of the pair of diamonds and their labels. All regions except the last two are defined with respect to  $D_1$  — for these there are analogous regions defined with respect to  $D_2$ . Note that the upper left and right diagonal regions as well as the left and right leg regions extend over both diamonds (as evident in their symbols). . . . . 92





# List of Figures

2.1.	An $N = 200$ sprinkling into a causal diamond in two-dimensional Minkowski space. Only the irreducible relations are shown (i.e. those not implied by others via transitivity). . . . .	22
3.1.	The left and right Rindler wedges of two-dimensional Minkowski space-time. . . . .	37
3.2.	The causal diamond, $u, v \in (-L, L)$ . The shaded portions of the diagram represent the centre ( <i>i</i> ) and corner ( <i>ii</i> ) regions of interest in Section 3.2.1. . . . .	42
3.3.	Plot of $\tan x$ and $2x$ along with vertical lines at $\frac{2n-1}{2}\pi$ for $n \in \mathbb{Z}$ . The values of the summation variable correspond to the positions of the intersections $\tan x = 2x > 0$ . . . . .	44
3.4.	An $N = 2^{11} = 2048$ element sprinkling into a diamond $C_L$ (with $L = 2^{\frac{9}{2}}$ in natural units). The subregions corresponding to the centre ( <i>i</i> ) and the corner ( <i>ii</i> ) are highlighted. . . . .	51
3.5.	The real parts of the continuum two-point function $W_{M,\lambda}(x, x')$ (black line) with $\lambda = 0.02$ and the discrete SJ two-point function $\mathbf{W}_{ij}$ (blue scatter) in the centre of the finite diamond $C_L$ with $L = 2^{\frac{9}{2}}$ , plotted against the proper time $ d $ for timelike separated events. . . . .	52
3.6.	Correlation plots for the two-point functions in the corner of the causal diamond. The horizontal axis represents the causal set two-point function $\mathbf{W}_{ij}$ . The vertical axes represent (from left to right, top to bottom): the SJ, the Minkowski, the mirror, and the Rindler two-point functions. . . . .	53
3.7.	Correlation plots for the two-point functions in the full causal diamond. The horizontal axis represents the causal set two-point function $\mathbf{W}_{ij}$ . The vertical axes represent (from left to right, top to bottom): the SJ, the Minkowski, the left mirror, the box (two mirrors) and the Rindler two-point functions. . . . .	54

- 
- 4.1. The Penrose diagram of de Sitter space. The shaded area represents the (expanding) Poincaré patch. Dotted lines are surfaces of constant  $t$  ( $d$ -spheres), dashed lines are surfaces of constant  $\eta$  ( $d$ -planes). . . . . 59
- 4.2. The SJ state in the global patch of  $3 + 1$  dimensional de Sitter space. The SJ modefunctions  $u_{L_j}^{S_J}$  are related to those of the Euclidean vacuum  $u_{L_j}^E$  by the Bogoliubov transformation  $u_{L_j}^{S_J} = \cosh(\alpha)u_{L_j}^E + \sinh(\alpha)e^{i\beta}\bar{u}_{L_j}^E$ , the second coefficient of which is plotted here. Depending on the product  $m\ell$ , where  $m$  is the mass of the field and  $\ell$  is the de Sitter radius, the SJ state corresponds to different  $\alpha$ -vacua. For  $m\ell \geq 3/2$  and  $m\ell = \sqrt{5/4}$ , it coincides with the Euclidean vacuum. The prescription fails for  $m\ell = \sqrt{2}$ . . . . . 74
- 4.3. An  $N = 1010$  element sprinkling with density  $\rho = 76\ell^{-2}$  into a causal diamond of length  $\tau = 8\ell$  in two-dimensional de Sitter space, visualised in the embedding three-dimensional Minkowski space (see Section 4.1). The de Sitter radius has been set to  $\ell = 1$ . . . . . 78
- 4.5. The Hadamard function  $\mathbf{H}_{S_J}$  on an  $N = 1010$  sprinkling of into a causal diamond of length  $\tau = 8\ell$  in  $1 + 1$  dimensional de Sitter space. The mass of the field is taken to be  $m = 2.36\ell^{-1}$ , and the de Sitter radius  $\ell$  is set to unity. The geodesic distance  $|d|$  between the two arguments of the function is plotted on the horizontal axis for timelike (above) and spacelike (below) separated points. The error bars show the standard deviation about the mean of  $\mathbf{H}_{S_J}$  for binned values of  $|d|$ .  $H_{\alpha,\beta}(x, y)$  refers to the Hadamard function of the  $\alpha$ -vacua (see Section 4.2). The function  $H_{0,1,0}$  has been omitted in (a), since it is indistinguishable from the Euclidean function  $H_E$ . . . . . 80
- 5.1. The “trousers” spacetime with topology-change  $S^1 \leftrightarrow S^1 \times S^1$ . . . . . 86
- 5.2. The trousers spacetime (left) and a two-dimensional representation of it (right) obtained by cutting and unwrapping the manifold. The coloured arrows indicate the respective identifications in the trunk (blue) and in the left and right legs (yellow and red). The crosses mark the location of the crotch singularity. . . . . 88
- 5.3. The pair of diamonds in more detail. The coloured arrows indicate the topological identifications inherited from the trousers (Figure 5.2). 89

---

5.4.	A naive ansatz for the retarded propagator $G_R(x, y) = -\frac{1}{2}\chi(x \succ y)$ in the trousers, drawn as a function of $y$ for fixed $x \succ x_c$ represented by the black dot. The function is equal to $-\frac{1}{2}$ in the shaded region and zero everywhere else. The dashed contour corresponds to the boundary of a causal diamond centred on the singularity. . . . .	93
5.5.	The modified propagator $G_R(x, y) = G_A(y, x)$ for fixed $x$ in  . In order for the integral version of Green's equation to vanish for a small contour around the singularity, we need $b_1 + b_2 = 1$ . . . . .	96
5.6.	The modified propagator $G_{A,p}(x, y) = G_{R,p}(y, x)$ for fixed $x$ in  . Here $q = 1 - p$ . . . . .	98
5.7.	The Pauli-Jordan function $\Delta_p(x, y)$ in the trousers as a function of $y$ , with the first argument $x$ fixed (at the dot) in the causal future of the crotch singularity. Here $q = 1 - p$ . . . . .	100
5.8.	$L^2(M \times M)$ -norm of $i\Delta_p(x, y)$ on the pair of diamonds as a function of $p$ . . . . .	101
A.1.	A plot of $\epsilon(u, v; u', v')$ in the centre (top) and in the corner (bottom) against $-\log_{10}(V_{\text{sub}}/V)$ . . . . .	110

# 1. Introduction

Quantum field theory (QFT) in curved spacetime is primarily a framework for studying the effect of spacetime geometry on quantum fields, in situations where the quantum effects of gravity itself can be ignored. Although not a fundamental theory of nature, predictions made within the framework have led to profound insights into the interplay between matter and spacetime geometry, such as the emission of thermal radiation by black holes [3], the Unruh effect [4, 5, 6], and the generation of Gaussian-distributed and nearly scale-invariant random perturbations in the theory of inflation [7]. In all of these applications, physical predictions are arrived at via the choice of a “vacuum” or some reasonable reference state for the quantum field. It is well known, however, that the unique Poincaré-invariant vacuum of flat spacetime does not admit an obvious generalisation to arbitrarily curved backgrounds, a notable exception being spacetimes with a timelike Killing vector  $\kappa = \frac{d}{dt}$ , for which a natural choice of vacuum is the ground state of the Hamiltonian on  $t = \text{const.}$  hypersurfaces.

This observation hints at a central tension in the subject as traditionally studied, as pointed out by S.A. Fulling at the end of his classic textbook *Aspects of Quantum Field Theory in Curved spacetime*:

One of the striking things about the subject is the intertwining of the conceptual issues with the mathematical tools. Historically there has been a close association between relativity and differential geometry, while rigorous research in quantum theory has looked more toward functional analysis. Field quantisation in a gravitational background brings these two alliances into head-to-head confrontation: A field is a function of a time and a space variable,

$$\phi(t, \mathbf{x}).$$

Relativity and modern geometry persuade one with an almost religious intensity that these variables must be merged and submerged; the true

---

domain of the field is a spacetime manifold:

$$\phi(\mathbf{x}), \mathbf{x} \rightarrow \{x^\mu\}$$

But quantum theory and its ally, analysis, are constantly pushing in the opposite direction. They want to think of the field as an element of some function space, depending on time as a parameter:

$$\phi_t(\mathbf{x}).$$

Taking the relativistic view that the physical world has a spacetime character indeed requires an approach to quantum field theory that is built on spacetime concepts, one that makes no fundamental appeal to “time as a parameter.” The approach of algebraic quantum field theory takes this view seriously and attempts to push the foundations towards greater covariance, basing the theory on appropriate algebras of operators associated to open spacetime regions. The focus on the quasi-local algebras as the central constructs of the theory has encouraged the point of view that in general, in curved spacetime, there is no preferred quantum state and that a choice of state is akin to a choice of coordinates (see *e.g.* [8]). However, the algebraic approach has not been completely successful in constructing the expectation value of the stress-energy tensor or dealing with interacting fields. It remains an open question whether quantum field theory requires in addition the identification of a distinguished “ground state” (or class of them) [9, 10, 11].

The split of spacetime into space plus time that Fulling assumes to be inherent in the quantum aspect of the field theory is actually an artefact of the choice to conceive of a quantum field as if it were the canonical quantisation of a classical Hamiltonian system. In a canonical approach, defining the Hamiltonian tends to demand the foliation of spacetime into spacelike hypersurfaces. However, there is an alternative, long ago identified by Dirac as more fundamental because it is essentially relativistic: the quantum analogue of the classical Lagrangian approach, namely the path integral [12].

In this thesis, we investigate a proposal for a “ground state of a spacetime region” for a free quantum field [10, 13] that, like the path-integral, is essentially relativistic in character. The proposal, implicit in work by S. Johnston on quantum field theory on a causal set [14], gives primacy to the “true domain”, the spacetime manifold itself and its coordinate independent causal structure. This “Sorkin-Johnston” (SJ)

---

ground state is defined in a covariant way starting from nothing more than the Pauli-Jordan function (or causal propagator)  $\Delta(x, y)$ .

The formulation of the quantum theory along these lines bears no resemblance to the “canonical quantisation” process: one does not solve the classical equations of motion or identify canonically conjugate variables or promote them to operators satisfying canonical commutation relations. Such a formulation seems much more compatible with a path integral approach to quantum theory, and indeed the SJ proposal serves as the starting point for the construction of a histories-based formulation of quantum field theory on a causal set [13] which admits a natural generalisation to interacting scalar fields and takes us one step further towards a quantum theory of causal sets.

From a more conservative point of view, even if a natural construction of quantum states in curved spacetime is not logically necessary for quantum field theory as such, finding such a construction can be fruitful for many reasons. For instance, one may hope to find what could be a “natural” state for a portion of spacetime such as the early universe [10], just as the Minkowski vacuum is “natural” for an infinite flat spacetime. Then, one might hope further that “natural” would coincide with “likely to be produced dynamically”, which in the cosmological case refers to the pre-geometric, quantum gravity era [15].

## 2. Background

We use a mostly + metric signature and natural units:  $G = \hbar = c = 1$ . The complex conjugate of  $c$  is  $\bar{c}$  and the Hermitian conjugate of  $h$  is  $h^\dagger$ .

### 2.1. Quantum fields in curved spacetime

Here we review the quantum theory of a free real scalar field  $\phi(x)$  in a  $D = d + 1$  dimensional spacetime  $(M, g_{\mu\nu})$ . We assume  $(M, g_{\mu\nu})$  to be globally hyperbolic, which implies that it admits a global time function  $t : M \rightarrow \mathbb{R}$  and a foliation by Cauchy surfaces  $\Sigma_t$  of constant  $t$ .

The classical equations of motion of the field are given by the Klein-Gordon equation

$$(\square - m^2)\phi(x) = 0 \quad (2.1)$$

where  $\square = g^{\mu\nu}\nabla_\mu\nabla_\nu = \frac{1}{\sqrt{-g}}\partial_\mu(\sqrt{-g}g^{\mu\nu}\partial_\nu)$  is the d'Alembertian operator and  $g$  is the determinant of the metric.

There exists a natural inner product on the space of solutions to (2.1), the so-called *Klein-Gordon product*:

$$(f, g) := i \int_\Sigma (\bar{f}n^\mu\nabla_\mu g - gn^\mu\nabla_\mu\bar{f}) d\Sigma, \quad (2.2)$$

where bar denotes complex conjugation,  $\Sigma$  is an arbitrary Cauchy surface in  $M$ ,  $n^\mu$  is the future-directed unit normal to  $\Sigma$ , and  $d\Sigma$  is the induced volume element on  $\Sigma$ . It is invariant under the evolution generated by (2.1), that is to say it is independent of the hypersurface  $\Sigma$  when evaluated on any pair of solutions to (2.1).

One defines advanced and retarded Green functions  $G_{R,A}(x, y)$  associated with (2.1) as solutions to

$$(\square - m^2)G_{R,A}(x, y) = \frac{1}{\sqrt{-g}}\delta^{(D)}(x - y), \quad (2.3)$$

where by definition  $G_R(x, y) = 0$  unless  $y \prec x$  and  $G_A(x, y) = 0$  unless  $x \prec y$ . Here, we have introduced the causal precedence relation  $\prec$ , where  $x \prec y$  means that  $x$

is in the causal past of (or causally precedes)  $y$ , i.e. there exists a future-directed causal (non-spacelike) curve from  $x$  to  $y$ . The relation  $\succ$  is defined analogously. The Green functions are unique when  $(M, g_{\mu\nu})$  is globally hyperbolic [16].

### 2.1.1. Canonical quantisation

In the usual construction of the QFT, one promotes  $\phi(x)$  to an operator in a Hilbert space  $\mathcal{H}$ , in such a way that  $\phi(x)$  solve the Klein-Gordon equation and satisfy the canonical commutation relations

$$[\phi(t, \mathbf{x}), \pi(t, \mathbf{y})] = i\delta^d(\mathbf{x} - \mathbf{y})\mathbf{1}. \quad (2.4)$$

Here  $\mathbf{1}$  is the identity operator on  $\mathcal{H}$  and both the field and its conjugate momentum  $\pi(x) = \sqrt{-g}g^{0\mu}\partial_\mu\phi(x)$  are specified on the same hypersurface  $\Sigma_t$  (we omit hats on operators). The two conditions are consistent with each other due to the invariance of (2.4) under the evolution generated by the field equations.

This is achieved concretely by first identifying a complete orthonormal set of positive-norm solutions to the Klein-Gordon equation,  $u_{\mathbf{k}}(x)$ , i.e. one for which  $(u_{\mathbf{k}}, u_{\mathbf{q}}) = \delta_{\mathbf{k}\mathbf{q}}$ . Any such set comes hand in hand with an orthogonal set of negative-norm solutions  $\bar{u}_{\mathbf{k}}$ :

$$(u_{\mathbf{k}}, u_{\mathbf{q}}) = -(\bar{u}_{\mathbf{k}}, \bar{u}_{\mathbf{q}}) = \delta_{\mathbf{k}\mathbf{q}}, \quad (u_{\mathbf{k}}, \bar{u}_{\mathbf{q}}) = 0. \quad (2.5)$$

Taken together the two sets form a complete basis. The field is expanded in terms of the modes  $u_{\mathbf{k}}$  and  $\bar{u}_{\mathbf{k}}$  by attaching appropriately normalised annihilation operators to the positive-norm modes:

$$\phi(x) = \sum_{\mathbf{k}} u_{\mathbf{k}}(x)a_{\mathbf{k}} + \bar{u}_{\mathbf{k}}(x)a_{\mathbf{k}}^\dagger. \quad (2.6)$$

The canonical commutation relations (2.4) then obtain if the operators  $a_{\mathbf{k}}$  and their Hermitian conjugates satisfy the usual commutation relations

$$[a_{\mathbf{k}}, a_{\mathbf{q}}^\dagger] = \delta_{\mathbf{k}\mathbf{q}} \quad \text{and} \quad [a_{\mathbf{k}}, a_{\mathbf{q}}] = [a_{\mathbf{k}}^\dagger, a_{\mathbf{q}}^\dagger] = 0. \quad (2.7)$$

Introducing, finally, the vacuum state  $|\Omega\rangle$  via the conditions  $a_{\mathbf{k}}|\Omega\rangle = 0 \ \forall \ \mathbf{k}$ , one obtains a concrete operator  $\phi(x)$  acting in a Hilbert space  $\mathcal{H}$  spanned by states of the form  $(a_{\mathbf{k}_1}^\dagger)^{n_1}(a_{\mathbf{k}_2}^\dagger)^{n_2}\dots|\Omega\rangle$ . We will refer to the state  $|\Omega\rangle$  defined in this manner



as the “vacuum associated with the modes  $u_{\mathbf{k}}$ ”.

The covariance of the canonical commutation relations is not explicit in their equal-time form (2.4). However, they can be restated in an entirely equivalent form due to Peierls as [17, 18]

$$[\phi(x), \phi(y)] = i\Delta(x, y)\mathbf{1}, \quad (2.8)$$

where  $\Delta(x, y)$  is the Pauli-Jordan (or commutator) function, which is defined as the difference between the retarded and advanced Green functions:

$$\Delta(x, y) := G_R(x, y) - G_A(x, y). \quad (2.9)$$

Note that the arguments  $x$  and  $y$  are not restricted to lie on any particular hypersurface, and further that  $\Delta(x, y)$  is a solution to the Klein-Gordon equation in both arguments since it is the difference between two Green functions.

### 2.1.2. Non-uniqueness of the quantum state

As is well-known, this construction is not unique. There are many ways to choose a set of positive-norm solutions, and with each choice comes a different set of annihilation operators and a different vacuum. Consider a new orthonormal set of positive-norm modes  $v_{\mathbf{k}}$  related by a so-called Bogoliubov transformation to the modes  $u_{\mathbf{k}}$ :

$$v_{\mathbf{k}}(x) = \sum_{\mathbf{q}} A_{\mathbf{kq}} u_{\mathbf{q}}(x) + B_{\mathbf{kq}} \bar{u}_{\mathbf{q}}(x), \quad (2.10)$$

where  $A_{\mathbf{kq}}$  and  $B_{\mathbf{kq}}$  are known as the Bogoliubov coefficients. These modes define a different representation of the field

$$\phi(x) = \sum_{\mathbf{k}} v_{\mathbf{k}}(x) b_{\mathbf{k}} + \bar{v}_{\mathbf{k}}(x) b_{\mathbf{k}}^{\dagger}, \quad (2.11)$$

which is consistent with the commutation relations (2.8) so long as

$$\begin{aligned} \sum_{\mathbf{k}} A_{\mathbf{ak}} B_{\mathbf{bk}} - B_{\mathbf{ak}} A_{\mathbf{bk}} &= 0 \\ \sum_{\mathbf{k}} A_{\mathbf{ak}} \bar{A}_{\mathbf{bk}} - B_{\mathbf{ak}} \bar{B}_{\mathbf{bk}} &= \delta_{\mathbf{ab}} \end{aligned} \quad (2.12)$$

(assuming that the new annihilation operators  $b_{\mathbf{k}}$  are given their usual normalisation (2.7)). The vacuum state  $|\tilde{\Omega}\rangle$  associated with these modes, i.e. the state defined

by  $b_{\mathbf{k}}|\tilde{\Omega}\rangle = 0 \forall \mathbf{k}$ , is different from  $|\Omega\rangle$  unless  $B_{\mathbf{k}\mathbf{q}} = 0 \forall \mathbf{k}, \mathbf{q}$ . A transformation for which the latter equality holds will be referred to as a *trivial* Bogoliubov transformation.

In the special case that the spacetime admits a global timelike Killing vector  $\kappa = \frac{d}{d\tau}$ , there exists a preferred basis of positive-norm modes  $u_{\mathbf{k}}$ , defined by the “positive-frequency” condition

$$\kappa u_{\mathbf{k}} = -i\omega(\mathbf{k})u_{\mathbf{k}} \quad (2.13)$$

for *positive* real  $\omega(\mathbf{k})$ . The Killing vector  $\kappa$  commutes with the Klein-Gordon operator, which implies that in a chart  $x = (\tau, \mathbf{x})$  the positive-frequency modes take the form

$$u_{\mathbf{k}}(x) = u_{\mathbf{k}}(\tau, \mathbf{x}) = n_{\mathbf{k}}e^{-i\omega(\mathbf{k})\tau}U_{\mathbf{k}}(\mathbf{x}) \quad (2.14)$$

where  $n_{\mathbf{k}}$  is a normalisation-factor,  $\omega(\mathbf{k}) > 0$ , and  $\mathbf{x}$  are the spatial coordinates of  $x$ . There is then a unique vacuum state corresponding to this choice of positive frequency modes, which is the ground state of the Hamiltonian associated to  $\kappa$ . In the absence of such symmetries, there is in general no preferred vacuum state.

### 2.1.3. Propagators

The Wightman (two-point) function of the field in a state  $|\Omega\rangle$  is defined as

$$W_{\Omega}(x, y) := \langle \Omega | \phi(x)\phi(y) | \Omega \rangle. \quad (2.15)$$

When  $|\Omega\rangle$  is a Gaussian state, knowledge of this function fully specifies the quantum theory, since Wick’s theorem then guarantees that all field correlators reduce to polynomials in  $W_{\Omega}(x, y)$ . We will assume that  $|\Omega\rangle$  is Gaussian in this thesis, since we are dealing with non-interacting fields. Using the definition of the commutation relations and the Wightman function, it follows that

$$W_{\Omega}(x, y) = \frac{1}{2}H_{\Omega}(x, y) + \frac{i}{2}\Delta(x, y), \quad (2.16)$$

where we have defined the Hadamard (or anticommutator) function

$$H_{\Omega}(x, y) := 2\text{Re} [W_{\Omega}(x, y)] = \langle \Omega | \phi(x)\phi(y) + \phi(y)\phi(x) | \Omega \rangle. \quad (2.17)$$

We see that the choice of a ground state  $|\Omega\rangle$  is equivalent to a choice of Hadamard function  $H_\Omega(x, y)$ , since *any* state consistent with the canonical commutation relations must have the same Pauli-Jordan function (as guaranteed by the commutation relations (2.8)).

Given a field expansion in terms of modes  $u_{\mathbf{k}}$ , the Wightman, Pauli-Jordan and Hadamard functions can be expressed as the mode sums

$$\begin{aligned} W_\Omega(x, y) &= \sum_{\mathbf{k}} u_{\mathbf{k}}(x)\bar{u}_{\mathbf{k}}(y), \\ i\Delta(x, y) &= \sum_{\mathbf{k}} [u_{\mathbf{k}}(x)\bar{u}_{\mathbf{k}}(y) - \bar{u}_{\mathbf{k}}(x)u_{\mathbf{k}}(y)], \\ H_\Omega(x, y) &= \sum_{\mathbf{k}} [u_{\mathbf{k}}(x)\bar{u}_{\mathbf{k}}(y) + \bar{u}_{\mathbf{k}}(x)u_{\mathbf{k}}(y)]. \end{aligned} \quad (2.18)$$

Note in this context that  $W_\Omega$  is always, in fact, positive semi-definite in the sense of a quadratic form:

$$\int_M \sqrt{-g(x)}dx \int_M \sqrt{-g(x')}dx' \overline{f(x)}W(x, x')f(x') \geq 0. \quad (2.19)$$

This follows directly from the positivity of the Hilbert norm:

$$\begin{aligned} &\int_M \sqrt{-g(x)}dx \int_M \sqrt{-g(y)}dx' \overline{f(x)}\langle\Omega|\phi(x)\phi(y)|\Omega\rangle f(y) \\ &= \left\langle\Omega\left|\left(\int_M \sqrt{-g(x)}dx \overline{f(x)\phi(x)}\right)\left(\int_M \sqrt{-g(x)}dx f(x)\phi(x)\right)\right|\Omega\right\rangle \\ &=: \langle\phi(f)|\phi(f)\rangle \geq 0. \end{aligned} \quad (2.20)$$

## 2.2. The discrete SJ state

Even though the central topic of this thesis is the study of the *continuum* SJ formalism (and its associated vacuum state), it seems appropriate to first introduce the SJ formalism on a causal set. For one, the discrete formalism is the historical precursor of the continuum formalism [14], wherefore it might better illustrate the original motivations for the idea. More importantly, perhaps, the mathematical formulation is much simpler in the discrete setting and hence the derivation cleaner.

The discrete version of the SJ prescription can be interpreted in two ways. In the context of quantum gravity, causal sets are considered to be fundamental — more fundamental than continuum spacetimes which are just approximations to the true

discrete physics [19]. On this view, the discrete SJ proposal is a starting point for building a theory of quantum fields on the physical discrete substratum of spacetime and one can hope that it will give us clues about quantum gravity, just as quantum field theory in curved continuum spacetime has done. From another viewpoint, the discrete formalism can be seen as simply a Lorentz-invariant discretisation of the continuum formalism and can therefore be used as a mathematical tool in the continuum theory when analytic calculations are difficult.

### 2.2.1. Background on causal sets

Let us briefly review the necessary background on causal sets (for more details on causal set theory the reader may refer to [19, 20, 21]). A *causal set*  $(\mathcal{C}, \prec)$  is a set  $\mathcal{C}$  with a partial order relation  $\prec$ , which is

- (i) transitive :  $x \prec y \prec z \implies x \prec z$
- (ii) irreflexive :  $x \not\prec x$
- (iii) locally finite :  $|[x, y]| < \infty$

for all  $x, y, z \in \mathcal{C}$ , where  $[x, y] := \{z \in \mathcal{C} \mid x \preceq z \preceq y\}$  is the (inclusive) order interval between two elements  $x, y \in \mathcal{C}$  and  $|\cdot|$  denotes cardinality. We write  $x \preceq y$  for ( $x \prec y$  or  $x = y$ ). In the presence of transitivity, irreflexivity implies the absence of cycles:  $x \prec x' \prec x'' \prec \dots \prec x$ , which can be taken as an alternative axiom to (ii). The condition (iii) of local finiteness is a formal way of saying that a causal set is discrete. Note that we use the same symbol  $\prec$  to denote the causal precedence relation on a causal set and that on a Lorentzian manifold (mainly for lack of symbols, but also as an indication of their kinship). It will always be clear which relation the symbol refers to, as it either relates two causal set elements or two spacetime points.

A causal set can be fully encoded in an adjacency or *causal matrix*  $\mathbf{C}$ , defined as the  $|\mathcal{C}| \times |\mathcal{C}|$ -matrix with entries

$$C_{ij} := \begin{cases} 1 & \text{if } x_i \prec x_j \\ 0 & \text{otherwise,} \end{cases} \quad (2.21)$$

for  $x_i, x_j \in \mathcal{C}$ , where  $i, j \in \{1, 2, \dots, |\mathcal{C}|\}$  are indices corresponding to a labelling of  $\mathcal{C}$ . A labelling is said to be faithful iff  $i \prec j \implies i < j$  and so, given a faithful labelling,  $\mathbf{C}$  will be represented by a strictly upper triangular matrix. In this thesis

labellings will always be faithful.

A technique that is widely used to test the discrete-continuum correspondence for causal sets is the *sprinkling*. Whenever we propose a new structure or a new model to describe discrete physics on a causal set (be it a formalism for quantum fields, a proposal for the spacetime action, a formula for geodesic distance...), a basic consistency requirement is that the proposed model reproduce known and tested continuum results in an appropriate “continuum limit”. A concrete implementation of this idea is afforded by the sprinkling, which is a procedure for generating a causal set  $(\mathcal{C}_M, \preceq)$  given a continuum spacetime region  $(M, g_{\mu\nu})$ . Points are placed at random in  $M$  using a Poisson process with “density”  $\rho = l^{-d}$ , where  $l$  denotes the discreteness scale. In other words we set the mean of the Poisson variable  $N_M := |\mathcal{C}_M|$  that counts the number of elements sprinkled into  $M$  to be  $\langle N_M \rangle = \rho V_M$ , thus obtaining an average of 1 element (or atom) per spacetime volume-element  $l^d$ . This procedure generates a causal set whose elements are the sprinkled points and whose partial order relation can be “read off” from that of the underlying spacetime. The causal set obtained in this manner provides a discretisation of  $(M, g_{\mu\nu})$  which, unlike a regular lattice, is statistically Lorentz invariant [21, Sec. 1.5]. The continuum limit then corresponds to the limit as  $l \rightarrow 0$  or  $\rho \rightarrow \infty$  (as  $M$  and thus  $V_M$  are fixed). An example of an  $N = 200$  sprinkling into a causal diamond in two-dimensional Minkowski space is shown in Figure 2.1 (corresponding to  $V = L^2$  and  $\rho = 200L^{-2}$  where  $L$  is an arbitrary length scale for the diamond).

The sprinkling  $(\mathcal{C}_M, \prec)$  as such carries no explicit information other than the causal order inherited from its ordinary manifold  $(M, g_{\mu\nu})$  — everything but  $\prec$  is forgotten. Yet the order relation is very rich. Indeed, in the continuum, the causal order of a distinguishing manifold encodes all geometric information of the spacetime up to a local scale factor.<sup>1</sup> This suggests that the causal set contains much information intrinsically — otherwise, of course, it would not be a good candidate for spacetime in the first place.

The example that will be relevant in this work is the timelike geodesic distance between two elements of a sprinkling. It can be shown that, given a sprinkling into a  $D$ -dimensional spacetime, a good estimator for the geodesic distance between two elements is given by  $c_D \rho^{\frac{1}{d}}$  times the length of the longest chain between the

---

<sup>1</sup>The precise statement is that if two distinguishing spacetimes are causally isomorphic then they are conformally isometric — the causal order contains within itself the topology (including dimension), the differentiable structure and the conformal metric  $g_{\mu\nu} / \sqrt{-g}$  [22, 23, 24].

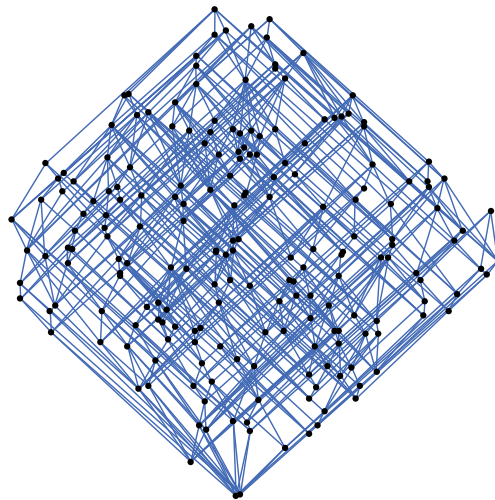


Figure 2.1.: An  $N = 200$  sprinkling into a causal diamond in two-dimensional Minkowski space. Only the irreducible relations are shown (i.e. those not implied by others via transitivity).

two elements (a chain being a sequence of elements, all of which are related, and  $c_D$  denoting a constant that only depends on  $D$ ) [25]. In order to reduce the computational cost of the simulations described in the following chapters, we will keep the geodesic distance information of  $(M, g_{\mu\nu})$  for all pairs of elements in  $\mathcal{C}_M$  rather than computing the geodesic distance from the sprinkling itself. This means that for all pairs  $\nu_i, \nu_j \in \mathcal{C}_M$  with coordinates  $x_i, x_j$  in  $M$ , we record the values  $d_{ij} := d(x_i, x_j)$ , where  $d(x_i, x_j)$  denotes geodesic distance in  $(M, g_{\mu\nu})$ . The results of [25] provide a priori justification for this workaround (at least for related pairs of elements), and the findings of Chapters 3 and 4 provide further a posteriori justification.

### 2.2.2. Definition

The canonical procedure for quantum field theory outlined in Section 2.1, relying on differential equations and Fourier decomposition, is hard to transpose to causal sets. On the other hand, the formulation in terms of the classical retarded and advanced propagators and the quantal Wightman function provides a much more natural starting point on causal sets. Indeed, the first step toward a theory of fields propagating on an underlying causal set was the discovery of a retarded propagator [26]. Let  $(\mathcal{C}_M, \preceq)$  be an  $N$ -element causal set generated by a sprinkling into a

1 + 1 dimensional spacetime  $(M, g_{\mu\nu})$ . The *discrete retarded propagator*  $\mathbf{R}$  in two dimensions is defined for a scalar field of mass  $m$  on  $\mathcal{C}_M$  as

$$\mathbf{R} = \frac{1}{2}\mathbf{C} \left( \mathbf{1} + \frac{m^2}{2\rho}\mathbf{C} \right)^{-1} \quad (2.22)$$

where  $\mathbf{C}$  denotes the causal matrix defined in (2.21). It has been shown that if  $(M, g_{\mu\nu})$  is a causal diamond<sup>2</sup> in two-dimensional Minkowski space, the mean of  $\mathbf{R}_{ij}$  as a function of the geodesic distance  $d_{ij} = d(x_i, x_j)$  is in agreement with the known continuum retarded propagator  $G_R(x, y) = \chi(y \prec x)J_0(m|d(x, y)|)$  for masses in the range  $0 < m/\sqrt{\rho} \ll 1$  [26]. (Here  $J_0$  denotes the Bessel function of the first kind and  $\chi$  is the Boolean function that maps propositions to  $\{0, 1\}$ :  $\chi(A) = 1$  if  $A$  is true and  $\chi(A) = 0$  if  $A$  is false). We will provide similar evidence for the case where  $(M, g_{\mu\nu})$  is a causal diamond in de Sitter space.

Given a retarded propagator, we define the *discrete Pauli-Jordan function* (or *Pauli-Jordan matrix*)  $\Delta$  on  $\mathcal{C}_M$  in analogy with its continuum counterpart [14]:

$$\Delta := \mathbf{R} - \mathbf{R}^T \quad (2.23)$$

where  $T$  denotes the matrix transpose. The matrix  $i\Delta$  is by construction skew-symmetric:  $i\Delta = -i\Delta^T$  and Hermitian:  $(i\Delta)^\dagger = i\Delta$ . By consequence, it has an even number of eigenvectors  $\mathbf{u}_a$  and its non-zero eigenvalues  $\lambda_a$  come in pairs of positive/negative real numbers:

$$(i\Delta)\mathbf{u}_a^\pm = \pm\lambda_a\mathbf{u}_a^\pm \quad (2.24)$$

(each eigenvector being a  $|\mathcal{C}|$ -dimensional vector  $[\mathbf{u}_a]_i$  with  $i \in \{1, 2, \dots, |\mathcal{C}|\}$ ). Their associated eigenvectors form complex conjugate pairs:

$$\bar{\mathbf{u}}_a^+ = \mathbf{u}_a^- \quad \forall a. \quad (2.25)$$

Eigenvectors corresponding to distinct eigenvalues are orthogonal, and we can always normalise them such that

$$\begin{aligned} \langle \mathbf{u}_a^+, \mathbf{u}_b^+ \rangle &= \langle \mathbf{u}_a^-, \mathbf{u}_b^- \rangle = \delta_{ab} \\ \langle \mathbf{u}_a^+, \mathbf{u}_b^- \rangle &= 0 \end{aligned} \quad (2.26)$$

---

<sup>2</sup>A causal diamond is the intersection of the interior of the past lightcone of a point  $q$  with the interior of the future light cone of a point  $p$  that lies to the causal past of  $q$ .

where  $\langle \mathbf{u}_1, \mathbf{u}_2 \rangle := \mathbf{u}_1^\dagger \cdot \mathbf{u}_2$ . By the spectral theorem for Hermitian matrices, we can now decompose  $i\Delta$  as follows:

$$i\Delta = \sum_a \lambda_a \mathbf{u}_a^+ (\mathbf{u}_a^+)^\dagger - \sum_a \lambda_a \mathbf{u}_a^- (\mathbf{u}_a^-)^\dagger. \quad (2.27)$$

If we then define the matrix

$$\mathbf{Q} = \sum_a \lambda_a \mathbf{u}_a^+ (\mathbf{u}_a^+)^\dagger, \quad (2.28)$$

the decomposition above takes the simple form

$$i\Delta = \mathbf{Q} - \overline{\mathbf{Q}}. \quad (2.29)$$

Remember that the commutation relations for the real scalar field in the continuum imply  $i\Delta(x, x') = W(x, x') - \overline{W(x, x')}$ . This suggests that  $\mathbf{Q}$  itself is the causal set analog of the two-point function! This leads to Sorkin and Johnston's proposal

$$\mathbf{W}_{SJ} := \mathbf{Q} = \sum_a \lambda_a \mathbf{u}_a^+ (\mathbf{u}_a^+)^\dagger. \quad (2.30)$$

The *discrete SJ Wightman function* (or *SJ Wightman matrix*) has hereby been defined as the positive spectral projection of  $i\Delta$ :

**Definition:** *The SJ Wightman function on a causal set is given by the positive part of the matrix  $i\Delta$ :*

$$\mathbf{W}_{SJ} := \text{Pos}(i\Delta). \quad (2.31)$$

By construction,  $\mathbf{W}_{SJ}$  is a Hermitian positive<sup>3</sup> matrix:

$$\mathbf{W}^\dagger = \mathbf{W} \quad \text{and} \quad \langle \mathbf{u}, \mathbf{W}_{SJ} \mathbf{u} \rangle \geq 0 \quad \forall \mathbf{u} \in \mathbb{C}^N. \quad (2.32)$$

Since  $i\Delta$  is itself a finite Hermitian matrix (at least for causal sets of finite cardinality), its positive part is completely well-defined and specifies  $\mathbf{W}_{SJ}$  uniquely. Before we move on we also define the discrete analogue of the Hadamard function

$$\mathbf{H}_{SJ} := 2\text{Re}[\mathbf{W}_{SJ}] \quad (2.33)$$

---

<sup>3</sup>In this text, *positive* will always mean *positive semi-definite*.



such that  $\mathbf{W}_{SJ} = \frac{1}{2}\mathbf{H}_{SJ} + \frac{i}{2}\mathbf{\Delta}$ .

### 2.2.3. Alternative definition

Note that  $\mathbf{W}_{SJ}\overline{\mathbf{W}}_{SJ} = \overline{\mathbf{W}}_{SJ}\mathbf{W}_{SJ} = \mathbf{0}$ , since

$$\begin{aligned}\mathbf{W}_{SJ}\overline{\mathbf{W}}_{SJ} &= \sum_{a,b} \lambda_a \lambda_b \mathbf{u}_a^+ (\mathbf{u}_a^+)^\dagger \mathbf{u}_b^- (\mathbf{u}_b^-)^\dagger \\ &= \sum_{a,b} \lambda_a \lambda_b \mathbf{u}_a^+ \langle \mathbf{u}_a^+, \mathbf{u}_b^- \rangle (\mathbf{u}_b^-)^\dagger = \mathbf{0}.\end{aligned}\tag{2.34}$$

To give this property a name, we shall say that two matrices  $\mathbf{A}$  and  $\mathbf{B}$  satisfying  $\mathbf{AB} = \mathbf{0}$  have ‘‘orthogonal support’’ (in analogy with two functions satisfying  $\int f(x)g(x)dx = 0$ ).<sup>4</sup> This provides an alternative definition of the SJ two-point function free of reference to its spectral decomposition, as the unique matrix that satisfies the three conditions:

**Definition:** *The SJ Wightman function on a causal set is given by the unique matrix satisfying the three conditions*

1. *Consistency with the Pauli-Jordan functional:*  $i\mathbf{\Delta} = \mathbf{W} - \overline{\mathbf{W}}$
2. *Positivity:*  $\langle \mathbf{u}, \mathbf{W}\mathbf{u} \rangle \geq 0$
3. *Orthogonal supports:*  $\mathbf{W}\overline{\mathbf{W}} = \mathbf{0}$ .

To see that these conditions specify  $\mathbf{W}_{SJ}$  uniquely, suppose  $\mathbf{W}_1$  and  $\mathbf{W}_2$  both satisfy the conditions. First note that if  $\mathbf{W}$  is positive, then so is  $\overline{\mathbf{W}}$ . We have  $\mathbf{W}_1\overline{\mathbf{W}}_1 = \overline{\mathbf{W}}_1\mathbf{W}_1 = \mathbf{W}_2\overline{\mathbf{W}}_2 = \overline{\mathbf{W}}_2\mathbf{W}_2 = \mathbf{0}$  and

$$\mathbf{W}_1 - \overline{\mathbf{W}}_1 = \mathbf{W}_2 - \overline{\mathbf{W}}_2.\tag{2.35}$$

Squaring both sides yields

$$\begin{aligned}(\mathbf{W}_1 - \overline{\mathbf{W}}_1)^2 &= (\mathbf{W}_2 - \overline{\mathbf{W}}_2)^2 \\ \Rightarrow (\mathbf{W}_1 + \overline{\mathbf{W}}_1)^2 &= (\mathbf{W}_2 + \overline{\mathbf{W}}_2)^2.\end{aligned}\tag{2.36}$$

<sup>4</sup>Since the ‘‘support’’ of a matrix is a word sometimes used to refer to the orthogonal complement of the matrix kernel ( $\text{supp}(\mathbf{A}) = \ker(\mathbf{A})^\perp$ ), ‘‘orthogonal support’’ could be interpreted as implying  $\text{supp}(\mathbf{A}) \perp \text{supp}(\mathbf{B})$ . To be clear, the term ‘‘orthogonal support’’ in this text merely means that  $\mathbf{AB} = \mathbf{0}$ . Two matrices satisfying this condition do not necessarily satisfy  $\text{supp}(\mathbf{A}) \perp \text{supp}(\mathbf{B})$ .

Both  $\mathbf{W}_1 + \overline{\mathbf{W}}_1$  and  $\mathbf{W}_2 + \overline{\mathbf{W}}_2$  are positive matrices and hence their squares are positive. Since every positive matrix has a unique positive square root, we can take the square root of (2.36) to obtain

$$\mathbf{W}_1 + \overline{\mathbf{W}}_1 = \mathbf{W}_2 + \overline{\mathbf{W}}_2. \quad (2.37)$$

This equation together with (2.35) implies that  $\mathbf{W}_1 = \mathbf{W}_2$ , hence proving that the above conditions specify  $\mathbf{W}_{SJ}$  uniquely.

## 2.3. The continuum SJ state

Conceptually, the formalism outlined in the previous section extends in a natural way to continuum spacetime manifolds [26]. In this section we present the continuum formalism, the study of which will constitute the core of this thesis. In essence, the move from the causal set to the continuum simply means replacing discrete causal set indices  $i$  by spacetime coordinates  $x^\mu$ , vectors  $[\mathbf{u}]_i$  by functions  $u(x)$  and matrices  $\mathbf{M}_{ij}$  by integral kernels  $M(x, y)$  (or rather their associated linear operators  $M : f(x) \rightarrow (Mf)(x) = \int M(x, y)f(y)dy$ ). However, as always, the move from finite to infinite dimensions comes along with technical complications.

Indeed to give a rigorous definition of the SJ state in globally hyperbolic spacetime manifolds, field operators should really be abstracted to symbols of a  $\star$ -algebra, propagators should be viewed as linear operators and  $n$ -point functions as distributions on appropriate function spaces, as it is customary in the algebraic approach to QFT [10, 11]. And even then, the rigorous construction relies on spacetime being *bounded* (of finite volume) or at least bounded in time in some appropriate sense (more on this below). The formalism that necessarily accompanies any such rigorous treatment would cloud the matters we wish to address in this thesis. We will therefore adopt the less rigorous approach (as we already did implicitly by writing down expressions such as  $\phi(x)$  in Section 2.1), but nevertheless we will encounter and address some of the questions regarding the status of the SJ state in unbounded regions of spacetime.

### 2.3.1. Definition

Recall that in the continuum the Pauli-Jordan function is defined as  $\Delta(x, y) = G_R(x, y) - G_A(x, y)$ . Hence the kernel  $i\Delta(x, y)$  is both antisymmetric:

$$i\Delta(y, x) = -i\Delta(x, y) \quad (2.38)$$

and Hermitian:

$$\overline{i\Delta(y, x)} = i\Delta(x, y). \quad (2.39)$$

This is the case because  $\Delta(x, y)$  is real and in a globally hyperbolic spacetime  $G_A(x, y) = G_R(y, x)$ .

Consider the space  $L^2(M)$  of square-integrable functions on  $(M, g_{\mu\nu})$  with the usual inner product

$$\langle f, g \rangle := \int_M \overline{f(x)}g(x)\sqrt{-g}dx \quad (2.40)$$

where  $f, g \in L^2(M)$  and  $dx := dx^0 dx^1 \dots dx^D$ . We define the *Pauli-Jordan operator* as the integral operator whose kernel is the Pauli-Jordan function  $\Delta(x, y)$ :

$$(\Delta f)(x) = \int_M \Delta(x, y)f(y)\sqrt{-g(y)}dy \quad (2.41)$$

Let us assume, for now, that (i)  $(M, g_{\mu\nu})$  is a globally hyperbolic manifold that is *bounded* (i.e. of finite spacetime volume  $V_M = \int_M \sqrt{-g}dx$ ) and (ii) that  $\Delta(x, y)$  is a square integrable kernel:  $\Delta(x, y) \in L^2(M \times M)$  (as in the case of a massless scalar field in two-dimensional Minkowski space — see Section 3.2). Then the operator  $i\Delta$  is a self-adjoint Hilbert-Schmidt integral operator [27, Thm. VI.23] and the spectral theorem for such operators guarantees that  $i\Delta$  has a set of real eigenvalues  $\lambda_{\mathbf{a}}$  and a complete orthonormal set of eigenvectors  $\mathbf{u}_{\mathbf{a}}(x)$  which satisfy

$$i\Delta\mathbf{u}_{\mathbf{a}} = \lambda_{\mathbf{a}}\mathbf{u}_{\mathbf{a}}, \quad \lambda_{\mathbf{a}} \in \mathbb{R}. \quad (2.42)$$

Since  $\Delta(x, y)$  is a real function, it follows that

$$i\Delta\mathbf{u}_{\mathbf{a}} = \lambda_{\mathbf{a}}\mathbf{u}_{\mathbf{a}}(x) \implies i\Delta\bar{\mathbf{u}}_{\mathbf{a}} = -\lambda_{\mathbf{a}}\bar{\mathbf{u}}_{\mathbf{a}}, \quad (2.43)$$

which means that the non-zero eigenvectors of  $i\Delta$  come in pairs:

$$i\Delta\mathbf{u}_{\mathbf{a}}^{\pm} = \pm\lambda_{\mathbf{a}}\mathbf{u}_{\mathbf{a}}^{\pm}, \quad (2.44)$$

where by definition  $\lambda_{\mathbf{a}} > 0$  and  $u_{\mathbf{a}}^- = \bar{u}_{\mathbf{a}}^+$ . Moreover, these functions (when appropriately normalised) are orthonormal in the  $L^2(M)$  inner product:

$$\begin{aligned}\langle u_{\mathbf{a}}^{\pm}, u_{\mathbf{b}}^{\pm} \rangle &= \delta_{\mathbf{ab}} \\ \langle u_{\mathbf{a}}^+, u_{\mathbf{b}}^- \rangle &= 0.\end{aligned}\tag{2.45}$$

We can now split  $i\Delta(x, y)$  into positive and negative parts

$$i\Delta(x, y) = Q(x, y) - \overline{Q(x, y)},\tag{2.46}$$

where

$$Q(x, y) = \sum_{\mathbf{a}} \lambda_{\mathbf{a}} u_{\mathbf{a}}^+(x) \bar{u}_{\mathbf{a}}^+(y).\tag{2.47}$$

The SJ state  $|SJ\rangle$  is then defined by

$$W_{SJ}(x, y) := Q(x, y) = \sum_{\mathbf{a}} \lambda_{\mathbf{a}} u_{\mathbf{a}}^+(x) \bar{u}_{\mathbf{a}}^+(y).\tag{2.48}$$

This is a valid definition for a two-point function because (i) it is positive:

$$\langle f, W_{SJ}f \rangle = \int_M \sqrt{-g(x)} dx \int_M \sqrt{-g(x')} dx' \overline{f(x)} W(x, x') f(x') \geq 0\tag{2.49}$$

(ii) its anti-symmetrisation produces the commutator:

$$W_{SJ}(x, y) - W_{SJ}(y, x) = [\phi(x), \phi(y)]\tag{2.50}$$

and (iii) it satisfies the Klein-Gordon equation:

$$(\square_x - m^2)W_{SJ}(x, y) = 0.\tag{2.51}$$

The last statement follows from the fact that  $\Delta(x, y)$  itself satisfies the Klein-Gordon equation  $(\square_x - m^2)\Delta(x, y) = 0$ , which implies that the functions  $u_{\mathbf{a}}^{\pm}$  are solutions, since  $(\square_x - m^2)u_{\mathbf{a}}(x) = \pm(\square_x - m^2)(i\Delta u_{\mathbf{a}})(x)/\lambda_{\mathbf{a}} = 0$ . Therefore,  $W_{SJ} = \sum_{\mathbf{a}} \lambda_{\mathbf{a}}^+ u_{\mathbf{a}} \bar{u}_{\mathbf{a}}^+$  satisfies the Klein-Gordon equation as well (in both arguments).

When the annihilation and creation operators that serve as the expansion coefficients are given their customary normalisation, the field operator  $\phi(x)$  can be

expanded as a mode sum

$$\phi(x) = \sum_{\mathbf{a}} u_{\mathbf{a}}^{SJ}(x) a_{\mathbf{a}} + \bar{u}_{\mathbf{a}}^{SJ}(x) a_{\mathbf{a}}^{\dagger}, \quad (2.52)$$

where the ‘‘SJ modes’’,  $u_{\mathbf{a}}^{SJ}$ , i.e. the modes normalised with respect to the Klein-Gordon product (as opposed to the  $L^2$  inner product), are given by

$$u_{\mathbf{a}}^{SJ}(x) := \sqrt{\lambda_{\mathbf{a}}} u_{\mathbf{a}}^+(x). \quad (2.53)$$

The SJ state is then defined by  $a_{\mathbf{a}}|SJ\rangle = 0 \forall \mathbf{a}$ . As shown above, the SJ modes  $u_{\mathbf{a}}^{SJ}(x)$  satisfy the Klein-Gordon equation.

Note, finally, that the eigenvalues  $\lambda_{\mathbf{a}}$  of  $i\Delta$  satisfy the useful identity [27, Thm. VI.23]:

$$\int_M \sqrt{-g(x)} dx \int_M \sqrt{-g(y)} dy |i\Delta(x, y)|^2 = \sum_{\mathbf{a}} \lambda_{\mathbf{a}}^2. \quad (2.54)$$

In words, the sum of the squared eigenvalues of  $i\Delta$  is equal to the  $L^2(M \times M)$  norm of its kernel. We will use this identity in Chapters 3 and 5.

The conditions imposed on  $\Delta(x, y)$  above are very restrictive. For example, already in 3+1 dimensional Minkowski space  $\Delta(x, y)$  is no longer a Hilbert-Schmidt integral kernel. However, it has been shown [10, 11] that the construction can be carried out on any *bounded* globally hyperbolic spacetime (where the SJ state then defines a ‘‘pure quasi-free state’’).  $i\Delta$  in that case belongs to the class of bounded self-adjoint operators, for which the spectral theorem guarantees the possibility to define the spectral decomposition and thus the ‘‘positive part’’. The authors of [11] point out that even if  $i\Delta$  is not bounded as an operator or essentially self-adjoint, the SJ two-point function can still be meaningfully defined so long as the weaker condition holds that  $\Delta f$  be square-integrable for any smooth  $f$  of compact support. The SJ Wightman function can then be obtained because an operator  $i\Delta$  for which the latter condition holds admits a ‘‘polar decomposition’’ that serves to define its positive part.

Still, for unbounded spacetimes it is not immediately clear how to arrive at a rigorous definition. In general,  $i\Delta(x, y)$  will have non-compact support and therefore it seems guaranteed that  $\Delta f$  will not be square-integrable for *any* non-zero function  $f$  (since convolution with  $\Delta(x, y)$  will spread the support of the function over an

infinite region).  $\Delta$  cannot then be defined as an unbounded (i.e. densely defined) linear operator on  $L^2$  at all. This prevents one from appealing to the procedures above (i.e. spectral decomposition of self-adjoint extensions or polar decomposition) in order to derive  $W_{SJ}$  as the positive part of  $i\Delta$ . Perhaps it may be possible to make sense of  $\Delta$ , not as an operator, but rather as a bilinear form  $\Delta(f, g) = \int \sqrt{-g(x)} dx \int \sqrt{-g(y)} dy f(x) \Delta(x, y) g(y)$  on some dense subset of  $L^2$ . One would then need to show that such an object may be decomposed uniquely into positive and negative parts. At present, these questions remain open.

Nevertheless, as we know well from quantum field theory, progress can be made even in the absence of a rigorous underpinning using limiting procedures and “formal” calculations. That will be the approach adopted in some of the sections below. We shall see that it is possible to obtain a meaningful answer to “What is the SJ state in an infinite spacetime?” following this approach, especially in the case of de Sitter space, but we will also encounter problems that shed further light on the continuum formalism.

### 2.3.2. Explicit construction

Here we derive an explicit construction of the SJ modes that define the SJ two-point function (and its associated state), in terms of an arbitrary (orthonormal) basis of solutions to the Klein-Gordon equation.

The eigenvalue problem (2.42) can be reduced to a set of algebraic equations as follows. Given an expansion of the field in terms of an arbitrary set of modes  $u_{\mathbf{k}}$ , the commutator function  $i\Delta(x, y)$  can be expressed as the mode sum (2.18)

$$i\Delta(x, y) = \sum_{\mathbf{k}} [u_{\mathbf{k}}(x)\bar{u}_{\mathbf{k}}(y) - \bar{u}_{\mathbf{k}}(x)u_{\mathbf{k}}(y)].$$

Substituting this into the eigenvalue equation (2.42) for an eigenfunction  $u_{\mathbf{a}}^{SJ}$  with positive eigenvalue  $\lambda_{\mathbf{a}}$ , we obtain

$$u_{\mathbf{a}}^{SJ}(x) = \sum_{\mathbf{k}} A_{\mathbf{a}\mathbf{k}} u_{\mathbf{k}}(x) + B_{\mathbf{a}\mathbf{k}} \bar{u}_{\mathbf{k}}(x), \quad (2.55)$$

where we have defined

$$\begin{aligned} A_{\mathbf{a}\mathbf{k}} &= \lambda_{\mathbf{a}}^{-1} \langle u_{\mathbf{k}}, u_{\mathbf{a}}^{SJ} \rangle, \\ B_{\mathbf{a}\mathbf{k}} &= -\lambda_{\mathbf{a}}^{-1} \langle \bar{u}_{\mathbf{k}}, u_{\mathbf{a}}^{SJ} \rangle. \end{aligned} \quad (2.56)$$

As the notation is meant to indicate, these coefficients define a Bogoliubov trans-

formation. This can be checked explicitly by acting on (2.55) with  $\langle u_{\mathbf{k}}, \cdot \rangle$  and  $\langle \bar{u}_{\mathbf{k}}, \cdot \rangle$ , which yields

$$\begin{aligned} A_{\mathbf{a}\mathbf{k}} &= \frac{1}{\lambda_{\mathbf{a}}} \sum_{\mathbf{q}} A_{\mathbf{a}\mathbf{q}} \langle u_{\mathbf{k}}, u_{\mathbf{q}} \rangle + B_{\mathbf{a}\mathbf{q}} \langle u_{\mathbf{k}}, \bar{u}_{\mathbf{q}} \rangle, \\ B_{\mathbf{a}\mathbf{k}} &= \frac{-1}{\lambda_{\mathbf{a}}} \sum_{\mathbf{q}} A_{\mathbf{a}\mathbf{q}} \langle \bar{u}_{\mathbf{k}}, u_{\mathbf{q}} \rangle + B_{\mathbf{a}\mathbf{q}} \langle \bar{u}_{\mathbf{k}}, \bar{u}_{\mathbf{q}} \rangle. \end{aligned} \tag{2.57}$$

Complementing these equations with the orthonormality conditions (2.45) on the SJ modes, we find the Bogoliubov conditions

$$\begin{aligned} \sum_{\mathbf{k}} A_{\mathbf{a}\mathbf{k}} B_{\mathbf{b}\mathbf{k}} - B_{\mathbf{a}\mathbf{k}} A_{\mathbf{b}\mathbf{k}} &= 0 \\ \sum_{\mathbf{k}} A_{\mathbf{a}\mathbf{k}} \bar{A}_{\mathbf{b}\mathbf{k}} - B_{\mathbf{a}\mathbf{k}} \bar{B}_{\mathbf{b}\mathbf{k}} &= \delta_{\mathbf{a}\mathbf{b}}. \end{aligned} \tag{2.58}$$

Finding the SJ state now reduces to solving the above system of equations for  $A_{\mathbf{a}\mathbf{k}}$  and  $B_{\mathbf{a}\mathbf{k}}$ . Note that this construction is, strictly speaking, only valid in a bounded region of spacetime, since otherwise the inner products diverge. One strategy for unbounded spacetimes is to impose temporal and (if necessary) spatial cut-offs, to compute the spectrum of  $i\Delta$  (which in this case is completely well-defined), and to then take the limit as the cut-off goes to infinity. The inner products and eigenvalues are then formally divergent, but we shall see below that the technique still leads to well-defined results in most cases, and can thus be justified in hindsight to some extent. (It fails in certain special cases, although, it seems, only in circumstances where the QFT suffers from otherwise known symptoms).

### 2.3.3. Alternative Definition

The alternative definition for the discrete SJ two-point function given in Section 2.2.3 can be translated to the continuous case as follows:

1. *Consistency with the Pauli-Jordan functional:*

$$i\Delta(x, x') = W_{SJ}(x, x') - \bar{W}_{SJ}(x, x')$$

2. *Positivity:*

$$\langle f, W_{SJ} f \rangle \geq 0.$$

3. Orthogonal supports:<sup>5</sup>

$$\int_M \sqrt{-g(x')} dx' W_{SJ}(x, x') \overline{W}_{SJ}(x', x'') = 0. \quad (2.59)$$

On this view the Wightman function is a positive bilinear form on the vector space of complex functions, a view that might lend itself better to generalisation to infinite spacetimes, as discussed above. The first two conditions must be satisfied by the two-point function of any state. It is the third and last requirement that acts as the “ground state condition.” For the conditions to specify a state fully, their solution must be unique. If we express the ground state condition as  $W\overline{W} = 0$ , then uniqueness will follow (in analogy to the matrix case above) if a positive bilinear form has a unique positive square root. Whether this is true is not known to the author, and we will return to this question in the coming chapters.

When  $(M, g_{\mu\nu})$  admits a timelike Killing vector  $\kappa = \frac{d}{d\tau}$ , we can show that the SJ state (formally extended to the case of a spacetime of infinite volume) is the ground state of the Hamiltonian associated with that Killing vector by showing that the Wightman function defined by the positive-frequency modes (2.14)

$$u_{\mathbf{k}}(x) = u_{\mathbf{k}}(\tau, \mathbf{x}) = N_{\mathbf{k}} e^{-i\omega(\mathbf{k})\tau} U_{\mathbf{k}}(\mathbf{x})$$

satisfies the SJ conditions. Clearly, the two-point function satisfies conditions (i) and (ii), and it only remains to check the ground state condition (iii). In a coordinate chart  $x^\mu = (\tau, \mathbf{x})^\mu$  we then have

$$\begin{aligned} W\overline{W}(x, x'') &= \int_M \sqrt{-g(x')} dx' W(x, x') \overline{W}(x', x'') \\ &= \sum_{k,l} u_k(x) u_l(x'') \int d\mathbf{x}' d\tau \sqrt{-g(x')} \overline{u}_k(x') \overline{u}_l(x') \\ &= \sum_{k,l} u_k(x) u_l(x'') \int d\mathbf{x}' \sqrt{-g(x')} \overline{U}_k(\mathbf{x}') \overline{U}_l(\mathbf{x}') \int_{-\infty}^{\infty} d\tau e^{-i\omega_k \tau} e^{-i\omega_l \tau} \\ &= \sum_{k,l} u_k(x) u_l(x'') \int d\mathbf{x}' \sqrt{-g(x')} \overline{U}_k(\mathbf{x}') \overline{U}_l(\mathbf{x}') \int_{-\infty}^{\infty} d\tau e^{-i(\omega_k + \omega_l)\tau} \\ &\propto \delta(\omega_k + \omega_l) = 0 \end{aligned} \quad (2.60)$$

---

<sup>5</sup>Strictly speaking, to multiply two quadratic forms together requires a metric, here given by a delta function.



since the sum over modes does not include the zero-mode  $\omega_k = 0$ . Thus, if the SJ conditions specify a unique state, that state is the appropriate ground state when there is a globally timelike Killing vector.

#### 2.3.4. The Hadamard property

Here is a good place to mention the question of whether the SJ state obeys the so-called Hadamard condition on its short-distance behaviour, i.e. the condition that the two-point function of a state coincide with the two-point function in flat spacetime in the coincidence limit of its two arguments. Hadamard states have a special status in the algebraic approach to QFT, not least because they admit a well-defined (“point-splitting”) regularisation scheme for the stress-energy tensor [9, 28]. In static spacetimes the Hamiltonian vacuum obeys this condition, so the SJ state does as well, as we have just seen. On the other hand, Fewster and Verch [29] have recently provided examples of spacetimes where the condition does not hold. We defer a discussion of this matter to Chapter 4, where we will see a concrete example in which the SJ state is not Hadamard.

### 3. The SJ state in the flat causal diamond in two dimensions

In this chapter we look at the SJ state for a free massless scalar field in a causal diamond of two-dimensional Minkowski spacetime. The analysis is restricted to the massless field because the Pauli-Jordan function takes on a particularly simple form in that case, which makes it possible to find the eigenmodes of  $i\Delta$  explicitly.

We will derive the SJ Wightman function for the diamond and we shall pay particular attention to the limit where the size of the diamond is large compared to the geodesic separation between the two arguments of  $W$ , and where the points lie either (i) far away from the left and right corners or (ii) close to one of the corners.

In the former limit one might hope to recover the unique Poincaré-invariant Minkowski vacuum state, if such a state existed. But in fact, no such vacuum exists, since  $W$  is logarithmic and depends on an arbitrary length-parameter or “infrared cut-off”, as is well known. In our finite diamond, we find that  $W$  has the expected form, but with a definite value of the length-parameter determined by the diamond’s area.

In the latter limit, one might expect to see the Rindler vacuum state, since the geometry of the corner approaches that of the familiar Rindler wedge as the diamond size tends to infinity. However, we find that this is not the case. Instead, the SJ state close to the corner is the vacuum state of Minkowski spacetime with a static mirror on the corner.

Further, we shall use the causal set QFT formulation to construct the ground state on a causal set that approximates the continuum causal diamond. We compare the results with the foregoing continuum analysis in the subregions of the causal set corresponding to the two limits (i) and (ii). In both cases, the Wightman function on the causal set is in good agreement with the continuum Wightman function.

**Comment on notation:** *We have been using plain letters  $x, y$  to denote space-time coordinates and boldface letters  $\mathbf{x}, \mathbf{y}$  to denote spatial coordinates. In two di-*

*mensions, however, there is only one spatial coordinate and it seems most appropriate to denote the single spatial coordinate by a plain letter as well. It should always be clear from the context whether we are referring to a spatial or spacetime coordinate.*

### 3.1. The massless scalar field in two-dimensional flat spacetimes

As background for our investigation of the massless scalar field in a two-dimensional causal diamond, we review the massless scalar field in Minkowski (M) and Rindler (R) spacetimes in two dimensions. The metric on Minkowski spacetime in Cartesian coordinates  $(t, x)$  is given by

$$ds_{\text{M}}^2 = -dt^2 + dx^2. \quad (3.1)$$

Since the spacetime is globally hyperbolic and static with timelike Killing vector  $\kappa_{\text{M}} = \frac{d}{dt}$ , we can separate the solutions to the Klein-Gordon equation into positive and negative frequency with respect to  $\kappa_{\text{M}}$ . The field equation is

$$\square_{\text{M}}\phi = -\partial_t^2\phi + \partial_x^2\phi = 0 \quad (3.2)$$

and the normalised positive frequency modes can be taken as

$$u_k^{\text{M}}(t, x) = \frac{1}{\sqrt{4\pi\omega_k}} e^{-i\omega_k t + ikx} \quad (3.3)$$

where  $\omega_k = |k|$ .

If we try to define a vacuum state  $|0_{\text{M}}\rangle$  in the usual way as the state annihilated by the operator coefficients of the positive frequency modes in the expansion of the field operator  $\phi(t, x)$ , then it is well-known that we encounter an infrared divergence [30, 31, 32]. The Wightman function is logarithmically divergent at  $k = 0$ :

$$\begin{aligned} W_{\text{M}}(t, x; t', x') &:= \langle 0_{\text{M}} | \phi(t, x) \phi(t', x') | 0_{\text{M}} \rangle \\ &= \frac{1}{4\pi} \int_{-\infty}^{\infty} \frac{dk}{|k|} e^{-i|k|(t-t') + ik(x-x')}. \end{aligned} \quad (3.4)$$

Following [31], we can remove the divergence in the integral by introducing an in-

frared momentum cut-off  $\lambda$ :

$$\begin{aligned}
 & \frac{1}{4\pi} \int_{-\infty}^{\infty} \frac{dk}{|k|} e^{-i|k|\delta t + ik\delta x} \theta(|k| - \lambda) \\
 &= \frac{1}{4\pi} \lim_{\epsilon \rightarrow 0^+} \int_{\lambda}^{\infty} \frac{dk}{k} \left[ e^{-ik(\delta t + \delta x - i\epsilon)} + e^{-ik(\delta t - \delta x - i\epsilon)} \right] \\
 &= -\frac{1}{4\pi} \lim_{\epsilon \rightarrow 0^+} \left[ \text{Ln} [i(\delta t + \delta x - i\epsilon)\mu] + \text{Ln} [i(\delta t - \delta x - i\epsilon)\mu] \right] + \mathcal{O}(\lambda\delta) \\
 &= -\frac{1}{2\pi} \text{Ln} \mu |d| - \frac{i}{4} \text{sgn}(\delta t) \theta(\delta t^2 - \delta x^2) + \mathcal{O}(\lambda\delta)
 \end{aligned} \tag{3.5}$$

where  $\mu = \lambda e^\gamma$ ,  $\gamma = 0.5772\dots$  is the Euler-Mascheroni constant, and  $\delta t = t - t'$ ,  $\delta x = x - x'$ , and  $d = \sqrt{-\delta t^2 + \delta x^2}$ . The complex logarithm here is given a branch cut on the negative real axis and  $\text{Ln}$  denotes its principal value. The quantity  $\delta$  stands collectively for  $\delta t$  and  $\delta x$ , such that small  $\lambda\delta$  implies that both coordinate distances  $\delta t$  and  $\delta x$  are small compared to  $\lambda^{-1}$ . With non-zero  $\lambda$ , the theory has a preferred frame. However, if we drop the  $\mathcal{O}(\lambda)$  term in (3.5), we obtain a one-parameter family of two-point functions that depend on  $\lambda$  but are fully frame-independent:

$$W_{\text{M},\lambda}(t, x; t', x') := -\frac{1}{2\pi} \text{Ln} \mu |d| - \frac{i}{4} \text{sgn}(\delta t) \theta(\delta t^2 - \delta x^2) \tag{3.6}$$

Unfortunately, (3.6) cannot itself serve as a physical Wightman function, because it fails to be positive as a quadratic form (see (2.19)). Nevertheless we will see that the form (3.6) will emerge in a natural manner as a certain limit of the two-point function we will derive for the diamond.<sup>1</sup>

It is worth noting that the theory whose fundamental field is the gradient of  $\phi$  rather than  $\phi$  itself is not infrared divergent, and in fact the vacuum expectation value

$$\langle 0_{\text{M}} | \nabla_{\mu} \phi(t, x) \phi(t', x') | 0_{\text{M}} \rangle = \frac{\delta x_{\mu}}{2\pi(\delta t^2 - \delta x^2)} \tag{3.7}$$

already converges, except for the singularity on the lightcone.

The Rindler metric [33, 34] arises from the Minkowski metric via the coordinate transformations  $t = a^{-1} e^{a\xi} \sinh a\eta$  and  $x = a^{-1} e^{a\xi} \cosh a\eta$ , where  $a > 0$  is a constant with dimensions of inverse length and  $-\infty < \xi, \eta < \infty$ . The coordinates  $\xi$  and  $\eta$  only cover a submanifold of the full Minkowski space, namely the right Rindler wedge,  $x > |t|$ ; but this submanifold is conformal to all of Minkowski space as one sees from

<sup>1</sup>Perhaps (3.6) could also be understood as defining an ‘‘approximate state’’ valid when  $\delta t$  and  $\delta x$  are small compared to the IR scale  $\lambda^{-1}$ .

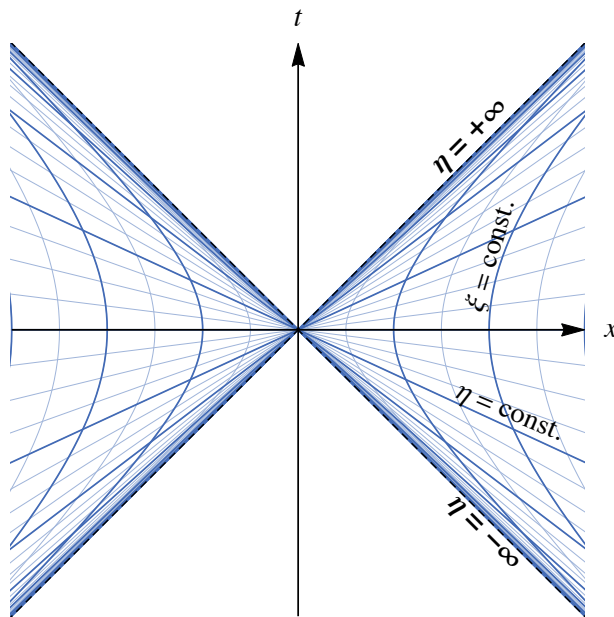


Figure 3.1.: The left and right Rindler wedges of two-dimensional Minkowski spacetime.

the form of the line element in  $(\xi, \eta)$  coordinates:

$$ds_{\text{R}}^2 = e^{2a\xi} (-d\eta^2 + d\xi^2). \quad (3.8)$$

Lines of constant  $\xi$  are hyperbolae that correspond to the trajectories of observers accelerating eternally at a constant acceleration  $ae^{-a\xi}$  (Figure 3.1), and are integral curves of the Killing vector  $\kappa_{\text{R}} = \frac{d}{d\eta}$ .

Since Rindler spacetime is globally hyperbolic and static in its own right, the canonical quantisation of the scalar field can be carried out in a completely self-contained manner [35]. Thanks to the conformal invariance of the massless theory in two dimensions, the field equation  $\square_{\text{R}}\phi = 0$  in Rindler coordinates (3.8) is just the usual wave equation, whose normalised positive frequency solutions, the Fulling-Rindler modes, are given by the plane waves

$$u_p^{\text{R}} = \frac{1}{\sqrt{4\pi\omega_p}} e^{-i\omega_p\eta + ip\xi}, \quad (3.9)$$

where  $\omega_p = |p|$ . Trying to define a Fulling-Rindler vacuum state  $|0_{\text{R}}\rangle$  as the state annihilated by the operator coefficients of the positive frequency Rindler modes in the expansion of  $\phi$  once again results in an infrared divergent integral for the two-point function  $W$ . Proceeding as before, one can introduce a cut-off at small “momentum”  $\lambda$  and discard a term of order  $\lambda$  to obtain a one-parameter family of two-point functions, which are the same functions of Rindler coordinates as the Minkowski two-point function (3.6) is of Cartesian coordinates:

$$W_{\text{R},\lambda}(\eta, \xi; \eta', \xi') := -\frac{1}{4\pi} \text{Ln} \mu^2 |\delta\eta^2 - \delta\xi^2| - \frac{i}{4} \text{sgn}(\delta\eta) \theta(\delta\eta^2 - \delta\xi^2) \quad (3.10)$$

where  $\mu = \lambda e^\gamma$ . As before, this two-point function is symmetric (boost-invariant) but fails to be positive and depends explicitly on the cut-off  $\lambda$ . At best it can have an approximate validity when the coordinate-differences  $\delta\eta$  and  $\delta\xi$  are small compared to  $\lambda^{-1}$ .

It is well known that the Minkowski and Fulling-Rindler “ground states” corresponding to (3.6) and (3.10) are not equal, since the Rindler mode functions  $u_k^{\text{R}}$  are linear combinations of both positive and negative frequency Minkowski mode functions  $u_k^{\text{M}}$  and  $\bar{u}_k^{\text{M}}$  (in other words, the two sets are related by a non-trivial Bogoliubov transformation). This phenomenon is by now well understood as an instance of the Fulling-Davies-Unruh effect [35, 36, 37]: if the Rindler wedge is understood as a sub-region of Minkowski space, and the field is in the usual Poincaré-invariant vacuum state (say in  $3 + 1$  dimensions, where the latter is well defined), observers that are confined to the wedge and that accelerate eternally at a uniform rate will feel themselves immersed in a thermal bath of particles.

The preceding calculations suffer from the appearance of infinite integrals and the consequent need for infrared cut-offs. Nevertheless, we will see that the two-point functions we have obtained in this section can be related to the case we study next, that of a *finite* two-dimensional causal diamond, where the the SJ construction and the integrals it gives rise to are completely well-defined. In this connection we comment also that inasmuch as both the Minkowski and Rindler spacetimes possess globally timelike Killing vectors, the formal demonstration of Section 2.3.3 would apply to show that the SJ vacua of these two spacetimes would coincide with the ground-states discussed in this section – were such states actually to exist. (See also [10].)

### 3.1.1. The SJ state in Rindler space

Both the Minkowski Rindler spacetimes are examples of spacetimes with global timelike Killing vectors and so the formal demonstration of Section 2.3.3 would apply to show that the SJ state for Minkowski space is  $|0_M\rangle$  and the SJ state for Rindler space is  $|0_R\rangle$ , were these states actually to exist. Here we give an alternative demonstration of the relation of the SJ state to the Fulling-Rindler (FR) vacuum using the technique of identifying the “positive SJ modes”,  $u_a^{SJ}$  — the appropriately (Klein-Gordon-) normalised eigenfunctions of  $i\Delta$  with positive eigenvalue — and writing down the Wightman function as the sum (2.48)  $W_{SJ} = \sum_a \bar{u}_a^{SJ} u_a^{SJ}$  over these modes. We will see that the positive SJ modes are proportional to the positive frequency FR modes, which can be interpreted as meaning that the SJ state for the Rindler wedge is the FR vacuum.

As a disclaimer, the calculations in the following paragraphs are of a particularly singular nature. Since Rindler space is unbounded,  $i\Delta$  is not just unbounded as an operator, it is not a well defined operator at all on any dense subset of  $L^2$ -functions on the spacetime. We will thus be comparing infinite quantities with slightly less infinite quantities and divide by delta-functions. Still, including the calculations here might be of some benefit since they offer a different angle on the formal calculation of Section 2.3.3.

The Pauli-Jordan function  $\Delta(x, x')$  for Rindler space is functionally equal to that for Minkowski space but the coordinates have different ranges, and since we seek the eigenfunctions of  $i\Delta$  for Rindler space, we choose to express it as a sum over Rindler modes  $u_p^R$ :

$$\begin{aligned} i\Delta(\eta, \xi; \eta', \xi') &= \int_{-\infty}^{\infty} \bar{u}_p^R(\eta, \xi) u_p^R(\eta', \xi') dp \\ &= \int_{-\infty}^{\infty} \frac{e^{-i|p|\delta\eta + ip\delta\xi} - e^{i|p|\delta\eta - ip\delta\xi}}{4\pi\omega_p} dp. \end{aligned} \quad (3.11)$$

Eigenfunctions of the Pauli-Jordan integral operator with non-zero eigenvalue must satisfy the Klein-Gordon equation, so we make the ansatz

$$u_p^{SJ}(\eta, \xi) = \frac{e^{-i|\bar{p}|\eta + i\bar{p}\xi}}{\sqrt{4\pi|\bar{p}|}} = u_{\bar{p}}^R(\eta, \xi). \quad (3.12)$$

This is not the most general ansatz: one could start with an arbitrary linear combination of positive/negative frequency modes. However, we shall see that in the

case of the Rindler wedge, the positive-eigenvalue eigenvectors of the Pauli-Jordan operator coincide with the positive frequency modes, in line with our general result above. The action of  $i\Delta$  on (3.12) is

$$\begin{aligned}
 (i\Delta u_{\tilde{p}}^{SJ})(\eta, \xi) &= \int_{-\infty}^{\infty} d\eta' \int_{-\infty}^{\infty} d\xi' e^{2\xi'} i\Delta(\eta, \xi; \eta', \xi') u_{\tilde{p}}^{SJ}(\eta', \xi') \\
 &= \int_{-\infty}^{\infty} dp \int_{-\infty}^{\infty} d\eta' \int_{-\infty}^{\infty} d\xi' e^{2\xi'} \frac{e^{-i|p|\delta\eta+ip\delta\xi} - e^{i|p|\delta\eta-ip\delta\xi}}{4\pi|p|\sqrt{4\pi|\tilde{p}|}} e^{-i|\tilde{p}|\eta'+i\tilde{p}\xi'} \\
 &= \int_{-\infty}^{\infty} dp \int_{-\infty}^{\infty} d\xi' e^{2\xi'} \delta(|p| - |\tilde{p}|) \frac{e^{i\xi'(\tilde{p}-p)}}{4\pi|p|} \frac{e^{-i|p|\eta+ip\xi}}{\sqrt{4\pi|\tilde{p}|}} \\
 &= \left[ \frac{1}{4\pi|\tilde{p}|} \int_{-\infty}^{\infty} d\xi' e^{2\xi'} \right] u_{\tilde{p}}^{SJ}(\eta, \xi) + \left[ \frac{1}{4\pi|\tilde{p}|} \int_{-\infty}^{\infty} d\xi' e^{2\xi'(1+i\tilde{p})} \right] u_{-\tilde{p}}^{SJ}(\eta, \xi) \\
 &= \lambda_{\tilde{p}} u_{\tilde{p}}^{SJ}(\eta, \xi).
 \end{aligned} \tag{3.13}$$

The last equality holds in the sense that the second term in square brackets is suppressed with respect to the first, as can be readily verified if one is willing to accept the divergent integrals as meaningful. We have defined the eigenvalue  $\lambda_p = (4\pi\omega_p)^{-1} \int d\xi' e^{2\xi'}$ , a real positive (although divergent) number, and used  $\delta(|p| - |\tilde{p}|) = \delta(p + \tilde{p}) + \delta(p - \tilde{p})$ , discarding any terms that force  $p = 0$  (i.e. we discard the zero-mode). Therefore, the RF positive frequency modes  $u_p^R(\eta, \xi)$  are eigenfunctions of  $i\Delta$  with real positive (although divergent) eigenvalues. It is easily verified that  $\bar{u}_p^{SJ}$  are the negative eigenvalue eigenfunctions of  $i\Delta$ . The ‘‘delta-function normalisation’’ of the eigenmodes is

$$\begin{aligned}
 \langle u_p^{SJ}, u_{\tilde{p}}^{SJ} \rangle &= \int d\eta \int d\xi e^{2\xi} \bar{u}_p^{SJ}(\eta, \xi) u_{\tilde{p}}^{SJ}(\eta, \xi) \\
 &= \frac{1}{4\pi|p|} \int d\xi e^{2\xi} e^{-i(p-\tilde{p})\xi} \delta(|p| - |\tilde{p}|) \\
 &= \left[ \frac{1}{4\pi|p|} \int_{-\infty}^{\infty} d\xi' e^{2\xi'} \right] \delta(p - \tilde{p}) + \left[ \frac{1}{4\pi|\tilde{p}|} \int_{-\infty}^{\infty} d\xi' e^{2\xi'(1+i\tilde{p})} \right] \delta(p + \tilde{p}) \\
 &= \lambda_p \delta(p - \tilde{p}),
 \end{aligned} \tag{3.14}$$

where again we used the fact that the second term in square brackets is suppressed with respect to the first. The SJ two-point function can be computed formally using these ‘‘normalised eigenfunctions’’. One sees that the infinite normalisation-factor



cancels the divergent eigenvalues in expression (2.18), and one obtains

$$\begin{aligned}
 W_{SJ}(\eta, \xi; \eta', \xi') &= \int dp \frac{\lambda_p}{||u_p||^2} u_p^{SJ}(\eta, \xi) \bar{u}_p^{SJ}(\eta', \xi') \\
 &= \int dp u_p^{SJ}(\eta, \xi) \bar{u}_p^{SJ}(\eta', \xi') \\
 &= W_R(\eta, \xi; \eta', \xi'),
 \end{aligned} \tag{3.15}$$

which is just the divergent Rindler two-point function we examined earlier, and which led us to (3.10).

The preceding calculations and arguments suffer from both the appearance of infinite integrals and the unphysical nature of the infrared cut-offs they presuppose, but we will see that they can be interpreted as limits of the *finite* 1 + 1 dimensional causal diamond, where the the SJ construction and the procedure outlined above are completely well-defined.

We will study this case next, and will then analyse the limiting behaviour of the resulting two-point function as the size of the diamond tends to infinity. For points that remain close to one corner of the diamond, the spacetime obtained in this limit corresponds to the Rindler wedge.

### 3.2. The massless SJ two-point function in the flat causal diamond

A causal diamond (or Alexandrov open set) is the intersection of the chronological future of a point  $x$  with the chronological past of a point  $y \succ x$ . Because such a causal diamond is a globally hyperbolic manifold in its own right, the scalar field possesses therein a unique Pauli-Jordan function  $\Delta$ . In this section we will follow the SJ procedure to derive from  $\Delta$  a two-point function  $W$  for the massless scalar field in a causal diamond in two-dimensional Minkowski space. We will then analyse the limit of  $W$  for points (i) in the centre of the diamond and (ii) in the corner of the diamond.

It will be most convenient to work with lightcone coordinates  $u = (t + x)/\sqrt{2}$  and  $v = (t - x)/\sqrt{2}$ , in which we have  $ds^2 = -2dudv$ ,  $\sqrt{-g} = 1$  and  $\square = -2\partial_u\partial_v$ . A causal diamond centred at the origin  $u = v = 0$  that corresponds to the region  $u, v \in (-L, L)$  is shown in Figure 3.2 and will be denoted by  $C_L$ . Its spacetime

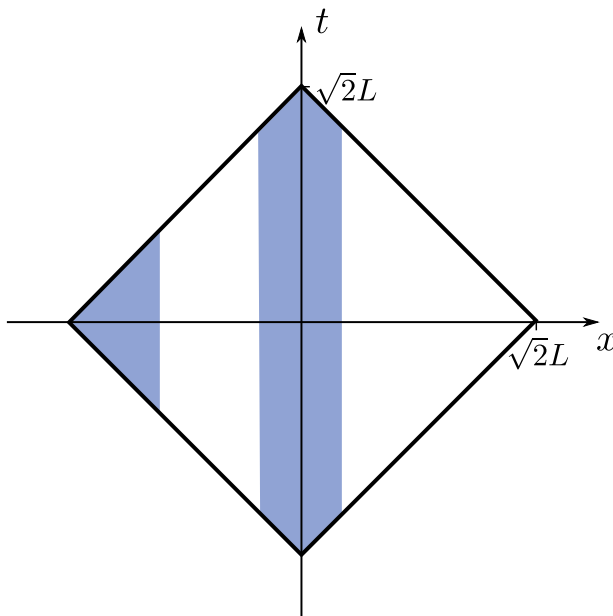


Figure 3.2.: The causal diamond,  $u, v \in (-L, L)$ . The shaded portions of the diagram represent the centre (i) and corner (ii) regions of interest in Section 3.2.1.

volume is  $V = 4L^2$ . The retarded propagator (2.3) must then solve

$$\partial_u \partial_v G_R(u, v; u', v') = -\frac{1}{2} \delta(u - u') \delta(v - v') \quad (3.16)$$

with retarded boundary condition  $G_R(u, v; u', v') = 0$  unless  $u > u'$  and  $v > v'$ , which leads uniquely to

$$G_R(u, v; u', v') = -\frac{1}{2} \theta(u - u') \theta(v - v'). \quad (3.17)$$

In words,  $G_R$  is equal to  $-\frac{1}{2}$  in the past lightcone of its first argument and zero everywhere else. The advanced propagator is given by the same formula with arguments transposed. The commutator function  $\Delta(x, x') = G_R(x, x') - G_A(x, x')$  can be written as follows:

$$\Delta(u, v; u', v') = -\frac{1}{2} [\theta(u - u') + \theta(v - v') - 1]. \quad (3.18)$$

The associated integral operator  $i\Delta$  defined in (2.41) is of Hilbert-Schmidt type,

since

$$\int_{-L}^L du \int_{-L}^L dv \int_{-L}^L du' \int_{-L}^L dv' |i\Delta(u, v; u', v')|^2 = 2L^4 < \infty. \quad (3.19)$$

Given that  $i\Delta(x, x') = [i\Delta(x', x)]^*$ , we find that  $i\Delta$  is also self-adjoint and so the spectral theorem applies. The (appropriately normalised) positive eigenfunctions  $u_k^{SJ}$  that satisfy  $i\Delta u_k^{SJ} = +\lambda_k u_k^{SJ}$ , are given by the two sets [26]

$$\begin{aligned} f_k(u, v) &:= e^{-iku} - e^{-ikv} && \text{with } k = \frac{n\pi}{L}, n = 1, 2, \dots \\ g_k(u, v) &:= e^{-iku} + e^{-ikv} - 2\cos(kL) && \text{with } k \in \mathcal{K}, \end{aligned} \quad (3.20)$$

where  $\mathcal{K} = \{k \in \mathbb{R} \mid \tan(kL) = 2kL \text{ and } k > 0\}$  and their eigenvalues are  $\lambda_k = L/k$ .<sup>2</sup> Their  $L^2$ -norms are  $\|f_k\|^2 = 8L^2$  and  $\|g_k\|^2 = 8L^2 - 16L^2\cos^2(kL)$ . It is clear that the eigenfunctions with negative eigenvalues are given by the complex conjugates  $\bar{u}_k^{SJ}$ . To verify that the functions (3.20) and their complex conjugates are indeed *all* the eigenfunctions with non-zero eigenvalue, we can use relation (2.54), which states that the sum over the squared eigenvalues of  $i\Delta$  must be equal to (3.19). A short calculation shows that

$$\sum_k \lambda_k^2 = \sum_{n=1}^{\infty} \frac{2L^4}{(\pi n)^2} + \sum_{k \in \mathcal{K}} \frac{2L^2}{k^2} = \frac{2L^4}{6} + \frac{10L^4}{6} = 2L^4, \quad (3.21)$$

as required (the analytic evaluation of the second sum in (3.21) can be found in [26, 38]). The SJ prescription defines the two-point function  $W_{SJ,L}(u, v; u', v')$  as the positive spectral projection of  $i\Delta$ :

$$W_{SJ,L}(u, v; u', v') = \sum_{n=1}^{\infty} \frac{L^2}{\pi n} \frac{1}{\|f_k\|^2} f_k(u, v) f_k^*(u', v') + \sum_{k \in \mathcal{K}} \frac{L}{k} \frac{1}{\|g_k\|^2} g_k(u, v) g_k^*(u', v'). \quad (3.22)$$

We denote the two sums in (3.22) by  $S_1$  and  $S_2$ , respectively.

The first sum

$$S_1 = \frac{1}{8\pi} \sum_{n=1}^{\infty} \frac{1}{n} \left[ e^{-\frac{iun\pi}{L}} - e^{-\frac{ivn\pi}{L}} \right] \left[ e^{\frac{iu'n\pi}{L}} - e^{\frac{iv'n\pi}{L}} \right] \quad (3.23)$$

can be evaluated in closed form. We recognise four Newton-Mercator series which

---

<sup>2</sup>There is a sign error in the commutator function in [26] which results in the  $f_k$  and  $g_k$  given here being the complex conjugates of those there.

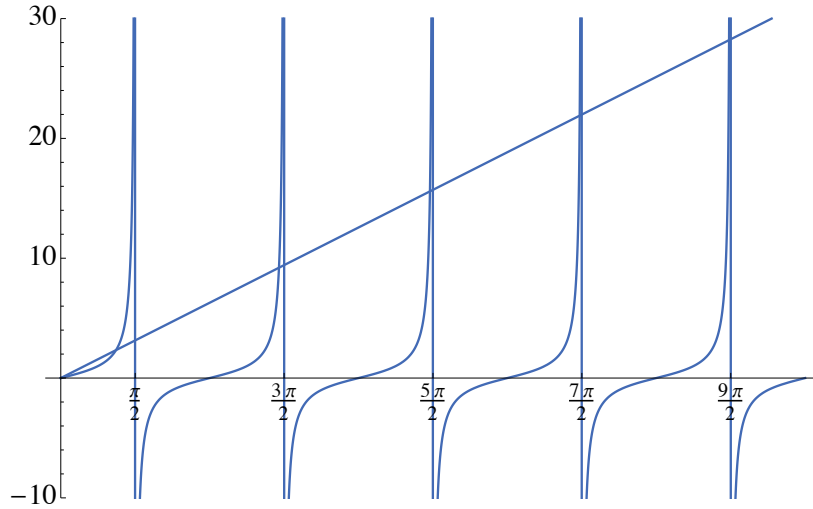


Figure 3.3.: Plot of  $\tan x$  and  $2x$  along with vertical lines at  $\frac{2n-1}{2}\pi$  for  $n \in \mathbb{Z}$ . The values of the summation variable correspond to the positions of the intersections  $\tan x = 2x > 0$ .

converge to the principal branch of the complex logarithm:

$$S_1 = \frac{1}{8\pi} \left\{ -\text{Ln} \left[ 1 - e^{-\frac{i\pi(u-u')}{L}} \right] - \text{Ln} \left[ 1 - e^{-\frac{i\pi(v-v')}{L}} \right] + \text{Ln} \left[ 1 - e^{-\frac{i\pi(u-v')}{L}} \right] + \text{Ln} \left[ 1 - e^{-\frac{i\pi(v-u')}{L}} \right] \right\}. \quad (3.24)$$

The second sum is

$$S_2 := \sum_{k \in \mathcal{K}} \frac{\left[ e^{-iku} + e^{-ikv} - 2 \cos(kL) \right] \left[ e^{iku'} + e^{ikv'} - 2 \cos(kL) \right]}{kL [8 - 16 \cos^2(kL)]}. \quad (3.25)$$

We have no closed form expression for this sum but as  $n \rightarrow \infty$ , the roots of the transcendental equation  $\tan(x) = 2x$  rapidly approach  $x_n = \frac{(2n-1)\pi}{2}$  with  $n \in \mathbb{N}$  (see Figure 3.3). Therefore if we approximate the sum by replacing  $k \in \mathcal{K}$  with  $x_n/L$ , we can expect the main error to come from a few modes of long wavelength. Consequently we can expect the resulting error term to be a slowly varying and small correction to the approximated sum. Let

$$\mathcal{K}_0 := \left\{ \frac{2n-1}{2L} \pi \mid n = 1, 2, 3, \dots \right\} \quad (3.26)$$

and define the error  $\epsilon(u, v; u', v')$  by

$$\begin{aligned} S_2 &= \sum_{k \in \mathcal{K}_0} \frac{\left[ e^{-iku} + e^{-ikv} - 2 \cos(kL) \right] \left[ e^{iku'} + e^{ikv'} - 2 \cos(kL) \right]}{kL [8 - 16 \cos^2(kL)]} + \epsilon(u, v; u', v') \\ &= \frac{1}{4\pi} \sum_{n=1}^{\infty} \frac{1}{2n-1} \left[ e^{-\frac{iu(2n-1)\pi}{2L}} + e^{-\frac{iv(2n-1)\pi}{2L}} \right] \left[ e^{\frac{iu'(2n-1)\pi}{2L}} + e^{\frac{iv'(2n-1)\pi}{2L}} \right] + \epsilon(u, v; u', v'). \end{aligned} \quad (3.27)$$

In other words  $\epsilon$  is the difference between the exact value of  $S_2$  and the value obtained in the approximation  $\mathcal{K} \rightarrow \mathcal{K}_0$ . The sums above converge to logarithmic terms when  $L < \infty$  and are most conveniently expressed in the form:

$$\begin{aligned} S_2 &= \frac{1}{4\pi} \left\{ \tanh^{-1} \left[ e^{-\frac{i\pi(u-u')}{2L}} \right] + \tanh^{-1} \left[ e^{-\frac{i\pi(v-v')}{2L}} \right] \right. \\ &\quad \left. + \tanh^{-1} \left[ e^{-\frac{i\pi(u-v')}{2L}} \right] + \tanh^{-1} \left[ e^{-\frac{i\pi(v-u')}{2L}} \right] \right\} + \epsilon(u, v; u', v') \end{aligned} \quad (3.28)$$

The two-point function of the SJ ground state in the causal diamond is given by the sum,  $W_{SJ,L} = S_1 + S_2$ . Using  $\tanh^{-1}(x) = \frac{1}{2} \text{Ln}(1+x) - \frac{1}{2} \text{Ln}(1-x)$  and the fact that  $\text{Ln}(1-e^x) - \text{Ln}(1 \pm e^{\frac{x}{2}}) = \text{Ln}(1 \mp e^{\frac{x}{2}})$ , we can combine the two sums to yield

$$\begin{aligned} W_{SJ,L} &= \frac{1}{4\pi} \left\{ -\text{Ln} \left[ 1 - e^{-\frac{i\pi(u-u')}{2L}} \right] - \text{Ln} \left[ 1 - e^{-\frac{i\pi(v-v')}{2L}} \right] \right. \\ &\quad \left. + \text{Ln} \left[ 1 + e^{-\frac{i\pi(u-v')}{2L}} \right] + \text{Ln} \left[ 1 + e^{-\frac{i\pi(v-u')}{2L}} \right] \right\} + \epsilon(u, v; u', v') \quad (3.29) \\ &= W_{\text{box},L} + \epsilon(u, v; u', v'), \end{aligned}$$

where  $W_{\text{box},L}$  is the exact continuum two-point function of the *ground state* of a massless scalar field in a box with reflecting boundaries at  $x = \pm\sqrt{2}L$ . We shall now investigate the form of the SJ ground state in the limits (i) and (ii) mentioned above.

### 3.2.1. The SJ state in the centre and corner

The limits we are concerned with require that two spacetime points be separated by a small geodesic distance compared to the diamond scale  $L$  and that they be confined to (i) the centre of the diamond or (ii) a region near the left/right corner (we choose the left corner without loss of generality). In these particular limits, we

want the arguments in the exponentials of the sums above to have a small magnitude so that we can Taylor expand the functions and obtain more illuminating forms of the two-point function. Keeping in mind that in  $u, v$ -coordinates, the centre of the diamond lies at  $(0, 0)$ , the limit that corresponds to a pair of points in the centre (i) can be defined as

$$\begin{aligned}
 |u - u'| &\ll L \\
 |v - v'| &\ll L \\
 |u - v'| &\ll L \\
 |v - u'| &\ll L.
 \end{aligned} \tag{3.30}$$

The limit that corresponds to the corner can be obtained in a similar manner by first translating the coordinate system such that the left corner of the diamond lies at the origin  $(0, 0)$  of the new coordinates. This corresponds to the (passive) coordinate transformation  $x \rightarrow x - \sqrt{2}L$ , or  $u \rightarrow u - L$  and  $v \rightarrow v + L$ . By “in the corner” we then mean the limit (ii) where we first perform this translation and then apply the restriction (3.30) to the translated coordinates.

The inequalities (3.30) constrain the pairs of spacetime points to be separated by a small geodesic distance  $|d| = (2|u - u'||v - v'|)^{\frac{1}{2}} \ll L$  and furthermore imply that  $|x|, |x'| \ll L$ . This means that the points are confined to a narrow vertical strip centred on (i) the centre of the diamond or (ii) the left corner of the diamond, as illustrated in Figure 3.2. Let the width of the strip be  $D \ll L$ .

### The centre

We first analyse the sum in the centre by expanding to lowest order in  $\delta/L$ , where  $\delta$  collectively denotes the coordinate differences  $u - u', v - v', u - v', v - u'$ . Using  $\text{Ln}(1 - e^x) = \text{Ln}(x) + \mathcal{O}(x)$  we identify the leading term in  $S_1$  as

$$S_1 = \frac{1}{8\pi} \left[ -\text{Ln} |u - u' ||v - v'| + \text{Ln} |u - v' ||v - u'| + C_1 \frac{i\pi}{2} \right] + \mathcal{O} \left( \frac{\delta}{L} \right) \tag{3.31}$$

where  $C_1 = \text{sgn}(u - u') + \text{sgn}(v - v') - \text{sgn}(u - v') - \text{sgn}(v - u')$ . Similarly, in  $S_2$ , we expand  $\tanh^{-1}(e^x) = -\frac{1}{2} \text{Ln} \frac{x}{2} + \mathcal{O}(x)$  to obtain

$$S_2 = \frac{1}{8\pi} \left[ -\text{Ln} |u - u'| |v - v'| - \text{Ln} |u - v'| |v - u'| - 4 \text{Ln} \frac{\pi}{4L} + C_2 \frac{i\pi}{2} \right] + \epsilon + \mathcal{O}\left(\frac{\delta}{L}\right) \quad (3.32)$$

where  $C_2 = \text{sgn}(u - u') + \text{sgn}(v - v') + \text{sgn}(u - v') + \text{sgn}(v - u')$ .

Now we deal with the correction,  $\epsilon$ . Over a small region,  $\epsilon$  should not vary much. To investigate this, we now further restrict the arguments of  $W$  to lie in a small square centred on the origin, of linear dimension  $D$ , the width of the strip. After an analysis and numerical investigation given in the appendix, we find that  $\epsilon$  is indeed approximately constant over the small diamond and tends to a value  $\epsilon_{\text{centre}} \approx -0.063$  as  $L$  tends to infinity.

The terms with arguments  $u - v'$  and  $v - u'$  cancel in  $S_1 + S_2$  so we obtain

$$W_{\text{centre}}(u, v; u', v') = -\frac{1}{4\pi} \text{Ln} |\delta u \delta v| - \frac{i}{4} \text{sgn}(\delta u + \delta v) \theta(\delta u \delta v) - \frac{1}{2\pi} \text{Ln} \frac{\pi}{4L} + \epsilon_{\text{centre}} + \mathcal{O}\left(\frac{\delta}{L}\right) \quad (3.33)$$

as  $L$  gets large. Recall now that  $|\delta u \delta v| = \frac{1}{2} |d|^2$ . It is then evident that (3.33) matches the ‘‘cut off’’ Minkowski two-point function  $W_{M,\lambda}$  (3.6) with a particular value of the cut-off  $\lambda$  given by

$$\lambda = \frac{\pi}{4\sqrt{2}} \exp(-\gamma - 2\pi\epsilon_{\text{centre}}) L^{-1} \approx 0.46 \times L^{-1}, \quad (3.34)$$

where  $\gamma$  is the Euler-Mascheroni constant. As one would expect,  $\lambda^{-1} \sim L$  for large  $L$ , leading to a logarithmic factor of the form  $\text{Ln} |L^2 / \delta u \delta v|$ .

Whilst strictly speaking we cannot take the  $L \rightarrow \infty$  limit of such an expression, it seems fair to say that the SJ state takes on the character of a Minkowski vacuum in the centre of a large diamond. Notice finally that in the limit, the imaginary part of the two-point function does satisfy the requirement  $\text{Im}(W) = \Delta/2$ , as had to be the case.

### The corner

For spacetime points close to the edges of the diamond, the boundaries of the diamond appear like the causal horizons of a Rindler wedge (see Figure 3.1). To evaluate the SJ two-point function in this limit, we perform the translation  $u \rightarrow u - L$  and  $v \rightarrow v + L$  described above, which shifts the corner of the diamond to the position  $(0, 0)$ . We then Taylor expand using (3.30) in the new coordinates.

The sums  $S_1$  and  $S_2$  can be evaluated as before, but the translation introduces  $\pm$  signs multiplying integer multiples of  $i\pi$ . A brief inspection shows that the first sum (3.23) is unaltered by the translation, since only factors of  $\exp(2\pi i)$  arise, while the second sum (3.25) picks up factors of  $\exp(\pi i)$  that induce sign changes in the terms involving  $u - v'$  and  $v - u'$ . The second sum now evaluates to

$$S_2 = \frac{1}{8\pi} \left[ -\text{Ln} |u - u'| |v - v'| + \text{Ln} |u - v'| |v - u'| + C_2 \frac{i\pi}{2} \right] + \epsilon + \mathcal{O} \left( \frac{\delta}{L} \right), \quad (3.35)$$

where  $C_2 = C_1 = \text{sgn}(u - u') + \text{sgn}(v - v') - \text{sgn}(u - v') - \text{sgn}(v - u')$ . The correction term  $\epsilon$  can again be analysed numerically — see Appendix A — and the result is that it varies very little over the small corner region for fixed  $L$  and tends to zero as  $L \rightarrow \infty$ . A consequence of the sign changes is that the constant terms that depend on  $L$  cancel in  $S_2$ , whence there is no longer any obstruction sending  $L \rightarrow \infty$ . Taking this limit, we obtain the two-point function

$$\begin{aligned} \lim_{L \rightarrow \infty} W_{\text{corner}}(u, v; u', v') &= -\frac{1}{4\pi} \text{Ln} \left| \frac{(u - u')(v - v')}{(u - v')(v - u')} \right| \\ &\quad - \frac{i}{4} \text{sgn}(\delta u + \delta v) \left[ \theta((u - u')(v - v')) - \theta((v' - u)(u' - v)) \right], \end{aligned} \quad (3.36)$$

which can be recognised as the two-point function of the scalar field in Minkowski space with a mirror at rest at the corner  $x = 0$  ( $x = -\sqrt{2}L$  in the original coordinates) [39, 40]:

$$W_{\text{corner}}(t, x; t', x') = W_{M,\lambda}(t, x; t', x') - W_{M,\lambda}(t, x; t', -x'). \quad (3.37)$$

This two-point function is scale-free and does *not* have the character of a canonical vacuum for a Rindler wedge.

What conclusions can we draw from this? Previously, we argued heuristically



that the SJ state in the Rindler wedge should be the Fulling-Rindler vacuum (to the extent that either is defined at all in the presence of the IR divergences). Now we have seen that a well-controlled limiting procedure gives a different result. As  $L$  gets large, the spacetime geometry approaches that of the Rindler wedge, as far as points that remain close to one corner of the diamond are concerned, but the SJ state approaches the ground state of a scalar field with reflecting boundary conditions at the corner.

In fact, this “mirror behaviour” is already visible at the level of the SJ modes themselves. The first set of modes  $f_k$  (3.20) vanish on the two vertical lines at the spatial positions of the corners  $f_k(x = \pm\sqrt{2}L, t) = 0$  (recall that the corners are at  $x = \pm\sqrt{2}L$  in the coordinate system before translation), while the second set  $g_k$  also vanish on these vertical lines in the approximation  $\mathcal{K} \rightarrow \mathcal{K}_0$ . The SJ conditions thus satisfy approximately the boundary conditions for two static mirrors, one at each corner of the diamond. How would such a two-mirror state appear near to the left corner? As the size of the diamond tended to infinity, one might expect the field in the left corner to become unaware of the right mirror, and this is consistent with our calculation above. On the other hand there remains the puzzle of where the left-hand mirror comes from in the limit. Its very existence selects a distinguished timelike direction, and since this direction can only be covariantly defined by reference to the right hand corner of the diamond, it seems difficult to avoid the conclusion that the presence of the right corner retains its influence no matter how large  $L$  becomes!

It seems reasonable to attribute these counter-intuitive effects to our having set the mass to zero. As an aspect of its infrared pathology, the massless field might be able to sense the boundaries of the finite system, no matter how far away they are. If this explanation is correct, one would not expect to find the same mirror behaviour for a massive scalar field, since the mass should shield it from such long range effects. It would also be interesting to study massless and massive fields in finite regions of Minkowski spacetime in  $3 + 1$  dimensions.

### 3.3. Comparison with the discrete SJ state

In this section, we will apply the SJ formalism to the massless scalar field on a causal set that is well-approximated by the two-dimensional flat causal diamond. In the case of non-zero mass, it has been shown [26] numerically that the mean of the discrete SJ two-point function approximates well the Wightman function of the continuum Minkowski vacuum. We will extend this study to the massless case and

compare with our results above for the continuum SJ state.

### 3.3.1. Causal sets and discrete propagators

When  $\mathcal{C}$  is obtained by sprinkling, each causal set element  $\nu_i$  corresponds to a point  $x_i$  in the embedding continuum spacetime.<sup>3</sup> This allows us to directly compare the values of the discrete two-point function  $\mathbf{W}_{ij}$  and those of the continuum Wightman function  $W_{ij} := W(x_i, x_j)$ .

We will compare the mean of the massless discrete two-point function  $\mathbf{W}$  with its continuum counterparts, using two separate methods. In the centre of the diamond, the continuum two-point function (3.33) is approximately a function of the geodesic distance only, in the limit of large  $L$ . We therefore plot the amplitudes  $\mathbf{W}_{ij}$  against the proper time  $d_{ij} := |d(x_i, x_j)|$  and ask how well they agree with the continuum result. In the corner, the continuum  $W$  does not reduce to a function of a single variable. In that case, we provide a “correlation plot” between the discrete two-point function and several continuum two-point functions (evaluated on the sprinkled points), so that the relative goodness of fit can be assessed.

We restrict ourselves here to timelike related points; the analysis for spacelike related points is similar. Furthermore we only need to analyze the real parts of  $W$  and  $\mathbf{W}$ . The imaginary parts add nothing new since they are given by the Pauli-Jordan function and tell us nothing about the quantum state.

We work in a causal diamond  $M = \mathbf{C}_L$  and evaluate the discrete propagator on an  $N = 2^{11} = 2048$  element sprinkling into this diamond. We use units in which  $\rho = 1$ , which implies  $L = \sqrt{V}/2 = \sqrt{N}/2 = 2^{\frac{9}{2}}$ . A typical sprinkling is shown in Figure 3.4. Highlighted are the two subregions in which we shall sample the discrete SJ two-point function. Each subregion occupies 8% of the area of the full diamond.

### 3.3.2. The SJ state in the centre

The data for the centre is taken from a sample of 181 points in the square, among which there were 7599 timelike related pairs. As discussed in Section 3.1 the two-point function of the massless scalar field in two-dimensional Minkowski spacetime is ill-defined owing to the infrared divergence, but there exists a one-dimensional family of “approximate Wightman functions”  $W_{M,\lambda}$  parameterised by an infrared

---

<sup>3</sup>We will sometimes use Greek letters for sprinkled elements to distinguish the causal set element from its coordinate values in the continuum manifold.

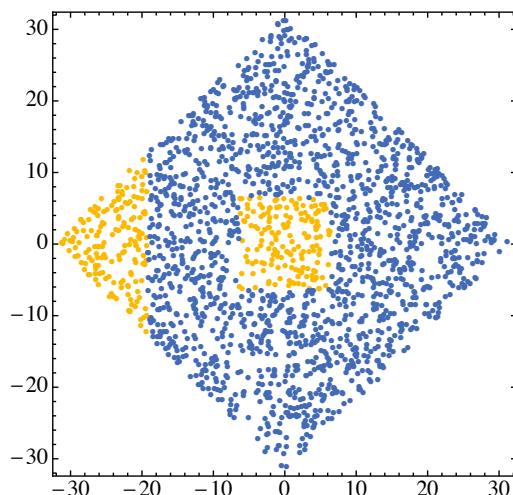


Figure 3.4.: An  $N = 2^{11} = 2048$  element sprinkling into a diamond  $C_L$  (with  $L = 2^{\frac{9}{2}}$  in natural units). The subregions corresponding to the centre ( $i$ ) and the corner ( $ii$ ) are highlighted.

scale or “cut-off”  $\lambda$ . It is thus natural to compare our discrete function  $\mathbf{W}$  with  $W_{M,\lambda}$ , where we fix  $\lambda = 0.02$  from the relation (3.34) between  $\lambda$  and  $L$  when  $L = 2^{\frac{9}{2}}$ . Then the real part of the continuum Wightman function we compare to is

$$\text{Re} [W_{M,\lambda}(x, x')] = -\frac{1}{2\pi} \text{Ln} |d(x, x')| + 0.53. \quad (3.38)$$

Figure 3.5 displays this function together with a scatter-plot of the discrete SJ amplitudes  $\mathbf{H}_{ij} = \text{Re} [\mathbf{W}_{ij}]$  taken from region ( $i$ ) in Figure 3.4. Evidently, the fit is good, with a slight hint of a deviation at larger values of proper time which, if real, can be attributed to  $\mathcal{O}(\delta/L)$  corrections, given that the centre region is still relatively large compared to  $L$ . From our previous analysis we know that  $W_{M,\lambda}(x, x')$  approximates the continuum SJ state in the centre of the diamond, and so our data also supports the conclusion that the continuum and discrete SJ Wightman functions approximate each other.

### 3.3.3. The SJ state in the corner and in the full diamond

For the corner, the type of plot we used for the centre is unsuitable because the continuum two-point functions we want to compare with depend on more variables than just the geodesic distance. Instead we plot the values of  $\mathbf{W}$  directly against

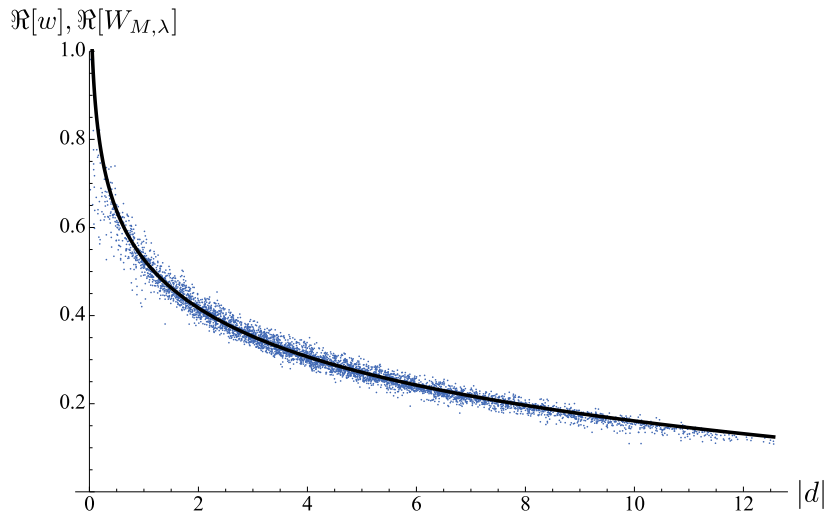


Figure 3.5.: The real parts of the continuum two-point function  $W_{M,\lambda}(x, x')$  (black line) with  $\lambda = 0.02$  and the discrete SJ two-point function  $\mathbf{W}_{ij}$  (blue scatter) in the centre of the finite diamond  $C_L$  with  $L = 2^{\frac{9}{2}}$ , plotted against the proper time  $|d|$  for timelike separated events.

those of the continuum  $W$  with which we are comparing. More specifically, we use the coordinate values of the sprinkled points to calculate the values of a particular continuum function  $W(x_i, x_j) =: W_{ij}$ . We then plot a point on the graph whose vertical coordinate is  $W_{ij}$  and whose horizontal coordinate is  $\mathbf{W}_{ij}$  at the corresponding pair of elements of the causet. In this manner, we will assess the correlation between the data sets  $\mathbf{W}_{ij}$  and  $W_{ij}$  for 4 different continuum two-point functions: the exact continuum SJ function  $W_{S,J,L}$  (before Taylor expansion), the Minkowski function  $W_{M,\lambda}$  (3.6), the single mirror  $W_{\text{mirror}}$  (3.37), and the Rindler function  $W_{R,\lambda}$  (3.10). Both the Rindler and Minkowski  $W$ -functions come with an arbitrary parameter  $\lambda$ , which shows up on the plots as an arbitrary vertical shift. We set this shift such that the intercept is zero. The corner subregion (Figure 3.4) contains 181 points, which produce a sample of 11230 pairs of timelike related points. The correlation plots for the real parts of the discrete and continuum propagators evaluated on this sample are shown in Figure 3.6. Evidently, the plot of the exact SJ function exhibits a good fit with the causal set data, confirming again that the discrete and continuum formalisms agree. As expected, the correlation with the mirror two-point function is also high, implying that the ground state in the corner is indeed that of flat space in the presence of a mirror. (The slightly positive intercept in the

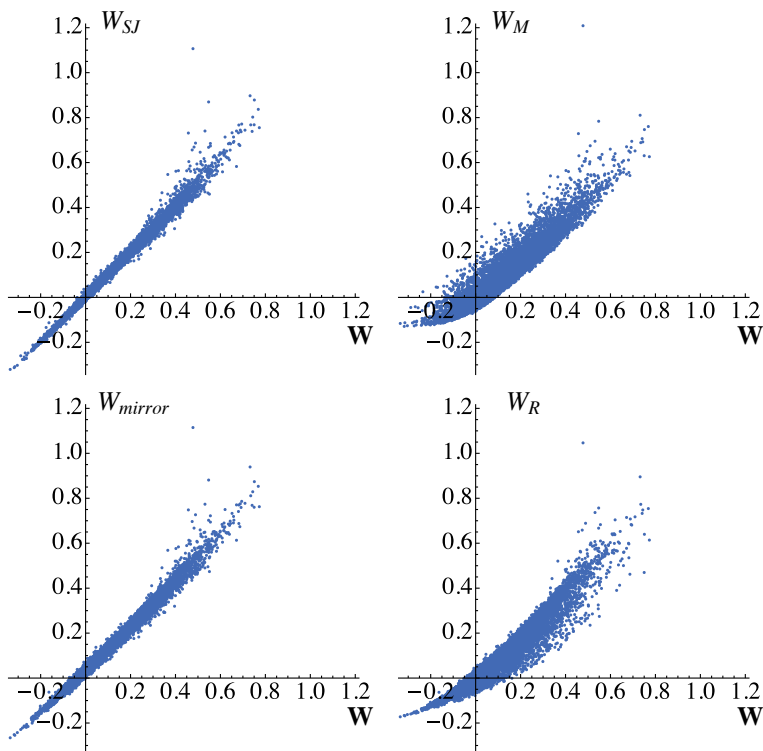


Figure 3.6.: Correlation plots for the two-point functions in the corner of the causal diamond. The horizontal axis represents the causal set two-point function  $\mathbf{W}_{ij}$ . The vertical axes represent (from left to right, top to bottom): the SJ, the Minkowski, the mirror, and the Rindler two-point functions.

causal set versus mirror plot, can plausibly be attributed to the  $\epsilon$  correction and to  $\mathcal{O}(\delta/L)$  effects, both of which would go away were the corner region made smaller.) As one would expect for the corner, the Minkowski and Rindler functions exhibit significantly worse correlations with the causal set data-set.

Turning to the full diamond, we use a smaller overall causal set with  $N = 256$ , which yields a sample of 16393 pairs of timelike related points. To the four comparison functions above we add a fifth: the reflecting box (mirrors at both corners)  $W_{\text{box},L}$ . Of these five continuum two-point functions, one should expect that in addition to the SJ state, only the reflecting box ground state would exhibit a reasonable degree of correlation with the causal set data. (As seen in equation (3.29) above, continuum SJ and reflecting-box are identical up to the error-term  $\epsilon(u, v; u', v')$ , which, however, can vary more appreciably now that we do not restrict ourselves to

a small subregion of the diamond.) The correlation plots of Figure 3.7 confirm this expectation, although the match with the discrete SJ function is not as sharp as in the case of the corner, perhaps reflecting the smaller overall sprinkling density.

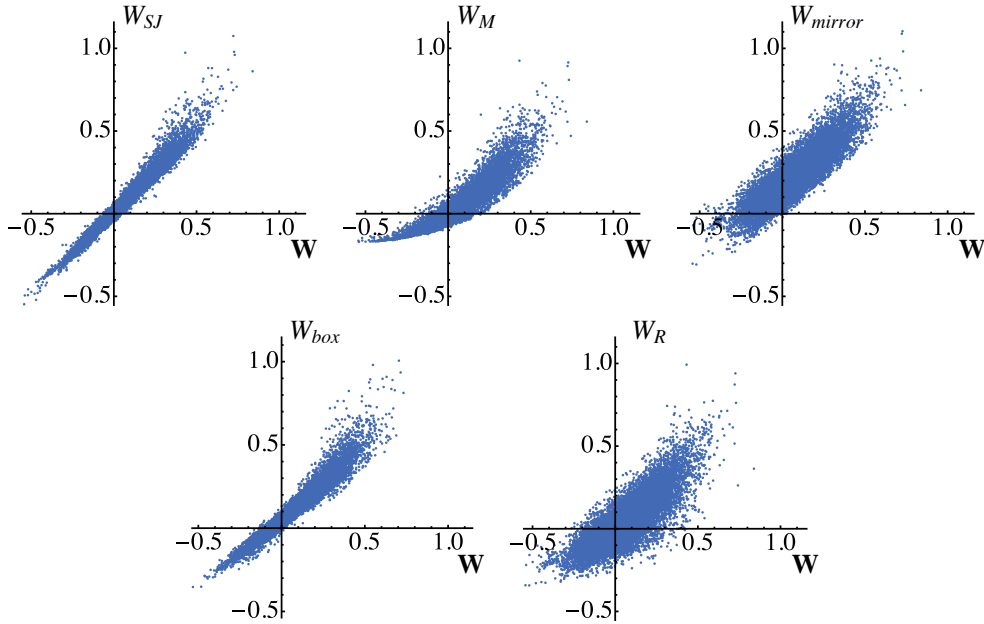


Figure 3.7.: Correlation plots for the two-point functions in the full causal diamond. The horizontal axis represents the causal set two-point function  $\mathbf{W}_{ij}$ . The vertical axes represent (from left to right, top to bottom): the SJ, the Minkowski, the left mirror, the box (two mirrors) and the Rindler two-point functions.

### 3.4. Conclusions

When we look near the centre of the diamond, we find that the SJ Wightman function agrees with the “Minkowski vacuum”, just as one might have expected. However, when we look in the corner of the diamond we do not see something having the form of a “Fulling-Rindler vacuum”. Instead we recognize the flat-space vacuum in the presence of a static mirror at that corner. This is confirmed by the numerical results. Thus, the continuum calculations in Section 2.3.3 giving the SJ state in the Rindler wedge do not agree with the limiting procedure of constructing the SJ state in the finite diamond and letting the size of the diamond tend to infinity, whilst keeping the

arguments of the two-point function at fixed locations with respect to the corner. It is important to understand the reason for this ambiguity which threatens the proposal of the SJ state as the distinguished ground state of a region: such a ground state, if it is defined at all, should be unique and be independent of any (physically sensible) limiting procedure. Of course, one cannot really speak of a disagreement between two functions, one of which is ill-defined, but the fact remains that the limiting procedure above yields very different results for the centre versus the corner of the diamond. It seems likely that these disagreements and ambiguities stem from the infrared divergences of the two-dimensional massless theory, and if one were to work instead with a massive field,<sup>4</sup> the SJ state for the wedge would be unique and in agreement with both the Fulling-Rindler vacuum and the limit of the diamond's SJ state. Some of these questions will need to be investigated in future work, but preliminary numerical results for the massive scalar field in the sprinkled diamond indicate that the discrete SJ function does fit the Fulling-Rindler vacuum better than the state with a mirror present.

If the foregoing expectations are born out, then one conclusion would be that the SJ state for the massive field is singular on the boundary of the diamond, which is the behaviour one would expect for a pure state in a bounded region. (The SJ state of a region is pure by construction.) Indeed, the highly entangled nature of quantum states possessing the local structure of the Minkowski vacuum means that their restrictions to any spatially bounded portion of Minkowski spacetime will be highly mixed and far from pure.

Before moving on, we should mention the recent work by Avilán et al. [41]. The authors compute the expectation value of the stress-energy tensor associated with the SJ state on the flat diamond, which they obtain by taking the coincidence limit of derivatives of the real part of the Wightman function (3.29) (i.e. the Hadamard function). More precisely, they obtain a renormalised expectation value  $\langle T_{\mu\nu} \rangle$  by first taking the  $L$ -derivative of the relevant derivatives of the Hadamard function, thus discarding  $L$ -independent terms, and then taking the coincidence limit of its arguments. The authors find that (i) the “correction term”  $\epsilon$  in fact contributes in a significant fashion to  $\langle T_{\mu\nu} \rangle$ , (ii) the theory develops a trace anomaly,  $\langle T_{\mu}^{\mu} \rangle \neq 0$ , and (iii) the ( $x$ -component of the) energy conservation equation  $\nabla_{\mu} \langle T^{\mu\nu} \rangle = 0$  is violated in the semi-classical theory. Since the SJ state breaks scale invariance, the authors claim that “we should have a coupling between the expectation value of the

---

<sup>4</sup>One might also consider working with the gradient of the field.

field and the metric, [i.e.] induced gravity”.<sup>5</sup> By starting with the most general two-dimensional metric and requiring that it take the appropriate form to restore the semi-classical energy conservation equation  $\nabla_\mu \langle T^{\mu\nu} \rangle = 0$ , they find that the metric thus obtained describes a spacetime that is asymptotically anti de Sitter ( $AdS_2$ ) with timelike boundaries at the positions of the corners  $x = \pm\sqrt{2}L$ . While the physical meaning of these results are not immediately apparent, it is certainly interesting to see the appearance of the timelike boundaries in the diamond spacetime again, here in the form of  $AdS_2$  boundaries, on which the SJ state appears to have picked its own boundary conditions. It also opens up interesting questions about the SJ formalism in non-globally hyperbolic spacetimes such as  $AdS_2$ , which we will revisit in Chapter 5.

In the next chapter, we will employ a somewhat different limiting procedure than the one used in this chapter to study the scalar field in de Sitter space. There, it turns out that the limiting procedure yields meaningful results *except* in a certain case, in which the mass of the field is below a threshold set by the Hubble scale. We shall see that this lends some support to the expectation that the failure of a unique limit in the SJ state always accompanies some other pathology of the theory.

---

<sup>5</sup>The SJ state is not conformally invariant because, unlike the Klein-Gordon inner product, the natural  $L^2$  inner product on the space on which  $i\Delta$  acts as an operator is not conformally invariant.



## 4. The SJ state in de Sitter space

In this chapter, we apply the SJ formalism to a free massive scalar field in de Sitter space, which is a particularly interesting setting for various reasons. Since de Sitter space and its globally hyperbolic submanifold known as the Poincaré half space are not static (or stationary), there is no unique canonical minimum-energy vacuum, and hence computing the SJ state is not merely another “consistency check”. (For that reason we do not consider the static patch of de Sitter in our analysis.)

Further, as demonstrated in [10], the SJ formalism is sensitive to the global structure of spacetime. By evaluating it on the the full de Sitter hyperboloid *as well as* on its Poincaré half space, we can investigate further the ways in which the state feels the global features of the spacetime it lives in. Indeed, we shall see that the SJ state on the Poincaré patch and the whole manifold are different in general.

The setup also provides further insight into the strategy of first computing the SJ state for a bounded globally hyperbolic subregion of an unbounded spacetime, and then taking appropriate limits to recover the state for the entire spacetime. In the case of de Sitter space, we will see that this procedure gives meaningful answers in most circumstances, but that it also fails in some cases. In this context, we also have the opportunity to further investigate in which circumstances the SJ state obeys the so-called Hadamard condition. We find that for certain ranges of the scalar field mass and for certain values of the spacetime dimension, the SJ state in de Sitter space is Hadamard, whereas for others it is not.

Finally, de Sitter space is of course interesting due to its relevance to cosmological models of the universe. Since one of the ultimate aims of our efforts is to develop the formalism to a stage at which it becomes possible to address questions of phenomenology, cosmological spacetimes are especially important.

We begin with a review of some relevant aspects of de Sitter geometry.

## 4.1. Geometry of de Sitter Space

De Sitter space is the maximally symmetric spacetime of constant positive curvature (a comprehensive review of de Sitter geometry can be found in [42]). We denote de Sitter space in  $D = d + 1$  dimensions by  $dS^D$ . It can be viewed as the hyperboloid

$$X \cdot X = +\ell^2 \quad (4.1)$$

in an embedding  $D + 1$  dimensional Minkowski space  $\mathbb{M}^{D+1}$  with Cartesian coordinates  $X^a$  ( $a = 0, 1, \dots, D$ ) and a Lorentzian metric  $\eta_{ab} = \text{diag}(-1, 1, \dots, 1)$  that defines the product  $X \cdot Y = \eta_{ab}X^aY^b$ . The de Sitter metric  $g_{\mu\nu}$  ( $\mu = 0, \dots, D - 1$ ) is induced by the restriction of  $\eta_{ab}$  onto the hyperboloid.

It can be shown that geodesics in de Sitter space correspond to intersections of planes through the origin of  $\mathbb{M}^{D+1}$  with the hyperboloid (4.1). Consequently, the geodesic distance between two points  $p, q \in dS^D$  takes a particularly simple form in terms of the Lorentzian product between the embedding coordinates, which we denote by

$$Z(p, q) := \ell^{-2} X(p) \cdot X(q). \quad (4.2)$$

In terms of  $Z$ , the geodesic distance is

$$d(p, q) := \ell \cos^{-1} Z(p, q). \quad (4.3)$$

For points that can be joined by a geodesic, the range of  $Z$  is  $-1 \leq Z < \infty$ , where  $Z > 1$ ,  $Z = 1$  and  $-1 \leq Z < 1$  correspond to timelike, null, and spacelike separations, respectively. The upper bound of  $\pi\ell$  on  $d$  for spacelike separation reflects the fact that not all spacelike separated points in de Sitter space can be joined by a spacelike geodesic. For instance, two points on opposite sides of the hyperboloid and at the same height  $X^0 \neq 0$  are spacelike but cannot be joined by a geodesic, since the intersection of the hyperboloid, with the plane through the origin that goes through both points, does not yield a curve connecting the two points (instead it corresponds to two disconnected timelike curves on opposite sides of the hyperboloid).

One of the symmetries of de Sitter space relevant to the discussion below is the antipodal map  $A : p \rightarrow p^A$ , which sends a point  $p \in dS^D$  to its ‘‘antipode’’, denoted by  $p^A$ . In embedding coordinates,  $A$  takes the simple form of a reflection about the

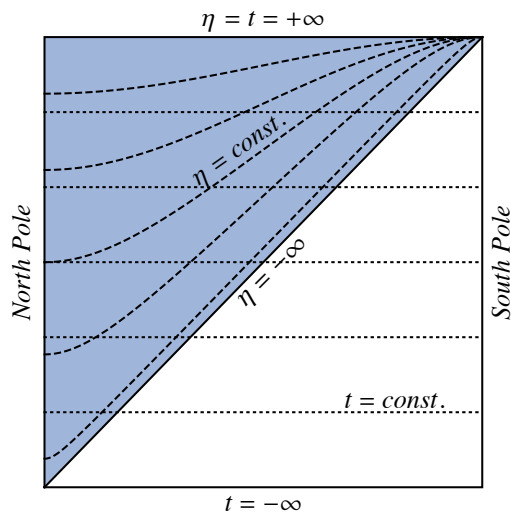


Figure 4.1.: The Penrose diagram of de Sitter space. The shaded area represents the (expanding) Poincaré patch. Dotted lines are surfaces of constant  $t$  ( $d$ -spheres), dashed lines are surfaces of constant  $\eta$  ( $d$ -planes).

origin of  $\mathbb{M}^{D+1}$ :

$$X^a(p^A) = -X^a(p). \quad (4.4)$$

Note that  $Z(p, q)$  and  $d(p, q)$  are invariant under the action of  $A$ .

We will consider two coordinate charts on de Sitter space: *closed global coordinates*, which cover the entire de Sitter manifold defined by (4.1), and *cosmological coordinates*, which cover only the half space  $X^0 + X^1 > 0$ , known as the (expanding) Poincaré patch (the contracting Poincaré patch corresponds to the other half  $X^0 + X^1 < 0$ ). We will denote the Poincaré patch by  $dS_P^D$ . It is highlighted in Figure 4.1 and corresponds to the causal future of an observer at the north pole of the  $d$ -sphere  $S^d$  at past timelike infinity (the bottom left corner of the Penrose diagram). In the field of cosmology, the word de Sitter space often refers implicitly to the Poincaré patch rather than the full hyperboloid, since a metric on the half space is used.

De Sitter space, as well as its upper and lower half spaces, constitute globally hyperbolic manifolds in their own right, but neither admits a global timelike Killing vector field [43] that would serve to define a unique “minimum energy” state.

#### 4.1.1. The global patch of de Sitter space, $dS^D$

The global chart is given by the coordinates  $x_G^\mu = (t, \theta^1, \dots, \theta^d) = (t, \boldsymbol{\theta})$  defined by

$$\begin{aligned} X^0 &= \ell \sinh(t/\ell) \\ X^i &= \ell \cosh(t/\ell) \omega^i \quad 1 \leq i \leq D, \end{aligned} \quad (4.5)$$

where  $\boldsymbol{\theta}$  stands collectively for the standard hyperspherical coordinates  $\theta^1, \theta^2, \dots, \theta^d$  on  $S^d$  and the symbols  $\omega^i$  ( $i = 1, \dots, D$ ) are given by

$$\begin{aligned} \omega^1 &= \cos(\theta^1) \\ \omega^2 &= \sin(\theta^1) \cos(\theta^2) \\ &\vdots \\ \omega^{D-1} &= \sin(\theta^1) \dots \sin(\theta^{d-1}) \cos(\theta^d) \\ \omega^D &= \sin(\theta^1) \dots \sin(\theta^{d-1}) \sin(\theta^d). \end{aligned} \quad (4.6)$$

The coordinates ranges are  $t \in (-\infty, \infty)$ ,  $\theta^d \in [0, 2\pi)$  and  $\theta^1, \dots, \theta^{d-1} \in [0, \pi]$  and the metric takes the form

$$ds^2 = -dt^2 + \ell^2 \cosh^2(t/\ell) d\Omega_d^2, \quad (4.7)$$

where  $d\Omega_d^2$  is the line element on  $S^d$ . The antipode of a point  $p$  with coordinates  $x_G^\mu(p) = (t, \theta^1, \theta^2, \dots, \theta^d)$  has coordinates  $x_G^\mu(p^A) = (-t, \pi - \theta^1, \pi - \theta^2, \dots, \pi - \theta^{d-1}, \theta^d \pm \pi)$ , where the  $+$  and  $-$  are for  $0 \leq \theta^d < \pi$  and  $\pi \leq \theta^d < 2\pi$ , respectively.

#### 4.1.2. The Poincaré patch of de Sitter space, $dS_P^D$

The Poincaré or cosmological chart is defined by the coordinates  $x_P^\mu = (\eta, \mathbf{x})$  where  $\mathbf{x} \in \mathbb{R}^d$  and

$$\begin{aligned} X^0 &= \frac{-1}{2\eta} (\ell^2 - \eta^2 + \mathbf{x}^2) \\ X^1 &= \frac{-1}{2\eta} (\ell^2 + \eta^2 - \mathbf{x}^2) \\ X^i &= \frac{-1}{\eta} x^{i-1} \quad 2 \leq i \leq D, \end{aligned} \quad (4.8)$$

with  $\mathbf{x}^2 = \sum_{i=1}^d (x^i)^2$ . The range of the (conformal) time coordinate is  $\eta \in (-\infty, 0)$  and we work in the convention where time flows in the positive  $\eta$ -direction. The line

element is then given by

$$ds^2 = \frac{\ell^2}{\eta^2} (-d\eta^2 + d\mathbf{x}^2), \quad (4.9)$$

where of course  $d\mathbf{x}^2 = \sum_{i=1}^d (dx^i)^2$ .

The antipodal map  $A$  is not defined on  $dS_P^D$ : if  $q$  is a point on the Poincaré patch, its antipode  $q^A$  is *not* a point on the Poincaré patch, since the antipodal map in cosmological coordinates takes the form  $x_P^\mu(q) = (\eta, \mathbf{x}) \implies x_P^\mu(q^A) = (-\eta, \mathbf{x})$ , and  $\eta$  is only defined on the negative real line. Bearing this in mind, we shall still use the notation  $x_P^A$  on cosmological coordinates to mean “switch the sign of  $\eta$ ” in  $x_P$ .

## 4.2. Vacuum states in de Sitter space

Here we briefly review some basic facts of scalar quantum field theory in de Sitter space. As mentioned in the previous section,  $dS^D$  and  $dS_P^D$  admit no global timelike Killing vector. Consequently there is no global definition of positive frequency that would serve to define a unique minimum-energy state. Requiring that the state of the field be invariant under the isometries of de Sitter space leaves a two-real-parameter family of quantum states known as the  $\alpha$ -vacua (or Mottola-Allen vacua) [44,45]. To single out a particular one, a number of different criteria have been called upon in the literature, depending on the context (Hadamard singularity structure [46], analyticity properties of the Green’s functions [47,48,49], minimisation of the Hamiltonian on a particular spatial hypersurface [50,51], ...). Our aim will be of course to find the ground state that is picked out by the Sorkin-Johnston formalism.

In order to diagonalise  $i\Delta$  using the prescription of Section 2.3.2, we need to pick an arbitrary complete set of modes  $u_{\mathbf{k}}$  and evaluate the Bogoliubov coefficients that relate the SJ modes to that set. A convenient choice is the set of modes associated with the so-called Euclidean or Bunch-Davies (BD) state  $|BD\rangle$  [52,53]. The modes that define this state on the full space  $dS^D$  are denoted by  $u_{L_j}^E(x_G)$  and they will be referred to as the Euclidean modes; those that define it on the Poincaré half-space  $dS_P^D$  are denoted by  $u_{\mathbf{k}}^{BD}(x_P)$  and they will be referred to as the Bunch-Davies modes. The derivation of the modes from the Klein-Gordon equations in Poincaré and global coordinates, as well as some useful properties, are given in detail in Appendix B. Here we present the expressions necessary for the next section.

### 4.2.1. BD modes

The positive-frequency modes that define the BD vacuum  $|BD\rangle$  on  $dS_P^D$  take the form (see Section B.1 of Appendix B):

$$u_{\mathbf{k}}^{BD}(\eta, \mathbf{x}) = \frac{e^{i\mathbf{k}\cdot\mathbf{x}}}{(2\pi)^{d/2}} \chi_k(\eta) \quad (4.10)$$

where

$$\chi_k(\eta) = \sqrt{\frac{\pi\ell}{4}} e^{i\pi(\frac{\nu}{2} - \frac{d+2}{4})} \left(\frac{-\eta}{\ell}\right)^{d/2} H_\nu^{(1)}(-k\eta) \quad (4.11)$$

and

$$\begin{aligned} \nu &= \ell\sqrt{m_*^2 - m^2}, \\ m_* &= \frac{d}{2\ell}. \end{aligned} \quad (4.12)$$

Here  $H_\nu^{(1)}$  is the Hankel function of the first kind and we will refer to  $m_*$  as the *critical mass*. As  $m$  increases from 0 to  $m_*$ ,  $\nu$  decreases along the real line from  $\frac{d}{2}$  to 0, and as  $m$  increases further across  $m_*$ ,  $\nu$  moves up the imaginary axis. These modes satisfy the Klein-Gordon equation and are orthonormal with respect to the Klein-Gordon inner product. The arbitrary phase of  $u_{\mathbf{k}}$  has been set to a value for which the mode functions satisfy the useful property

$$\bar{u}_{\mathbf{k}}(x_P) = u_{-\mathbf{k}}(x_P^A) := u_{-\mathbf{k}}(-\eta - i\epsilon, \mathbf{x}), \quad (4.13)$$

where  $x_P^A$  is the antipode of  $x_P$  (the  $i\epsilon$  term is there because the Hankel function in (4.11) has a branch cut that we have placed on the positive real axis).

### 4.2.2. Euclidean modes

The positive-frequency modes that define the Euclidean vacuum on  $dS^D$  take the form (see Section B.2 of Appendix B)

$$u_{Lj}^E(t, \boldsymbol{\theta}) = y_L^E(t) Y_{Lj}(\boldsymbol{\theta}) \quad (4.14)$$

where

$$y_L^E(t) = n_L e^{(a+\nu)t/\ell} \cosh^L(t/\ell) F(a, a + \nu; 2a; z(t) - i\epsilon) \quad (4.15)$$

and  $z(t) = 1 + e^{2t/\ell}$ . The normalisation constant is

$$n_L = \frac{e^{i\frac{\pi}{2}(a+\nu)} \sqrt{\Gamma(a+\nu)\Gamma(a-\nu)}}{2^a \ell^{\frac{d-1}{2}} \Gamma(a+\frac{1}{2})} \quad \text{with} \quad a = L + d/2. \quad (4.16)$$

Here  $F$  is short-hand for the hypergeometric function  ${}_2F_1$  and  $-i\epsilon$  determines the side of the branch cut (from 1 to  $\infty$  along the real axis) on which it should be evaluated. The functions  $Y_{Lj}(\boldsymbol{\theta})$  are spherical harmonics on  $S^d$ , whose relevant properties are listed in Appendix B.2. The index  $L$  takes values  $L \in \{0, 1, 2, \dots\}$  and  $j$  is a collective index for the numbers  $j_1, j_2, \dots, j_{d-1}$ , which run over values  $|j_{d-1}| \leq j_{d-2} \leq \dots \leq j_1 \leq L$ . These modes satisfy the Klein-Gordon equation and are orthonormal with respect to the Klein-Gordon inner product. Again the phase of the normalisation constant has been set so that the modes satisfy

$$u_{Lj}(x_G^A) = \bar{u}_{Lj}(x_G). \quad (4.17)$$

### 4.2.3. Two-point functions and $\alpha$ -vacua

The Euclidean and the BD modes define the same physical state in the sense that the two-point function  $W_E$  obtained as a mode sum of the Euclidean modes (4.14), when restricted to the Poincaré patch, coincides with the two-point function  $W_{BD}$  associated with the Bunch-Davies modes (4.10). (Both are functions of the geodesic distance and the causal relation between their arguments, which are coordinate independent quantities.) This two-point function is given by [52, 54]

$$W_E(x, y) = \frac{\Gamma[h_+] \Gamma[h_-]}{4\pi \ell^2 \Gamma[\frac{D}{2}]} F\left(h_+, h_-, \frac{D}{2}; \frac{1 + Z(x, y) + i\epsilon \operatorname{sgn}(x^0 - y^0)}{2}\right), \quad (4.18)$$

where  $h_{\pm} = \frac{d}{2} \pm \nu$  and  $F(a, b, c; z)$  is the hypergeometric function. The  $i\epsilon$  prescription selects the side of the branch cut from  $Z = 1$  to  $Z = +\infty$  on which the function should be evaluated when  $x$  and  $y$  are causally related (when  $x$  and  $y$  are spacelike, then  $Z < 1$  and the values of the function below and above the real line coincide). Note that The Hadamard function is equal to the real part  $H_E(x, y) = 2\operatorname{Re}[W_E(x, y)]$ , which depends only on the coordinate-independent quantity  $Z(x, y)$ . The Pauli-Jordan function and the retarded Green function can be written in terms of  $W_E(x, y)$ , since  $i\Delta(x, y) = 2\operatorname{Im}[W_E(x, y)]$  and  $G_R(x, y) = \theta(x^0 - y^0)\Delta(x, y)$ .

We denote the two-real-parameter family of  $dS$ -invariant  $\alpha$ -vacua by  $|\alpha, \beta\rangle$ . Their

modefunctions can be obtained through a Bogoliubov transformation [45]

$$u_{\mathbf{k}}^{(\alpha,\beta)} = \cosh(\alpha)u_{\mathbf{k}}^{BD} + \sinh(\alpha)e^{i\beta}\bar{u}_{-\mathbf{k}}^{BD}, \quad (4.19)$$

for the BD modes, and

$$u_{Lj}^{(\alpha,\beta)} = \cosh(\alpha)u_{Lj}^E + \sinh(\alpha)e^{i\beta}\bar{u}_{Lj}^E, \quad (4.20)$$

for the Euclidean modes. Here  $\alpha \in \mathbb{R}^+$  and  $\beta \in \mathbb{R}$  is defined modulo  $2\pi$ . Thanks to the relations (4.13) and (4.17) relating positive frequency modes to negative frequency modes evaluated on antipodal arguments, it is possible to express the two-point function  $W_{\alpha,\beta}(x, y)$  associated to an arbitrary  $\alpha$ -vacuum in terms of the Euclidean/BD two-point function  $W_E(x, y)$  (4.18). The imaginary part of  $W_{\alpha,\beta}(x, y)$  is always equal to  $i\Delta(x, y)$  and hence identical for all  $\alpha$ -vacua. The real part, i.e. the Hadamard function, depends on  $\alpha$  and  $\beta$ . By computing the mode sums using the  $\alpha$ -modes, the family of de Sitter invariant Hadamard functions  $H_{\alpha,\beta}(x, y)$  can be obtained and reads [45]:

$$H_{\alpha,\beta}(x, y) = \cosh 2\alpha H_E(x, y) + \sinh 2\alpha [\cos \beta H_E(x^A, y) - \sin \beta \Delta(x^A, y)]. \quad (4.21)$$

It can be verified that

$$W_{\alpha,\beta}(x, y) = \frac{1}{2}H_{\alpha,\beta}(x, y) + \frac{i}{2}\Delta(x, y). \quad (4.22)$$

In this particular parametrisation of the  $\alpha$ -vacua [45], the Euclidean state corresponds to  $\alpha = 0$ .<sup>1</sup> The derivation of (4.21) for modes on the Poincaré patch requires evaluating the BD Hadamard function outside its domain of validity. Specifically, one uses the property that

$$\begin{aligned} H_{BD}(\eta_x, \mathbf{x}; -\eta_y - i\epsilon, \mathbf{y}) &:= \int d^d \mathbf{k} [u_{\mathbf{k}}^{BD}(\eta_x, \mathbf{x})\bar{u}_{\mathbf{k}}^{BD}(-\eta_y - i\epsilon, \mathbf{y}) \\ &\quad + \bar{u}_{\mathbf{k}}^{BD}(\eta_x, \mathbf{x})u_{\mathbf{k}}^{BD}(-\eta_y - i\epsilon, \mathbf{y})] \\ &= H_E(x, y^A), \end{aligned} \quad (4.23)$$

---

<sup>1</sup>The relation between the parametrisation used here and that of [44, 51], which uses a single complex parameter  $\tilde{\alpha}$ , is  $\text{Re}(\tilde{\alpha}) = \text{Ln} \tanh \alpha$  and  $\text{Im}(\tilde{\alpha}) = \beta$ . The notation used here will be more convenient in the analysis of the SJ state on a causal set, because the Euclidean state then corresponds to a finite value  $\alpha = 0$  instead of  $\tilde{\alpha} = -\infty$ .



where  $H_E(x, y^A)$  is the Hadamard function of the Euclidean vacuum, which is of course defined on all of de Sitter space. This implies that for a given choice of  $\alpha$  and  $\beta$ , the two-point function associated with the modes (4.19) is the restriction of the global two-point function to the Poincaré patch.

Two  $\alpha$ -vacua that will be of special interest to us are the *in*- and *out*-vacua [44, 51]. In our parametrisation they correspond to

$$\alpha_{in} = \alpha_{out} = \tanh^{-1} e^{-\pi|\nu|}, \quad \beta_{in} = -\beta_{out} = \frac{D+1}{2}\pi. \quad (4.24)$$

These states have respectively no incoming/outgoing particles at past/future infinity. In other words, they minimise the Hamiltonian on spatial slices at  $t \rightarrow \pm\infty$  in global coordinates (see Figure 4.1).<sup>2</sup> Notice that in odd spacetime dimensions, the *in*- and *out*-vacua are the *same* state, i.e. they are related by a trivial Bogoliubov transformation, since then  $\exp(i\beta_{in}) = \exp(i\beta_{out})$ . The physical interpretation of this observation is somewhat delicate. The fact that the Bogoliubov transformation between the *in*- and *out*-states is trivial means that if we model the quantum scalar field on the *whole* de Sitter hyperboloid, and there are no particles coming in at  $t = -\infty$  (i.e. we choose the minimum energy state with respect to  $\partial_t$  on that surface), then there will be no particles going out at  $t = +\infty$ : “odd-dimensional de Sitter space is transparent” [51, 55]. Note that these observations have the usual “asymptotic” character of statements about particle creation in semi-classical calculations, where we associate different states with different hypersurfaces, and study the relationship between them. For instance, if one instead calculates the instantaneous response rate of an Unruh-deWitt detector travelling along an integral curve of  $t$  in the *in*- or *out*-state, the answer is in fact non-zero [51]. Note also that for the SJ state, there will be *one state only* for the de Sitter hyperboloid: by construction, the state depends on the entire spacetime manifold (more below). Whether there is an underlying physically intuitive reason for the coincidence of the *in*- and *out*-vacua in odd spacetime dimensions is an interesting question, the answer to which is as yet unknown to the author. One observation that might first come to mind is the fact that for massless Klein-Gordon fields in flat spacetime, the strict version of Huygen’s principle only holds when the spacetime dimension is even. However, in de Sitter spacetime, the principle holds instead when the mass of the field is related to the

<sup>2</sup> The modefunctions associated with these choices of  $\alpha$  and  $\beta$  correspond to  $\tilde{\phi}_{Lj}^{in}$  and  $\tilde{\phi}_{Lj}^{out}$  defined in [51], which differ from the usually defined in/out modes by a constant phase. Of course, these two choices define the same vacuum state because the two-point function is insensitive to any constant-phase rescaling of modefunctions.

dimension by  $m = \frac{1}{2\ell}\sqrt{d^2 - 1}$  [56]! It appears that, to date, a satisfying physical account for these mathematical peculiarities is still to be found.

Finally, it is also worth pointing out that for masses corresponding to a Compton wavelength much smaller than the Hubble radius,  $m \gg m_* = d/2\ell$ , the *in/out* states are “exponentially close” to the Euclidean state, since then  $|\nu| = \frac{1}{2}\ell\sqrt{m^2 - m_*^2} \gg 1$  and  $\sinh(\alpha) \sim e^{-\pi|\nu|}$ . We shall return to this observation in Section 4.3.3.

### 4.3. The SJ state in de Sitter space

In this section we compute the SJ state in  $D = d + 1$  dimensional de Sitter space. We will proceed by evaluating the Bogoliubov coefficients in (2.55)

$$u_{\mathbf{a}}^{SJ}(x) = \sum_{\mathbf{k}} A_{\mathbf{a}\mathbf{k}} u_{\mathbf{k}}(x) + B_{\mathbf{a}\mathbf{k}} \bar{u}_{\mathbf{k}}(x),$$

which define the SJ modes in terms of the BD/Euclidean modes. Recall that these can be found by solving the relations (2.57)

$$\begin{aligned} A_{\mathbf{a}\mathbf{k}} &= \frac{1}{\lambda_{\mathbf{a}}} \sum_{\mathbf{q}} A_{\mathbf{a}\mathbf{q}} \langle u_{\mathbf{k}}, u_{\mathbf{q}} \rangle + B_{\mathbf{a}\mathbf{q}} \langle u_{\mathbf{k}}, \bar{u}_{\mathbf{q}} \rangle, \\ B_{\mathbf{a}\mathbf{k}} &= \frac{-1}{\lambda_{\mathbf{a}}} \sum_{\mathbf{q}} A_{\mathbf{a}\mathbf{q}} \langle \bar{u}_{\mathbf{k}}, u_{\mathbf{q}} \rangle + B_{\mathbf{a}\mathbf{q}} \langle \bar{u}_{\mathbf{k}}, \bar{u}_{\mathbf{q}} \rangle. \end{aligned}$$

and (2.58)

$$\begin{aligned} \sum_{\mathbf{k}} A_{\mathbf{a}\mathbf{k}} B_{\mathbf{b}\mathbf{k}} - B_{\mathbf{a}\mathbf{k}} A_{\mathbf{b}\mathbf{k}} &= 0 \\ \sum_{\mathbf{k}} A_{\mathbf{a}\mathbf{k}} \bar{A}_{\mathbf{b}\mathbf{k}} - B_{\mathbf{a}\mathbf{k}} \bar{B}_{\mathbf{b}\mathbf{k}} &= \delta_{\mathbf{a}\mathbf{b}}. \end{aligned}$$

Since the inner products are divergent on the full spacetime manifolds, we introduce cutoffs in terms of global coordinates on  $dS^D$  and in terms of cosmological coordinates on  $dS_P^D$ . We then take appropriate limits to recover the infinite spacetimes. Of course, the validity of any such limiting procedure is not guaranteed a priori, and in particular, it may depend on the boundary conditions one needs to introduce on spatial boundaries introduced by the cut-offs. However, the results obtained below indicate that such issues may not be a serious concern in the case of de Sitter space. On the global patch, the spatial sections are compact spheres, so the only cut-off we need to introduce is a temporal one,  $t \in (-T, T)$ . On the Poincaré patch, the spatial

sections are non-compact, but we will work formally with delta-normalised modes and only introduce temporal cut-offs  $\eta \in (\eta_1, \eta_2)$  where  $\eta_1, \eta_2 < 0$ . This procedure clearly breaks de Sitter invariance, but we shall see that when the limit is taken, we obtain states that are de Sitter invariant.

### 4.3.1. The SJ state in the Poincaré patch

We need the following  $L^2$  inner products of the BD modes:

$$\begin{aligned}\langle u_{\mathbf{k}}^{BD}, u_{\mathbf{q}}^{BD} \rangle &= \delta^{(d)}(\mathbf{k} - \mathbf{q}) \langle \chi_k, \chi_k \rangle_\eta \\ \langle u_{\mathbf{k}}^{BD}, \bar{u}_{\mathbf{q}}^{BD} \rangle &= \delta^{(d)}(\mathbf{k} + \mathbf{q}) \langle \chi_k, \bar{\chi}_k \rangle_\eta\end{aligned}\tag{4.25}$$

where we have defined the inner product  $\langle \cdot, \cdot \rangle_\eta$  which integrates over  $\eta$  only:

$$\langle f, g \rangle_\eta := \int_{\eta_{\min}}^{\eta_{\max}} \overline{f(\eta)} g(\eta) \left( \frac{-\ell}{\eta} \right)^{d+1} d\eta.\tag{4.26}$$

We have introduced  $\eta_{\min}$  and  $\eta_{\max}$  as regulators which will be sent to  $-\infty$  and 0 (respectively). The algebraic relations (2.57) and (2.58) can now be solved by setting the Bogoliubov coefficients that specify the SJ modes in terms of the Bunch-Davies modes to

$$\begin{aligned}A_{\mathbf{kq}} &= \delta^{(d)}(\mathbf{k} - \mathbf{q}) \cosh(\alpha_k) \\ B_{\mathbf{kq}} &= \delta^{(d)}(\mathbf{k} + \mathbf{q}) \sinh(\alpha_k) e^{i\beta_k}\end{aligned}$$

where

$$\alpha_k = \frac{1}{2} \tanh^{-1} |r_k|, \quad \beta_k = \arg(r_k) + \pi,\tag{4.27}$$

and

$$r_k := \frac{\langle \bar{\chi}_k, \chi_k \rangle_\eta}{\langle \chi_k, \chi_k \rangle_\eta}.\tag{4.28}$$

The associated eigenvalues are given by

$$\lambda_{\mathbf{k}} = \sqrt{\langle \chi_k, \chi_k \rangle_\eta^2 - \left| \langle \bar{\chi}_k, \chi_k \rangle_\eta \right|^2}.\tag{4.29}$$

These will in general diverge as the inner products diverge, but the Bogoliubov coefficients only depend on the ratio  $r_k$  and hence they remain well-defined as long as  $|r_k| \neq 1$ . When  $|r_k| = 1$ , the Bogoliubov coefficients blow up and the SJ prescription is no longer valid. We need to compute  $r_k$  in the limit  $\eta_{\min} \rightarrow -\infty$  and  $\eta_{\max} \rightarrow 0^-$ .

It follows from the definition of  $\chi_k^{BD}$  that

$$\begin{aligned}\langle \bar{\chi}_k, \chi_k \rangle_\eta &= \frac{\pi \ell}{4} e^{i\pi(\nu - \frac{d+2}{2})} \int_{\eta_{min}}^{\eta_{max}} \left[ H_\nu^{(1)}(-k\eta) \right]^2 \left( \frac{-\ell}{\eta} \right) d\eta \\ \langle \chi_k, \chi_k \rangle_\eta &= \frac{\pi \ell}{4} e^{-\pi \text{Im}(\nu)} \int_{\eta_{min}}^{\eta_{max}} \left| H_\nu^{(1)}(-k\eta) \right|^2 \left( \frac{-\ell}{\eta} \right) d\eta.\end{aligned}\quad (4.30)$$

Changing integration variables to  $x = -k\eta$ , and defining  $\Lambda = -k\eta_{min} > 0$  and  $\epsilon = -k\eta_{max}$ , we obtain:

$$r_k = e^{i\pi(\text{Re}(\nu) - \frac{d+2}{2})} F(\epsilon, \Lambda) \quad (4.31)$$

where

$$F(\epsilon, \Lambda) = \frac{\int_\epsilon^\Lambda \frac{dx}{x} \left[ H_\nu^{(1)}(x) \right]^2}{\int_\epsilon^\Lambda \frac{dx}{x} \left| H_\nu^{(1)}(x) \right|^2}. \quad (4.32)$$

The limits  $\eta_{min} \rightarrow -\infty$  and  $\eta_{max} \rightarrow 0$  correspond to  $\Lambda \rightarrow +\infty$  and  $\epsilon \rightarrow 0^+$ . Let us list a few useful properties of the Hankel function  $H_\nu^{(1)}(z)$ . It satisfies the Bessel equation  $[z^2 \frac{d^2}{dz^2} + z \frac{d}{dz} + (z^2 - \nu^2)] H_\nu^{(1)}(z) = 0$  and has the defining property (see [57, Eq. 10.2.5])

$$H_\nu^{(1)}(z) \rightarrow \sqrt{\frac{2}{\pi z}} e^{i(z - \frac{\pi\nu}{2} - \frac{\pi}{4})}, \quad (4.33)$$

as  $z \rightarrow \infty$  in  $-\pi + \delta \leq \text{ph}(z) \leq 2\pi - \delta$ , where  $\delta$  is an arbitrary small positive number. It has a branch point at  $z = 0$  and its principal branch corresponds to the principal value of the square root in (4.33), with a branch cut along  $(-\infty, 0]$  ( $\text{PV}(z^{-\frac{1}{2}}) = e^{-\frac{1}{2} \text{Ln} z}$  where  $\text{Ln} z = \text{Ln} r + i\vartheta$  with  $z = re^{i\theta}$  and  $-\pi < \vartheta \leq \pi$ ). From here on out  $H_\nu^{(1)}(z)$  will denote the principal value of the Hankel function. We also need the asymptotic behaviour of  $H_\nu^{(1)}(z)$  as  $z \rightarrow 0$  [57, Eqs. 10.7.2 – 10.7.7, 10.4.3]:

$$\begin{aligned}H_0^{(1)}(z) &\xrightarrow{z \rightarrow 0} \frac{2i}{\pi} \text{Ln} z \\ H_\nu^{(1)}(z) &\xrightarrow{z \rightarrow 0} -\frac{i}{\pi} \Gamma(\nu) e^{-\nu \text{Ln}(z/2)} \quad \text{for } \text{Re}(\nu) > 0 \\ H_{i\nu}^{(1)}(z) &\xrightarrow{z \rightarrow 0} A_\nu e^{i\nu \text{Ln}(z/2)} + B_\nu e^{-i\nu \text{Ln}(z/2)} \quad \text{for } \nu \in \mathbb{R}, \nu \neq 0\end{aligned}\quad (4.34)$$

where

$$A_\nu = \frac{1 + \coth(\pi\nu)}{\Gamma(1 + i\nu)}, \quad B_\nu = -\frac{\text{csch}(\pi\nu)}{\Gamma(1 - i\nu)} \quad (4.35)$$

Since our goal is to evaluate (4.32), we are here only interested in positive values of  $z$ . For finite  $\epsilon$ , as can be seen from (4.33), both integrals in the numerator and denominator of  $F(\epsilon, \Lambda)$  converge as  $\Lambda \rightarrow \infty$ . Moreover, the relations in (4.34) show that both integrals diverge in the limit  $\epsilon \rightarrow 0$ , which means we can first take  $\Lambda \rightarrow \infty$  and only concern ourselves with the behaviour of the integrands close to zero. Doing so, the second and third lines of (4.34) imply

$$\lim_{\epsilon \rightarrow 0} \lim_{\Lambda \rightarrow \infty} F(\epsilon, \Lambda) = -1 \quad \text{for} \quad \nu \geq 0. \quad (4.36)$$

and

$$\lim_{\epsilon \rightarrow 0} \lim_{\Lambda \rightarrow \infty} F(\epsilon, \Lambda) = \frac{2A_\nu B_\nu}{|A_\nu|^2 + |B_\nu|^2} = -\operatorname{sech} \pi |\nu| \quad \text{for} \quad \nu = i|\nu| \neq 0. \quad (4.37)$$

To derive this last equality, we have used the following properties of the Gamma function [57, Eqs. 5.5.1, 5.5.3, 5.4.3]:

$$\begin{aligned} \Gamma(z+1) &= z\Gamma(z) \\ \Gamma(z)\Gamma(1-z) &= \pi / \sin \pi z && \text{for } z \neq 0, \pm 1, \pm 2, \dots \\ |\Gamma(iy)| &= \sqrt{\pi/y \sinh \pi y} && \text{for } y \in \mathbb{R}. \end{aligned} \quad (4.38)$$

From these we can derive that  $\Gamma(1+i|\nu|)\Gamma(1-i|\nu|) = (i|\nu|)\Gamma(i|\nu|)\Gamma(1-i|\nu|) = i|\nu|\pi / \sin(i\pi|\nu|) = \pi|\nu| / \sinh \pi|\nu|$  and

$$|\Gamma(1 \pm i|\nu|)| = |\pm i|\nu|\Gamma(\pm i|\nu|)| = \sqrt{\pi|\nu| / \sinh \pi|\nu|}. \quad (4.39)$$

We thus obtain

$$\frac{2A_\nu B_\nu}{|A_\nu|^2 + |B_\nu|^2} = \frac{-2(1 + \coth \pi|\nu|) \operatorname{csch} \pi|\nu|}{(1 + \coth \pi|\nu|)^2 + \operatorname{csch}^2 \pi|\nu|} = -\operatorname{sech} \pi|\nu|, \quad (4.40)$$

which proves (4.37). Summarising our results:

$$r_k = \begin{cases} e^{i\pi(\nu - \frac{d}{2})} & \text{when } m \leq m_*, \\ e^{-i\pi\frac{d}{2}} \operatorname{sech} \pi|\nu| & \text{when } m > m_*. \end{cases} \quad (4.41)$$

Note that  $r_k$  does not, in fact, depend on  $k$ . We see that for masses  $m \leq m_*$ , the SJ prescription is not well defined in the limit  $\eta_{max} \rightarrow 0$ , since in that case  $|r_k| \rightarrow 1$ .

When  $m > m_*$ , we find that the Bogoliubov coefficients are

$$\alpha_k = \tanh^{-1} e^{-\pi|\nu|} \quad \text{and} \quad \beta_k = -\frac{D+1}{2}\pi. \quad (4.42)$$

This corresponds to the particular  $\alpha$ -vacuum known as the *out*-vacuum (see Section 4.2). More specifically, when  $m > m_*$ , the two point function of the SJ state in the Poincaré patch is equal to the restriction of the out-vacuum two-point function in this region.

### 4.3.2. The SJ state in the global patch

Again, we need the following  $L^2$  inner products:

$$\begin{aligned} \langle u_{Lj}^E, u_{L'j'}^E \rangle &= \langle y_L^E, y_L^E \rangle_t \delta_{LL'} \delta_{jj'}, \\ \langle \bar{u}_{Lj}^E, u_{L'j'}^E \rangle &= \langle \bar{y}_L^E, y_L^E \rangle_t (-1)^L \delta_{LL'} \delta_{jj'}, \end{aligned} \quad (4.43)$$

where we have defined the inner product  $\langle \cdot, \cdot \rangle_t$  that integrates over  $t$  only:

$$\langle f, g \rangle_t = \int_{-T}^T \overline{f(t)} g(t) \ell^d \cosh^d(t/\ell) dt. \quad (4.44)$$

We have introduced  $T$  as a regulator which will be sent to infinity below. The algebraic relations (2.57) and (2.58) can now be solved for in complete analogy to the previous section:

$$\begin{aligned} A_{Lj,L'j'} &= \cosh \alpha_L \delta_{LL'} \delta_{jj'} \\ B_{Lj,L'j'} &= \sinh \alpha_L e^{i\beta_L} \delta_{LL'} \delta_{jj'} \end{aligned}$$

and

$$\lambda_{Lj} = \sqrt{\langle y_L^E, y_L^E \rangle_t^2 - |\langle \bar{y}_L^E, y_L^E \rangle_t|^2}, \quad (4.45)$$

where

$$\alpha_L = \frac{1}{2} \tanh^{-1} |r_L|, \quad \beta_L = \arg(r_L) + \pi \quad (4.46)$$

and

$$r_L := (-1)^L \frac{\langle \bar{y}_L^E, y_L^E \rangle_t}{\langle y_L^E, y_L^E \rangle_t}. \quad (4.47)$$

We now evaluate this ratio. Substituting the mode functions into the inner products we obtain the expressions

$$\begin{aligned}\langle y_L^E, y_L^E \rangle_t &= 2 \int_0^T |y_L^E(t)|^2 l^d \cosh^d(t/l) dt \\ \langle \bar{y}_L^E, y_L^E \rangle_t &= 2 \int_0^T \operatorname{Re} [y_L^E(t)^2] l^d \cosh^d(t/l) dt.\end{aligned}\tag{4.48}$$

If we change the integration variables to  $z(t) = 1 + e^{2t/l}$ , these integrals become

$$\begin{aligned}\langle \bar{y}_L^E, y_L^E \rangle_t &= \frac{l^D}{2^{2a}} \operatorname{Re} \left[ \int_2^Z n_L^2 I_1(z) dz \right], \\ \langle y_L^E, y_L^E \rangle_t &= \frac{l^D}{2^{2a}} \int_2^Z |n_L|^2 I_2(z) dz,\end{aligned}\tag{4.49}$$

where

$$\begin{aligned}I_1(z) &:= (z-1)^{\nu-1} z^{2a} F(a, a+\nu; 2a; z(t) - i\epsilon)^2, \\ I_2(z) &:= (z-1)^{\operatorname{Re}(\nu)-1} z^{2a} |F(a, a+\nu; 2a; z(t) - i\epsilon)|^2.\end{aligned}\tag{4.50}$$

We have defined  $Z = z(T)$  and consequently the  $T \rightarrow \infty$  limit corresponds to  $Z \rightarrow \infty$ . With these definitions we have

$$\lim_{Z \rightarrow \infty} \frac{\langle \bar{y}_L^E, y_L^E \rangle_t}{\langle y_L^E, y_L^E \rangle_t} = \lim_{Z \rightarrow \infty} \frac{\operatorname{Re} \left[ n_L^2 \int_2^Z I_1(z) dz \right]}{|n_L|^2 \int_2^Z I_2(z) dz}.\tag{4.51}$$

At the lower end  $z = 2$  of the integration range both integrands are completely well-behaved, but they diverge in the limit where  $Z \rightarrow \infty$ . Therefore, it suffices to study the integrands in the limit  $Z \rightarrow \infty$ . There are two cases to consider.

When  $m \leq m_*$ , corresponding to real  $\nu$ , the asymptotic behaviour of the hypergeometric function given in (B.28) leads to

$$\begin{aligned}I_1(z) &\xrightarrow{z \rightarrow \infty} \gamma^2 e^{-2i\pi a} z^{\nu-1}, \\ I_2(z) &\xrightarrow{z \rightarrow \infty} |\gamma|^2 z^{\nu-1}.\end{aligned}\tag{4.52}$$

where (B.29)

$$\gamma = \frac{\Gamma(\nu)\Gamma(2a)}{\Gamma(a+\nu)\Gamma(a)}, \quad \xi = \frac{\Gamma(-\nu)\Gamma(2a)}{\Gamma(a-\nu)\Gamma(a)}$$

as derived in Section B.2 of Appendix B. Given that both quantities have the same

scaling with  $z$  in this limit, their ratio must converge to a constant when  $Z \rightarrow \infty$ :

$$\lim_{Z \rightarrow \infty} \frac{\langle \bar{y}_L^E, y_L^E \rangle_t}{\langle y_L^E, y_L^E \rangle_t} = \frac{\text{Re} [ |n_L|^2 e^{2i\vartheta_L} e^{-2i\pi a} ]}{|n_L|^2} = \cos[\pi(\nu - a)], \quad (4.53)$$

where  $\vartheta_L = \frac{\pi}{2}[a + \text{Re}(\nu)]$ . Here we have used the fact that  $\gamma$  is real when  $\nu$  is real.

When  $m > m_*$ , corresponding to imaginary  $\nu$ , it follows from (B.28) that

$$\begin{aligned} I_1(z) &\xrightarrow{z \rightarrow \infty} e^{-2i\pi a} z^{-1} \left[ 2\gamma\xi e^{\pi|\nu|} + \gamma^2 e^{i|\nu| \ln z} + \xi^2 e^{\pi|\nu|} e^{-i|\nu| \ln z} \right] \\ I_2(z) &\xrightarrow{z \rightarrow \infty} z^{-1} \left[ |\gamma|^2 + |\xi|^2 e^{2\pi|\nu|} + \gamma\bar{\xi} e^{i|\nu| \ln z} e^{\pi|\nu|} + \bar{\gamma}\xi e^{-i|\nu| \ln z} e^{\pi|\nu|} \right]. \end{aligned} \quad (4.54)$$

Again, since both quantities have the same scaling with  $z$  in this limit, the ratio of their integrals converges to a constant as  $Z \rightarrow \infty$ :

$$\lim_{Z \rightarrow \infty} \frac{\langle \bar{y}_L^E, y_L^E \rangle_t}{\langle y_L^E, y_L^E \rangle_t} = \frac{\text{Re} [ 2\gamma\xi |n_L|^2 e^{2i\vartheta_L} e^{-2i\pi a} ]}{|n_L|^2 (|\gamma|^2 + |\xi|^2 e^{2\pi\nu})} = \cos \pi a \text{sech} \pi |\nu|, \quad (4.55)$$

having used the fact that  $\gamma = \bar{\xi}$  when  $\nu$  is imaginary. Notice now that

$$\begin{aligned} \cos [\pi(\nu - a)] &= \cos(\pi L + \pi d/2 - \pi\nu) \\ &= (-1)^L \cos(\pi d/2 - \pi\nu) \\ &= (-1)^L \cos(\pi D/2 - \pi\nu - \pi/2) \\ &= (-1)^L \sin(\pi D/2 - \pi\nu). \end{aligned} \quad (4.56)$$

Similarly,  $\cos \pi a = (-1)^L \sin(\pi D/2)$ . Summarising our results:

$$r_L = \begin{cases} \sin\left(\frac{D}{2}\pi\right) \text{sech} \pi |\nu| & \text{if } m \geq m_*, \\ \sin\left[\left(\frac{D}{2} - \nu\right)\pi\right] & \text{if } 0 < m \leq m_*. \end{cases} \quad (4.57)$$

Again, we see that  $r_L$  is independent of  $L$ . Hence, so long as its modulus is not unity, the SJ state corresponds to one of the  $\alpha$ -vacua. The cases of even and odd spacetime dimensions look quite different, so we consider them in turn. For even  $D$ , (4.57) reduces to

$$r_L = \begin{cases} 0 & \text{if } m \geq m_*, \\ (-i)^{D-2} \sin \pi\nu & \text{if } 0 < m \leq m_*, \end{cases} \quad (4.58)$$



and for odd  $D$  we have

$$r_L = \begin{cases} (-i)^{D-1} \operatorname{sech} \pi|\nu| & \text{if } m \geq m_*, \\ (-i)^{D-1} \cos \pi\nu & \text{if } 0 < m \leq m_*. \end{cases} \quad (4.59)$$

When  $m \geq m_*$  and  $D$  is even,  $\alpha_L = 0$  and the SJ state is equal to the Euclidean state. In odd spacetime dimensions and above the critical mass we have

$$\alpha_L = \tanh^{-1} e^{-\pi|\nu|} \quad \text{and} \quad \beta_L = -\frac{D+1}{2}\pi, \quad (4.60)$$

which means that the SJ state is the *in/out*-vacuum. (The *in* and *out*-vacua are the same in odd dimensions as described in Section 4.2.3.) Below the critical mass, the Bogoliubov coefficients for even  $D$  are:

$$\alpha_L = \frac{1}{2} \tanh^{-1} |\sin \pi\nu| \quad \text{and} \quad \beta_L = \left[ \frac{D}{2} + \theta(-\sin(\pi\nu)) \right] \pi \quad (4.61)$$

and for odd  $D$ :

$$\alpha_L = \frac{1}{2} \tanh^{-1} |\cos \pi\nu| \quad \text{and} \quad \beta_L = \left[ \frac{D+1}{2} + \theta(-\cos(\pi\nu)) \right] \pi, \quad (4.62)$$

where  $\theta(x)$  is the Heaviside step function. In even dimensions, we obtain  $\alpha = 0$  whenever  $|\nu|$  is an integer, in which case the SJ state then corresponds to the Euclidean state. Whenever  $|\nu|$  is a half-integer, the Bogoliubov coefficients diverge. The same holds in odd dimensions but with integer  $\leftrightarrow$  half-integer. A summary of the different SJ vacua in the global and Poincaré patches of de Sitter space is shown in Table 4.1 in the conclusion of this chapter.

It is worth noting that the conformally coupled massless field corresponds in every spacetime dimension to the value  $\nu = \frac{1}{2}$ : through its coupling to the constant Ricci scalar, the conformally coupled field acquires an effective mass of

$$m_{cc} = \frac{1}{2} \sqrt{(D-2)/(D-1)R} = \frac{1}{2\ell} \sqrt{D(D-2)}, \quad (4.63)$$

which yields  $\nu = \ell \sqrt{m_*^2 - m_{cc}^2} = \frac{1}{2}$  (which is always below the critical mass  $m_*$ ). Hence, the SJ state for the conformally coupled massless scalar field on the global patch is ill-defined in even dimensions, but corresponds to the Euclidean state in odd dimensions (and is therefore Hadamard). It was found in [11] that the SJ state is *never* Hadamard on finite sections of the Einstein static universe (ESU)  $\mathbb{R} \times S^d$ .

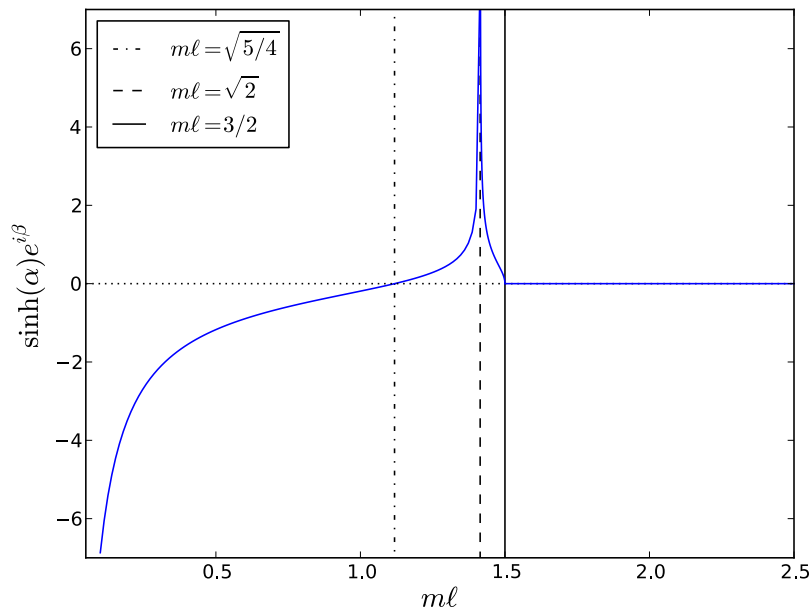


Figure 4.2.: The SJ state in the global patch of 3+1 dimensional de Sitter space. The SJ modefunctions  $u_{L_j}^{SJ}$  are related to those of the Euclidean vacuum  $u_{L_j}^E$  by the Bogoliubov transformation  $u_{L_j}^{SJ} = \cosh(\alpha)u_{L_j}^E + \sinh(\alpha)e^{i\beta}\bar{u}_{L_j}^E$ , the second coefficient of which is plotted here. Depending on the product  $m\ell$ , where  $m$  is the mass of the field and  $\ell$  is the de Sitter radius, the SJ state corresponds to different  $\alpha$ -vacua. For  $m\ell \geq 3/2$  and  $m\ell = \sqrt{5}/4$ , it coincides with the Euclidean vacuum. The prescription fails for  $m\ell = \sqrt{2}$ .

While de Sitter space is conformally related to a finite section of the ESU, these findings are not in contradiction with each other, since the SJ state is not invariant under conformal transformations even for conformally coupled fields (as mentioned above, this follows essentially from the fact that the  $L^2$  inner product, unlike the Klein-Gordon inner product, is not conformally invariant).

Let us take a closer look at the case of macroscopic physical spacetime,  $D = 3 + 1$ . As we have shown above, the SJ state is the Euclidean state when  $m \geq m_* = 3/2\ell$ . Below the critical mass, the SJ state is a de Sitter invariant  $\alpha$ -vacuum, except when  $m = m_{cc} = \sqrt{2}/\ell$ , in which case the SJ prescription is not well-defined because the Bogoliubov coefficients diverge. The magnitude of the second Bogoliubov coefficient as a function of  $m$  is shown in Figure 4.2.

### 4.3.3. The critical mass $m_*$

Some comments regarding the critical mass are in order, since it plays such a prominent role in the results above. Most notable is the peculiar behaviour of the SJ state for fields of subcritical mass. It is perhaps not surprising that *something* changes in this regime, since  $m_* = \frac{d}{2\ell} \sim \ell^{-1}$  is the mass scale below which the Compton wavelength of the field becomes larger than the Hubble scale. The first relevant observation is that in global coordinates, the *in*- and *out*-modes have the asymptotic expansions

$$\begin{aligned} u_{L_j}^{in}(t, \theta) &\sim e^{(\frac{d}{2}-i|\nu|)t} & \text{as } t \rightarrow -\infty \\ u_{L_j}^{out}(t, \theta) &\sim e^{(-\frac{d}{2}-i|\nu|)t} & \text{as } t \rightarrow +\infty \end{aligned} \quad (4.64)$$

for  $m > m_*$  and

$$\begin{aligned} u_{L_j}^{in}(t, \theta) &\sim e^{(\frac{d}{2}+|\nu|)t} & \text{as } t \rightarrow -\infty \\ u_{L_j}^{out}(t, \theta) &\sim e^{(-\frac{d}{2}+|\nu|)t} & \text{as } t \rightarrow +\infty \end{aligned} \quad (4.65)$$

for  $m \leq m_*$ . The first equation illustrates explicitly the statement made earlier, that the *in*- and *out*-modes are the “positive frequency” modes with respect to  $\partial_t$  at  $t \rightarrow \pm\infty$  (since they have factors of the form  $e^{-i\omega t}$  with  $\omega > 0$ ). We see, however, that for  $m \leq m_*$ , this characterisation loses its meaning: in the asymptotic limits, the modes fail to oscillate with respect to  $t$  and instead just decay exponentially (that the exponentials in (4.65) are always decaying is guaranteed by the fact that  $|\nu| < \frac{d}{2}$  for  $m \leq m_*$ ). A related observation was made by E. A. Tagirov in a 1972 paper [52]: the de Sitter propagators, as functions of the geodesic distance rather than some particular time coordinate, decrease “aperiodically and more slowly” for  $m < m_*$  than for  $m \geq m_*$  in the limit of large time-like separation between their arguments (he also goes on to argue that this is by itself no reason to label the theory unphysical for  $m \leq m_*$ ). Recall that on the upper Poincaré patch, the SJ state corresponds to the out state above the critical mass and is ill-defined below the critical mass. Given that the usual physical interpretation of the *in*- and *out*-vacua loses its justification for fields of subcritical mass, it is not unreasonable to imagine that the breakdown of the SJ procedure is tied to these observations. How this happens concretely is, however, not yet clear, especially since we obtain such different results on the Poincaré patch and on the global patch. The breakdown of the SJ prescription on the Poincaré patch for  $m \leq m_*$  also resonates with some previous findings in the literature. For instance, it is possible to define a unique

quantum state on de Sitter space by smearing the positive frequency modes of the embedding Minkowski space onto the de Sitter hyperboloid [58, 59], but the method only works when  $m > m_*$ . Taken together, these observations help put our results into context and shed some light on the phenomena encountered above, but it is safe to say that some questions about the deeper physical picture remain open.

#### 4.4. The discrete SJ state on a sprinkling into $dS^2$

Let us now compare the discrete SJ two-point function with the known propagators in continuum de Sitter space, we evaluate it on a causal set that is obtained by a sprinkling into a causal interval (diamond) in  $1 + 1$  dimensional continuum de Sitter space. In de Sitter space, the spacetime volume  $V$  of the causal interval between two timelike points depends only on their Lorentzian distance  $\tau$ :  $V = 4\ell^2 \ln(\cosh(\tau\ell^{-1}/2))$ . We shall refer to a causal diamond of *length*  $\tau$  as one whose volume is given by the formula above.

##### 4.4.1. Sprinkling into a causal diamond in $dS^2$

To produce a sprinkling  $(\mathcal{C}_D, \prec)$  into a causal diamond  $D$  in  $dS^2$ , we need to pick a coordinate chart. The cosmological coordinates  $x_p^\mu$  defined in (4.8) are well suited because they have a conformally flat metric, which makes it particularly simple to compute the causal relation between points, given their coordinate values. Even though this chart only covers half of de Sitter space, there is no loss of generality because the symmetries of de Sitter space imply that any causal diamond can be isometrically mapped to a causal diamond entirely contained in the Poincaré patch.

So let  $D$  be a causal diamond between two points  $p, q \in dS^2_P$  such that  $p \prec q$ . Denote the (timelike) geodesic distance between  $p$  and  $q$  by  $\tau$ . Since any two causal diamonds with the same value of  $\tau$  are isometric, we choose  $x_p^\mu = (\eta_\tau, 0)$  and  $x_q^\mu = (\ell^2/\eta_\tau, 0)$  with

$$\eta_\tau = -\ell e^{\tau/2\ell} < -\ell, \tag{4.66}$$

without loss of generality. To obtain a sprinkling  $(\mathcal{C}_D, \prec)$  into  $D$  we first generate a uniform Poisson distribution of  $N$  points in the square  $[0, 1]^2$  using a Mersenne Twister algorithm [60]. We use Cartesian coordinates  $y_1, y_2$  on  $[0, 1]^2$  and find an

embedding  $\varphi : [0, 1]^2 \rightarrow R$ , which for any subset  $A \subset [0, 1]^2$  satisfies

$$V_D \int_A dy_1 dy_2 = \int_{\varphi(A)} d^2x \sqrt{-g}. \quad (4.67)$$

The factor  $V_D$  on the left hand side guarantees that the embedding scales the volume correctly. Its value for the causal diamond of length  $\tau$  is

$$V_D = 4\ell^2 \ln \cosh \frac{\tau}{2\ell}. \quad (4.68)$$

By inspection it can be shown that the embedding  $\varphi : (y_1, y_2) \rightarrow (\eta, x)$  defined by [61]

$$\begin{aligned} \eta &= \frac{-\ell e^{\tau/2\ell}}{1 + y_1(e^{\tau/\ell} - 1)}, \\ r &= (1 - 2y_2) \sinh \frac{\tau}{2\ell}, \end{aligned} \quad (4.69)$$

satisfies the above condition (4.67). By keeping only such points for which  $|x| < \min(\eta_\tau - \eta, \eta - \ell^2/\eta_\tau)$  and recording the causal relations among them, we obtain a sprinkling  $(\mathcal{C}_D, \prec)$  into  $D$ . Note that, as explained above, we also calculate the geodesic distance between any two points using the metric on the manifold, even though this data is not explicitly part of  $(\mathcal{C}_D, \prec)$ .

#### 4.4.2. Simulation results

In order to compare causal set results with those of the continuum, we have computed the retarded propagator  $\mathbf{R}$ , and subsequently the discrete Hadamard function  $\mathbf{H}_{SJ}$ , on an  $N = 1010$  element sprinkling into a causal diamond of length  $\tau = 8\ell$  in  $1 + 1$  dimensional de Sitter space (implying  $\rho \simeq 76\ell^{-2}$ ). The sprinkling is shown in Figure 4.3, where we have set  $\ell = 1$ .

Figure 4.4 shows values of the retarded propagator  $\mathbf{R}_{ij}$  for all pairs of related events  $(\nu_i, \nu_j) \in \mathcal{C}_D$ , plotted as a function their geodesic distance  $d_{ij}$ . There is good agreement between the mean of  $\mathbf{R}$  and the continuum retarded Green function (whose functional form may be obtained from (4.18) as described in Section 4.2.3), which further validates the proposal (2.22). At large  $\tau \gg \ell$ , we see a slight deviation between the mean of the causal set data and the continuum retarded Green function. This discrepancy can be associated with edge-effects due to the finite size of the causal diamond: pairs of points separated by a geodesic distance comparable to

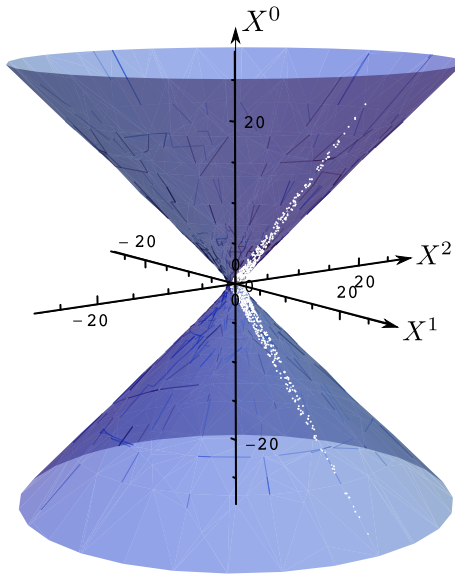


Figure 4.3.: An  $N = 1010$  element sprinkling with density  $\rho = 76\ell^{-2}$  into a causal diamond of length  $\tau = 8\ell$  in two-dimensional de Sitter space, visualised in the embedding three-dimensional Minkowski space (see Section 4.1). The de Sitter radius has been set to  $\ell = 1$ .

the size of the diamond will feel the boundaries of the spacetime region (the effect of spacetime boundaries has been addressed in more detail in [1]). Figure 4.5 shows the discrete SJ Hadamard function  $\mathbf{H}_{SJ}$ , computed for both timelike and spacelike pairs of events. Since we have no expression for the continuum SJ state in the causal diamond itself, we cannot compare  $\mathbf{H}_{SJ}$  with its *exact* continuum counterpart. However, the expectation would be that the discrete SJ two-point function approximates that of a de Sitter invariant vacuum in the centre of the diamond (where the boundaries of the diamond are felt the least). Indeed, Figure 4.5 shows a very good agreement between the mean of  $\mathbf{H}_{SJ}$  and the Hadamard function associated with the Euclidean vacuum ( $\alpha = 0$ ). At large  $\tau \gg \ell$ , the boundary effects become noticeable again. To highlight the particular agreement with the Euclidean ( $\alpha = \beta = 0$ ) Hadamard function, we have also plotted in Figure 4.5 the Hadamard function of two other  $\alpha$ -vacua with  $(\alpha, \beta) = (1, 0)$  and  $(\alpha, \beta) = (0.1, 0)$ . Note that  $H_{\alpha, \beta}(x, y)$  is more sensitive to variations in  $\alpha$  for spacelike separated arguments because of the extra antipodal singularity at  $d(x, y) = \pi\ell$ , i.e.  $Z(x, y) = -1$ , present in every  $\alpha$ -vacuum except the Euclidean one (see Section 4.2). For instance, for the range of parameters we have probed in our simulations, including those of Figure 4.5, the

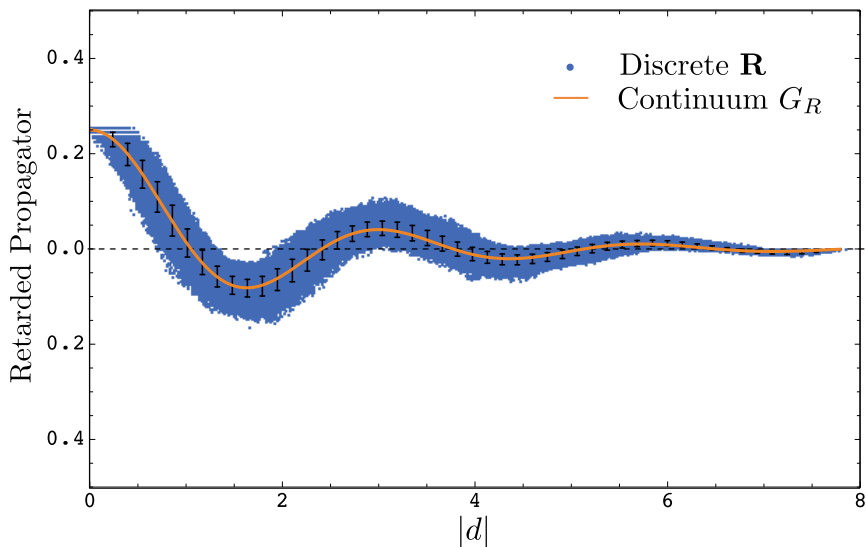


Figure 4.4.: The retarded propagator  $\mathbf{R}$ , computed on a causal set obtained via a  $N = 1010$  sprinkling into a causal diamond of length  $\tau = 8\ell$  in  $1 + 1$  dimensional de Sitter space. The mass of the field is  $m = 2.36\ell^{-1}$  and the de Sitter radius  $\ell$  is set to unity. The geodesic distance  $|d|$  between the two arguments of the function is plotted on the horizontal axis. The error bars show the standard deviation about the mean of  $\mathbf{R}$  for binned values of  $|d|$ . The continuum propagator  $G_R$  is shown with the thick black line.

function  $H_{0,1,0}$  as a function of the geodesic distance can be distinguished from the Euclidean Hadamard function for spacelike separated arguments, whereas it lies on top of the Euclidean Hadamard function for timelike separated arguments (and has thus been omitted from the timelike plot). With the parameters probed in our simulations, we cannot discriminate between the in/out and the Euclidean vacua, since they are very “close” unless  $m \sim m_*$ . Indeed, for the values presented here we have  $\alpha_{in} = \alpha_{out} = \mathcal{O}(10^{-4})$ . Discriminating between the in/out and Euclidean vacua is more demanding computationally. A full treatment of this matter will require more extensive simulations.

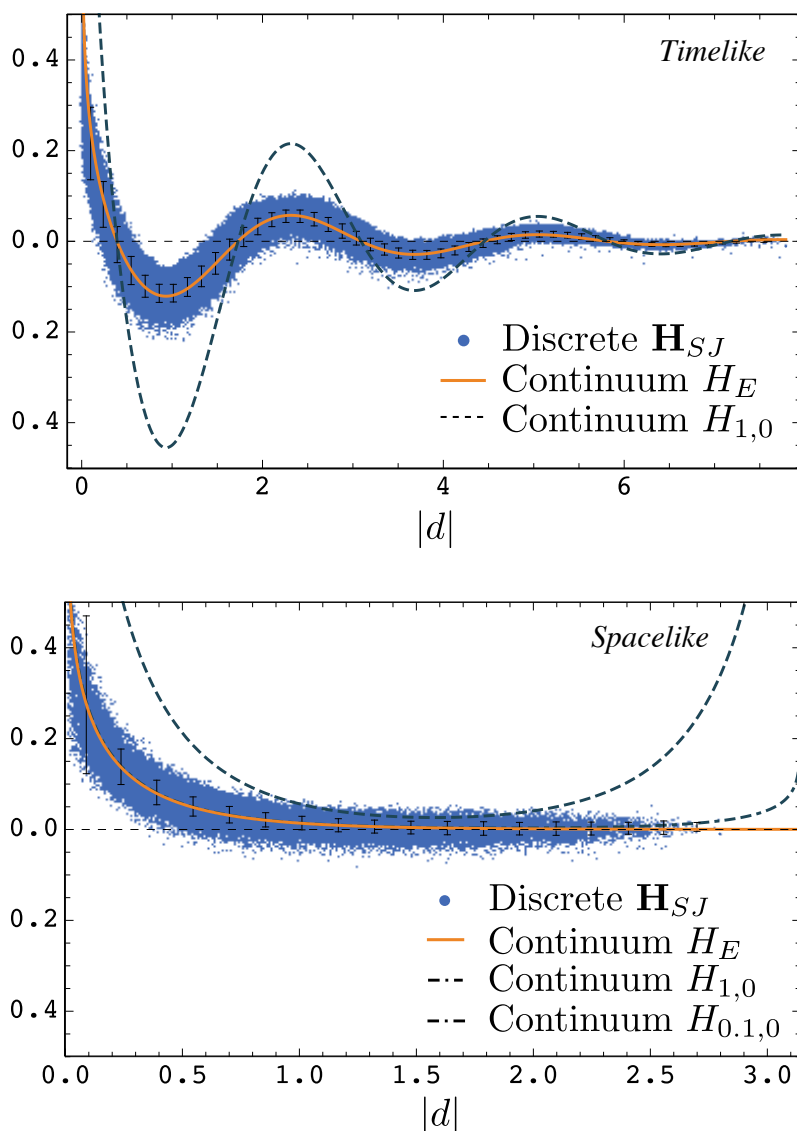


Figure 4.5.: The Hadamard function  $\mathbf{H}_{SJ}$  on an  $N = 1010$  sprinkling of into a causal diamond of length  $\tau = 8\ell$  in  $1+1$  dimensional de Sitter space. The mass of the field is taken to be  $m = 2.36\ell^{-1}$ , and the de Sitter radius  $\ell$  is set to unity. The geodesic distance  $|d|$  between the two arguments of the function is plotted on the horizontal axis for timelike (above) and spacelike (below) separated points. The error bars show the standard deviation about the mean of  $\mathbf{H}_{SJ}$  for binned values of  $|d|$ .  $H_{\alpha,\beta}(x,y)$  refers to the Hadamard function of the  $\alpha$ -vacua (see Section 4.2). The function  $H_{0.1,0}$  has been omitted in (a), since it is indistinguishable from the Euclidean function  $H_E$ .



Patch	Dimension	SJ state for $m \geq m_*$	SJ state for $m < m_*$
Global	even	Euclidean	$\alpha$ -vacuum (4.61)
	odd	in = out	$\alpha$ -vacuum (4.62)
Poincaré	even	out	not defined
	odd	in = out	not defined

Table 4.1.: The SJ state in the global and Poincaré patches of de Sitter space. Depending on the mass  $m$  of the field, the SJ state corresponds to different  $\alpha$ -vacua (the Euclidean, in- and out- vacua are all special cases of  $\alpha$ -vacua and in odd spacetime dimensions the in- and out-vacua coincide). The critical mass that marks these transitions is  $m_* = \frac{d}{2\ell}$ , where  $d$  is the spatial dimension and  $\ell$  is the de Sitter radius.

## 4.5. Conclusions

To summarise, let us state the results we have derived for the SJ state in the continuum, as given in Table 4.1. In the cases where the prescription gives well-defined results, the SJ state always corresponds to one of the de Sitter-invariant  $\alpha$ -vacua. This is reassuring, because a covariant approach should give rise to a vacuum state that respects the symmetries of the underlying spacetime. Furthermore, we find that the SJ state depends on (i) whether the mass of the field is above or below the critical value  $m_* = \frac{D-1}{2\ell}$  (where  $\ell$  is the de Sitter radius and  $D$  is the spacetime dimension), (ii) whether it is evaluated on the complete de Sitter manifold or its Poincaré half-space, and (iii) whether the spacetime dimension is even or odd.<sup>3</sup> For a field of mass  $m \geq m_*$  in even spacetime dimensions, the SJ state corresponds to the Euclidean vacuum on the global patch and to the out-vacuum on the Poincaré patch. For  $m < m_*$  on the Poincaré patch, as well as for a discrete set of mass values below  $m_*$  on the global patch, the SJ prescription cannot be applied to the entire spacetime, but only to a bounded globally hyperbolic subregion of it.

It would be interesting to investigate whether a physical account can be given for the failure of the procedure in this particular case (an example of another vacuum prescription which fails for light masses is the instantaneous ground state of the Hamiltonian, particularly in the global patch [63]). Here it is worth noting that the complementary and principal series also exhibit different behaviours in the case of

<sup>3</sup>The critical mass  $m_*$  separates the so-called principal ( $m \geq m_*$ ) and complementary ( $m < m_*$ ) series of de Sitter representations [62].

interacting theories [64, 65]. For instance, quantum-corrected fields whose bare mass belong to the principal series, unlike the complementary series, decay faster than the free Klein-Gordon field in past/future infinity. This has important consequences for objects such as the S-matrix for QFTs on global de Sitter space [66, 67, 68].

We return briefly to the observation, made by Fewster and Verch [11], that the SJ state in general fails to be a Hadamard state. With de Sitter space we have a concrete example at hand, since the  $\alpha$ -vacua are not Hadamard unless  $\alpha = 0$  (their two-point functions have an additional divergence when the antipode of one argument is on the light-cone of the other; see (4.21) and [45]). The main advantage of Hadamard states is that for such states it is known how to construct physically relevant expectation values, such as those of the stress-energy tensor, on arbitrarily curved spacetimes [69, 70, 71]. Although it has not been proven that this cannot be done for  $\alpha$ -vacua, it is known that standard prescriptions such as point-splitting and normal ordering fail [72]. One explanation proposed in [1], is that the non-Hadamard singularity structure of the SJ state arises as a consequence of the sharp spacetime boundaries that are implicit in the definition of the SJ modes (c.f. the sharp limits in the  $L^2$  inner products for the bounded spacetime regions above). The effect of these boundaries will be felt most heavily by high-frequency modes and so, by “smoothing the boundary”, one could hope to tweak the ultraviolet behavior of the SJ state so that it becomes Hadamard. That this idea bears out to some extent has recently been proven by Brum and Fredenhagen [73]. They study a modification of the SJ state that relies on a smooth cut-off of the commutator function and find that this modification *always* leads to Hadamard states on the class of spacetimes they study (static and “expanding” spacetimes with compact Cauchy surfaces). Due to the smoothing, these modified states are, however, no longer uniquely associated to the spacetime. At the end of this thesis we will offer some further comments on the question as to whether or not the failure of the Hadamard condition spoils the original (un-smoothened) SJ proposal as such.

Using the discrete SJ formalism on a causal set, we have determined the SJ state on a sprinkling of a causal diamond in  $1 + 1$  dimensional de Sitter space. As part of our analysis, we have found evidence that the “discrete retarded propagator” proposed in [74] agrees well with the continuum retarded propagator in de Sitter space. Our simulation also shows that the mean of the discrete SJ two-point function is consistent with that of an  $\alpha$ -vacuum and in particular with that of the Euclidean va-

---

cuum in the centre of the diamond (away from the edges) for a field of mass  $m \ll \sqrt{\rho}$ . This is encouraging, since the QFT defined on causal sets by the SJ formalism seems to reproduce what one would expect: a state that respects the spacetime isometries in the appropriate “continuum limit”. It would be interesting to carry out further simulations to determine, with more statistical significance, which continuum state is best approximated by the discrete SJ state. This might be particularly illuminating when  $m < m_*$ , since the procedure in the continuum becomes pathological in the Poincaré patch in that case.

It is natural to wonder whether the SJ formalism could have phenomenological implications in relation to cosmology. Two questions seem particularly relevant here. Firstly, because of its non-local nature, it is not clear what portion of spacetime one should use to compute the SJ state. For instance, should one consider the behaviour of late-time cosmology to determine the SJ state for the early universe? In any case, our current calculations are not realistic because the cosmos is not *always* in a de Sitter phase. It would be more interesting to compute the SJ state in the case of a single-field slow-roll inflationary background, in which case the near-de Sitter phase does end. These are all questions that could be addressed in future work.

## 5. Remarks on the SJ state in the trousers spacetime

So far, the spacetimes we have considered have all been globally hyperbolic. Global hyperbolicity is an important property in the usual construction of quantum field theory in flat and curved spacetime, since it guarantees that linear hyperbolic equations such as the Klein-Gordon equation admit a well-posed initial value problem and have well defined global advanced and retarded propagators [16, 75]. Yet there are situations in which one may like to consider spacetimes that fall short of the criterion. Anti de Sitter space is perhaps the most famous example of a spacetime that is not globally hyperbolic and yet of tremendous interest in the context of the gauge-gravity (AdS/CFT) correspondence [76]. Another case, the one that we will pay attention to in this chapter, is that of spacetimes experiencing topology-change. Such spacetimes cannot be globally hyperbolic: a globally hyperbolic Lorentzian manifold must be homeomorphic to  $\Sigma \times \mathbb{R}$  [77] and hence its spatial topology frozen in time.

At the level of the manifold topology itself, a frozen spatial topology is certainly not forced upon us. In fact, in  $D = 3 + 1$  and lower dimensions, given *any* two initial and final topologically distinct  $(D - 1)$ -dimensional (compact) manifolds  $V_i$  and  $V_f$ , there always exists a (compact)  $D$ -dimensional manifold  $M$  that interpolates between the two.<sup>1</sup> When attempting to put a Lorentzian metric on  $M$ , a theorem by Geroch [78] tells us that the metric must contain closed timelike curves. If we want to avoid the pathologies that go along with closed timelike curves [79, 80], we are still left with the alternative of considering metrics that are Lorentzian *almost everywhere* (degenerating at a finite set of isolated points) and which retain a well-defined causal structure [81], or, going further, considering metrics with signature change [82] or Euclidean signature [83].

In the context of quantum gravity, there are reasons to believe that topology-change is part of the story. Wheeler [84], using order-of-magnitude arguments and

---

<sup>1</sup>The manifold  $M$  with  $\partial M = V_i \sqcup V_f$  is known as a topological cobordism.

---

applying the uncertainty principle to the gravitational field, argued that fluctuations in spacetime curvature at Planckian scales should become so violent as to cause portions of space to pinch off or become multiply connected. From the point of view of a gravitational sum-over-histories, dimensional analysis also suggests that structures of Planckian size will have a gravitational action of order  $\hbar$ , which would lead to very little suppression in the gravitational path-integral [79]. Such considerations imply that, at least on a kinematical level, Planck scale topology-change should be taken into account in a quantum theory of gravity. To some workers in the field, topology-change is in fact *desirable*. For instance, the particle picture of quantum gravity — the theory that particles of ordinary matter are made of non-trivial topological structures in space (“topological geons”) [85, 86] — suffers from violations of the spin-statistics correlation and other problems in a framework with frozen spatial topology. Allowing topological fluctuations might help resolve some of these issues [81, 87].

If Planck scale topology-change is kinematically plausible, the question remains whether it is dynamically possible. This may seem impossible to answer without a theory of quantum gravity, but we can hope to find clues by following one of the usual top-down (semi-classical) approaches: fix a classical topology-changing spacetime (i.e. a non-trivial topological cobordism endowed with a metric according to one of the alternatives compatible with Geroch’s theorem) and study the action of the classical metric with linear-order quantum fluctuations. A first step in this direction can be made by investigating a free massless scalar quantum field coupled to the classical metric, thus placing the question within the framework of “scalar quantum field theory in curved spacetime” of the preceding chapters.

The first work along these lines was carried out by Anderson and DeWitt [88], who studied the quantum theory of a free massless scalar field on the topology-changing two-dimensional “trousers” spacetime, in which a circle splits into two (or vice-versa), viz. Figure 5.1. This spacetime admits an almost everywhere Lorentzian metric, which is the flat Minkowski metric everywhere except at an isolated singular point — the “crotch singularity” — on the spatial hypersurface which separates the two spatial topologies. At the singular point the equations of motion degenerate and hence the rule by which to propagate solutions past it must be specified by hand. Expanding the scalar field in terms of modes on a spacelike hypersurface in one region (the “in”-region) and choosing a particular “shadow rule” to propagate the modes past the topology-changing hypersurface into an “out”-region, Anderson and DeWitt found that the expectation value of the “out” stress-energy tensor

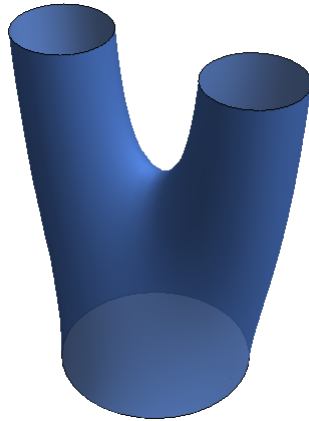


Figure 5.1.: The “trousers” spacetime with topology-change  $S^1 \leftrightarrow S^1 \times S^1$ .

evaluated in the “in”-vacuum has incurable (squared Dirac-delta) divergences on the lightcone of the singular point. They concluded that the trousers-type topology-change is dynamically forbidden. Manogue et al. [89] revisited the problem in a more careful analysis. They argued that the propagation rule of Anderson and DeWitt is unphysical because the Klein-Gordon product between two solutions obtained by propagating forward initial data past the topology-changing hypersurface is not conserved. Deriving a one-parameter family of propagation laws that conserve the inner product they arrived at the same conclusion, an infinite burst of energy emanating from the crotch singularity.

These results may at first be disappointing to those who hope that a quantum theory of gravity will incorporate topology-change. Of course, it could always be the case that the approximations made in such top-down calculations turn out to be wrong, but then again, without a bottom-up theory at hand, semi-classical calculations are one of the only tools we have to guide us. There are, however, good reasons why topology-change may still be physically viable even if the particular type of topology-change of the trousers spacetime is disallowed. The transition in the trousers belongs in a sense to a particularly singular class of topology-changes [90], those in which the spacetime exhibits “causal discontinuity”, which means (roughly) that the volume of the causal past or future of a point can change discontinuously as the point moves continuously around the manifold. The authors of [91] found that causally discontinuous topology changing processes in  $1 + 1$  dimensions are indeed

suppressed in a sum-over-histories, while causally continuous ones are enhanced. Such observations lend some support to Sorkin’s conjecture that infinite energy production occurs in a topology-changing spacetime<sup>2</sup> *if and only if* it contains a causal discontinuity.

In this chapter we present the results of first efforts to address the problem within the framework of the SJ formalism. This approach works directly with propagators rather than with the field operator expanded in modes. The freedom in specifying a propagation law corresponds to a freedom in choosing retarded and advanced Green functions. Once these are specified, however, the formalism should select a quantum state without further input. In light of the previous paragraph, the expectation would be to *confirm* previous findings in the trousers spacetime. The hope is to gain new insights by revisiting the problem from a new point of view, to understand the SJ framework in a more general setting, and to lay the foundation for semiclassical calculations in other topology-changing spacetimes.

## 5.1. Quantum Fields in the trousers spacetime

Keeping with tradition we hang the trousers upside down and use a coordinate chart in which  $t = 0$  separates the “legs” and the “trunk”. The spatial coordinate  $x$  lies in the range  $[-\lambda, \lambda]$  and the crotch singularity lies at the origin:  $x_c = (0, 0)$ . The coordinates in the trunk extend to coordinates in the left and right legs, i.e. we identify points  $(x, 0^+)$  in the legs with points  $(x, 0^-)$  in the trunk for  $x \neq 0$ . In the trunk, i.e. for  $t < 0$ , we identify  $x = -\lambda$  with  $x = \lambda$ . In the left leg, i.e. for  $t > 0$ , we identify  $x = -\lambda$  with  $x = 0^-$  and in the right leg we identify  $x = \lambda$  with  $x = 0^+$ . An illustration of the spacetime is shown in Figure 5.2.

We will attempt to build the SJ state by identifying the positive eigenmodes of  $i\Delta$  as we did in the analysis of the flat diamond. For this, we need the Pauli-Jordan function  $\Delta = G_R - G_A$ , and thus the retarded and advanced Green functions in the trousers.

There are two ways in which the Green functions in the trousers differ from those in Minkowski space. The first is due solely to the topology of the spatial sections before and after the topology-change and is largely independent of the questions

---

<sup>2</sup>More precisely, a topological cobordism endowed with an almost everywhere Lorentzian metric, i.e. the first alternative of those mentioned above for turning topological cobordisms into geometries.

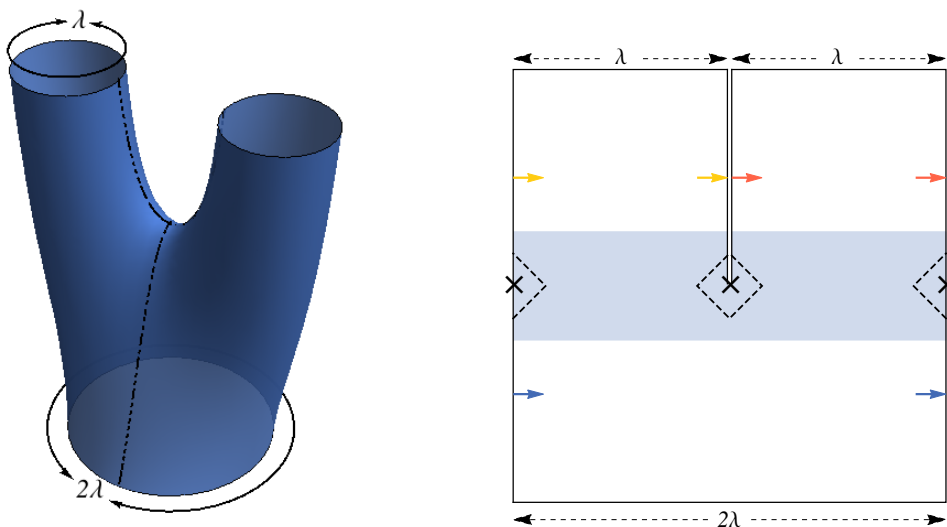


Figure 5.2.: The trousers spacetime (left) and a two-dimensional representation of it (right) obtained by cutting and unwrapping the manifold. The coloured arrows indicate the respective identifications in the trunk (blue) and in the left and right legs (yellow and red). The crosses mark the location of the crotch singularity.

pertaining to topology-change. Consider the quantum field theory on a flat cylinder  $S^1 \times \mathbb{R}$  (no topology-change). The metric is Minkowskian and so the propagators are locally Green functions to the usual wave equation. However, the future/past lightcone of any point will wrap around the cylinder, which makes it inconsistent to use the naive solution  $G_R^M(x, y)$  of two-dimensional Minkowski space  $\mathbb{M}$ , which is equal to  $-\frac{1}{2}$  in the causal past of  $x$  (and zero everywhere else). At the first conjugate point  $p_x$  to the past of  $x$  (the point where the two past-directed null geodesics emanating at  $x$  meet again), the naive Green function will take on the form  $-\frac{1}{2}(1 - \theta(-u)\theta(-v))$  in light-cone coordinates centred at  $p$ . This produces a negative Dirac-delta type source  $-\delta^{(2)}(x - p_x)$  in  $\square_x G_R(x, y)$  and therefore the naive propagator will not be a Green function. However, it is not hard to obtain a modification that *will* be a Green function, by simply taking  $G_R^M(x, y)$  and adding to it a (multiple of)  $G_R^M(p_x, y)$  for every conjugate point  $p_x$  such that the divergences in the original function are cancelled.

The observations in the previous paragraph are not particular to the trousers — they simply concern well-known facts of quantum field theory on the cylinder. In order to isolate the features of the trousers spacetime that are most pertinent to the



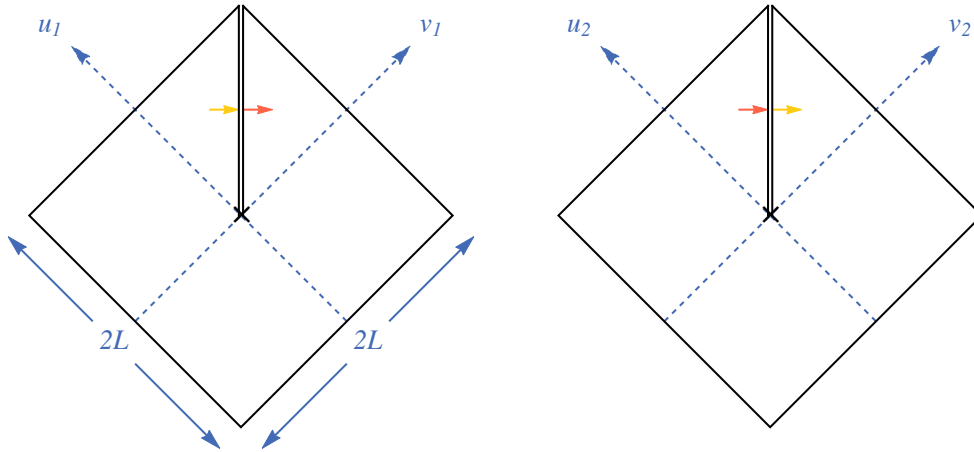


Figure 5.3.: The pair of diamonds in more detail. The coloured arrows indicate the topological identifications inherited from the trousers (Figure 5.2).

physics of topology-change, we can first restrict ourselves to a small enough section of the trousers containing the singularity such that no wrapping around occurs, e.g.  $|t| \leq t_{max}$  for some  $t_{max} < \frac{\lambda}{4}$  as shown in Figure 5.2 (the upper bound of  $\frac{\lambda}{4}$  guarantees that the future lightcone of a point in the causal past of the singularity does have time to wrap around one of the legs). In fact, it will be most convenient to restrict our analysis to a small causally convex neighbourhood around the singularity. Hence consider two points, one in the left and one in the right leg, both in the chronological future of the singularity:  $x_L^\pm = (t_0, \pm\epsilon)$ . Take the intersection of the union of their causal pasts with the causal future of a point in the trunk,  $x_T = (-t_0, 0)$ , which lies in the chronological past of the singularity. In the limit that the two points  $x_L^\pm$  are chosen to lie arbitrarily close to  $x = 0$  this region of spacetime will consist of the two diamonds drawn with dashed lines in Figure 5.2. We refer to this spacetime as the *pair of diamonds*. Figure 5.3 gives a more detailed depiction of the pair of diamonds, with the topological identifications inherited from the trousers. This spacetime has the same essential causal properties as the topology-changing trousers.

## 5.2. The pair of diamonds

In order to discuss the pair of diamonds and functions on it we need to construct a coordinate chart that covers the spacetime. When we depict the two diamonds next to each other, the left diamond is meant to correspond to the diamond seen in

the centre of the trousers (Figure 5.2) and the right diamond is made up of the two halves at the sides of the trousers. We will refer to the left and right diamonds as diamond 1 (symbol  $D_1$ ) and diamond 2 (symbol  $D_2$ ). Hence the upper left and right corners in diamond 1 respectively belong to the left and right legs, whereas the upper left and right corners in diamond 2 respectively belong to the right and left legs. Now define two identical coordinate systems with subscripts 1 and 2 on  $D_1$  and  $D_2$ . We will use both Cartesian and light-cone coordinates below and we shall label them in the obvious manner, e.g.  $(u_1, v_1)$  and  $(u_2, v_2)$  denote light-cone coordinates on  $D_1$  and  $D_2$  respectively. The relationship between the trousers coordinates (without subscript) defined above and the coordinates on the two diamonds are as follows. On diamond 1 the coordinate systems agree since their origin is the same. So  $t_1 = t, x_1 = x, u_1 = u$  and  $v_1 = v$ . On diamond 2, the left side comes from the right edge of the trousers and the right side comes from the left edge of the trousers, so the relations between the coordinates on  $D_2$  and those in the trousers are

$$\begin{array}{l}
 t_2 = t \\
 x_2 = x - \lambda \quad \text{for } x > 0 \\
 x_2 = x + \lambda \quad \text{for } x < 0
 \end{array}
 \iff
 \begin{array}{l}
 \left. \begin{array}{l}
 u_2 = u + \lambda/\sqrt{2} \\
 v_2 = v - \lambda/\sqrt{2}
 \end{array} \right\} \text{ for } x > 0 \\
 \left. \begin{array}{l}
 u_2 = u - \lambda/\sqrt{2} \\
 v_2 = v + \lambda/\sqrt{2}
 \end{array} \right\} \text{ for } x < 0.
 \end{array}
 \quad (5.1)$$

The coordinate ranges are  $u_i, v_i \in [-L, L]$  for  $i = 1, 2$  where  $L < \lambda$  sets the length scale of the diamonds. In both coordinate systems the crotch singularity is at the origin of coordinates. For  $0 < t_1, t_2 < \sqrt{2}L$  we identify  $x_1 = (v_1 - u_1)/\sqrt{2} = 0^-$  with  $x_2 = (v_2 - u_2)/\sqrt{2} = 0^+$  and vice versa. This gives us a complete chart on the pair of diamonds. Of course the two coordinate systems do not correspond to a split into left and right legs in the embedding trousers manifold: for example, both the top left part of  $D_1$  (i.e.  $u_1 > v_1 > 0$ ) and the top right part of  $D_2$  (i.e.  $v_2 > u_2 > 0$ ) belong to the left leg of the trousers.

To make expressions simpler we will typically use coordinates without subscript to describe functions on the pair of diamonds, and we will use an indicator function to restrict support onto subregions. Hence for a subregion  $R$  we write  $R(x)$  to denote the function which is equal to 1 when  $x \in R$  and zero otherwise (this is commonly also seen as  $\mathbf{1}_R(x)$ ). For instance,  $f(x) = e^{iku}$  is shorthand for  $f(x) = e^{iku_1} D_1(x) + e^{iku_2} D_2(x)$ , and  $g(x) = e^{iku} D_1(x)$  is shorthand for the function that is equal to  $e^{iku_1}$  in diamond 1 and zero in diamond 2. (This function should not be confused with the Boolean function  $\chi$  defined earlier, which we will also use below

and which maps propositions to  $\{0, 1\}$ :  $\chi(A) = 1$  if  $A$  is true and  $\chi(A) = 0$  if  $A$  is false.) Note that, in these conventions,  $f(u)D_2(x)$  is *not* equal to  $f(u)$  on  $D_2$ : it is equal to  $f(u_2) = f(u - \lambda/\sqrt{2})$ .

Each diamond splits naturally into five regions:

1. Bottom: the causal past of the singularity
2. Centre Left: the region spacelike to and to the left of the singularity
3. Centre Right: the region spacelike to and to the right of the singularity
4. Top Left: the left part of the causal future of the singularity
5. Top Right: the right part of the causal future of the singularity

These regions, along with some additional ones that will be used below, are defined more comprehensively for diamonds 1 and 2 on Table 5.1. As described above, we will also use the symbols defined here as indicator functions, e.g.  $\diamond\blacklozenge(x)$  is one if  $x$  is in the bottom of diamond 1 and zero otherwise.

Whether one considers the crotch as excised from the manifold or as a point that is present but at which the metric degenerates, the wave equation invariably loses its meaning there. For field modes this requires the specification of a propagation law, and in particular a rule for how a solution before/after the topology-change is to be propagated past the singularity. In terms of Green functions we are faced with a choice of what the retarded and advanced propagators look like near the singularity. This leads to a departure of the usual story in a number of ways. Not only is there a need to motivate any specific functional form of the retarded and advanced propagators, but the symmetry between the two is not forced upon us anymore.

### 5.3. Propagators in the trousers

Since the d'Alembertian degenerates at the singularity, it is unclear what is meant by a propagator as a Green function to the equations of motion. For pairs of points whose causal interval  $[x, y]$  does not contain the singularity, the retarded propagator should take its usual M-form  $G_R(x, y) = -\frac{1}{2}\chi(x \succ y)$ , since  $G_R$  satisfies the equations of motion and retarded boundary conditions everywhere in  $[x, y]$ . But what happens when the interval  $[x, y]$  contains the singularity, i.e. when the topology-change “registers” in the evolution between two spacetime points? The most naive

Symbol	Name	Definition
	Top Left 1	$u_1 > v_1 > 0$
	Top Right 1	$v_1 > u_1 > 0$
	Middle Left 1	$v_1 < 0$ and $u_1 > 0$
	Middle Right 1	$v_1 > 0$ and $u_1 < 0$
	Bottom 1	$v_1 < 0$ and $u_1 < 0$
	Upper Left Diagonal 1	
	Upper Right Diagonal 1	
	Lower Left Diagonal 1	
	Lower Right Diagonal 1	
	Left Leg	
	Right Leg	
	Pair of Diamonds	$\cup$ all of the above

Table 5.1.: Some subregions of the pair of diamonds and their labels. All regions except the last two are defined with respect to  $D_1$  — for these there are analogous regions defined with respect to  $D_2$ . Note that the upper left and right diagonal regions as well as the left and right leg regions extend over both diamonds (as evident in their symbols).

ansatz would be to set  $G_R(x, y) = -\frac{1}{2}\chi(x \succ y)$  for *all* pairs of points in the trousers, leaving the evolution law unchanged. This is illustrated in Figure 5.4. This however leads to inconsistencies, as a more careful analysis in the following paragraphs shows.

### 5.3.1. Integral form of Green's equation

We start with the following observation. In any neighbourhood  $D \subset \mathbb{M}$  of ordinary (two-dimensional) Minkowski space the operator  $\square$  is well-defined and we call  $G(x, y)$  a Green function if it satisfies  $\square_x G(x, y) = \square_y G(x, y) = \delta^{(d)}(x, y)$  for all  $x, y \in D$ , denoting by  $\square_x$  the d'Alembertian with respect to argument  $x$ . Let us assume for now that  $D$  is a causal diamond. We will work in light-cone coordinates  $y^\mu = (u, v)$  and we define  $G_x(y) := G(x, y)$ , by which we mean that  $G_x(y)$  is to be thought of

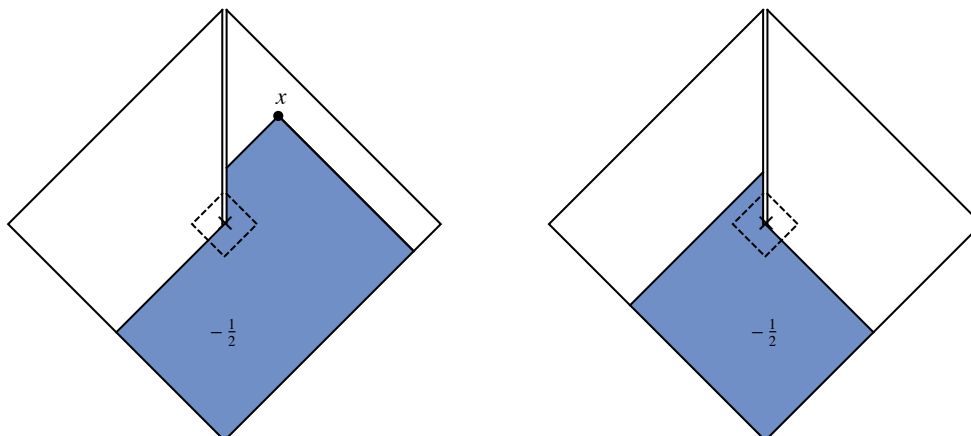


Figure 5.4.: A naive ansatz for the retarded propagator  $G_R(x, y) = -\frac{1}{2}\chi(x \succ y)$  in the trousers, drawn as a function of  $y$  for fixed  $x \succ x_c$  represented by the black dot. The function is equal to  $-\frac{1}{2}$  in the shaded region and zero everywhere else. The dashed contour corresponds to the boundary of a causal diamond centred on the singularity.

as a function of a single argument  $y$  for fixed  $x$ . Then Green's equation on one hand implies

$$\int_D dudv \square G_x(u, v) = \int_D \delta(u - u_x) \delta(v - v_x) dudv = D(x), \quad (5.2)$$

recalling that  $D(x)$  is the indicator function equal to 1 if  $x \in D$  and zero otherwise. On the other hand, using Green's theorem for a right-handed Cartesian coordinate system  $(u, v)$ :

$$\int_D (\partial_v M - \partial_u L) dudv = \oint_{\partial D} Ldv + Mdu \quad (5.3)$$

with  $M = -\partial_u G_x$  and  $L = \partial_v G_x$  we find

$$\int_D dudv \square G_x(u, v) = \oint_{\partial D} (\partial_v G_x(u, v) dv - \partial_u G_x(u, v) du) \quad (5.4)$$

where the null boundary  $\partial D$  of the causal diamond is to be traversed in anti-clockwise fashion.<sup>3</sup> Hence for any causal diamond  $D$  in  $M$ , a Green function will

<sup>3</sup> This formula of course only holds in flat space. The direction of the contour integral on the right hand side is determined by the handedness of the coordinate system on  $D$ . The general (curved spacetime) formula afforded by Stokes' theorem is more subtle in the Lorentzian setting (especially in the presence of null boundaries) due to the indefinite signature of the metric. See [92, 93] for details.

satisfy

$$\oint_{\partial D} [\partial_v G_x(u, v) dv - \partial_u G_x(u, v) du] = D(x). \quad (5.5)$$

This relation is valid for both arguments and applies to the retarded and advanced Green functions. For instance, it can easily be verified for  $G_R(u, v) = -\frac{1}{2}\theta(u)\theta(v)$ . Let us denote the integral in (5.5) by  $\mathfrak{B}_y^D G(x, y)$ . Then we can write an integral version of Green's equation as

$$\mathfrak{B}_y^D [G_R(x, y)] = D(x). \quad (5.6)$$

### 5.3.2. The field equations near the singularity

We turn to the pair of diamonds. For ease of notation we denote by  $\mathfrak{B}_y [G(x, y)]$  (with no superscript) the contour integral for which  $D$  is a small causally convex neighbourhood  $D$  whose interior contains the singularity  $x_c$  but *not*  $x$ . Similarly,  $\mathfrak{B}_x [G(x, y)]$  is the contour integral around a contour whose interior contains  $x_c$  but not  $y$ . In order for  $G(x, y)$  to “satisfy Green's equation” at the singularity we then need (5.5)

$$\mathfrak{B}_y [G_R(x, y)] = \mathfrak{B}_x [G_R(x, y)] = 0. \quad (5.7)$$

Now it can easily be seen that this will *not* be the case for the naive ansatz  $G_R(x, y) = -\frac{1}{2}\chi(x \succ y)$ . As illustrated in Figure 5.4, we obtain +1 instead of zero on the right hand sides of (5.7). There are two ways to see this. One is to note that the only contributions to the contour integral come from the places where the propagator changes between  $-\frac{1}{2}$  and 0, and at both places the derivative in  $\mathfrak{B}_y [G_R(x, y)]$  picks up  $+\frac{1}{2}$ . The other way is to see that in effect the “shadow” of the retarded propagator doubles up below the singularity, which corresponds to an extra Dirac-delta type term centered at the singularity in Green's equation. The same can be observed for  $G_A(x, y)$ , whose support “streams out” into both legs when  $x \prec x_c$ . Therefore  $\Delta = G_R - G_A$  constructed from the naive propagators will not be a solution to the equations of motion near the crotch in the sense that  $\mathfrak{B}_y [\Delta(x, y)] \neq 0$  and  $\mathfrak{B}_x [\Delta(x, y)] \neq 0$ .

These observations are reminiscent of the singularities in  $G_R^M(x, y)$  at conjugate points on the cylinder: the crotch singularity appears as a spurious source in the equations of motion. On the cylinder a physically satisfying propagator can be constructed by adding to the naive propagator appropriate scalar multiples of itself centred at the conjugate points. We shall follow a similar line of thought in order

to construct viable propagators in the trousers. The situation is not as simple, however. To begin with, there is no time-reversal symmetry in the trousers spacetime and hence the usual a priori assumption of perfect symmetry between retarded and advanced propagators seems unwarranted. Furthermore, in the globally hyperbolic case it is true that  $\square_x G_R(x, y) = \delta^{(2)}(x - y) \iff \square_y G_R(x, y) = \delta^{(2)}(x - y)$  provided the boundary conditions are satisfied, while the analog relation

$$\mathfrak{B}_y [G_R(x, y)] = 0 \iff \mathfrak{B}_x [G_R(x, y)] = 0 \quad (5.8)$$

does not obviously obtain without global hyperbolicity. This is closely related to the following fact: if  $x \in \blacklozenge\blacklozenge$ ,  $y \in \blacklozenge\blacklozenge$  and  $y' \in \blacklozenge\blacklozenge$ , then it is a priori not required that  $G_R(x, y)$  take the same value for  $(x, y)$  as it does for  $(x, y')$  — different such values implying different “strengths of propagation” into the left and right legs — so there is a potentially richer class of propagators corresponding to different physics. To construct a general family of propagators for the trousers, a more careful review is in order.

### 5.3.3. A one-parameter family of propagators

Recall that in the usual construction of the quantum theory, the primary role of the retarded and advanced propagators is their appearance in the Pauli-Jordan function  $\Delta = G_R - G_A$ . The latter enforces the causality structure of the theory, which is imposed through the commutation relations  $[\phi(x), \phi(y)] = i\Delta(x, y)$  (or their equal-time version, the canonical commutation relations). In order to act as a commutator of fields  $i\Delta$  should thus be antisymmetric. Antisymmetry also guarantees that  $i\Delta$  is a Hermitian integral kernel, which is essential in the construction of the SJ state. It is therefore reasonable to require that the propagators should *at least* be consistent with  $\Delta$  being antisymmetric and a solution to the field equations in both arguments in the sense of (5.5):

$$\mathfrak{B}_y^D [\Delta(x, y)] = \mathfrak{B}_x^D [\Delta(x, y)] = 0. \quad (5.9)$$

So let us define  $G_R$  and  $G_A$  to be the retarded and advanced parts of the commutator

$$\begin{aligned} G_R(x, y) &= \chi(x \succ y) \Delta(x, y) \\ G_A(x, y) &= -\chi(y \succ x) \Delta(x, y). \end{aligned} \quad (5.10)$$

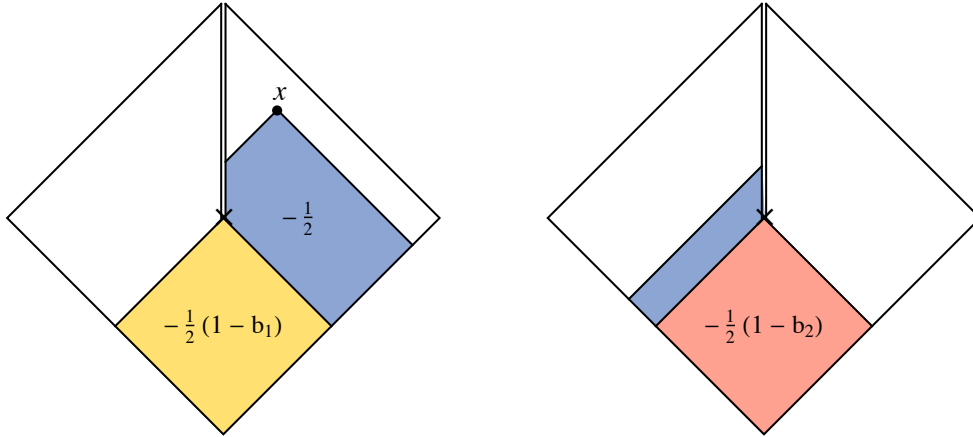


Figure 5.5.: The modified propagator  $G_R(x, y) = G_A(y, x)$  for fixed  $x$  in  $\diamond\diamond$ . In order for the integral version of Green's equation to vanish for a small contour around the singularity, we need  $b_1 + b_2 = 1$ .

and impose the conditions  $\Delta = -\Delta^T$  and  $\mathfrak{B}\Delta = 0$  in both arguments. By consequence of (5.10),  $G_R$  and  $G_A$  as well as any one  $G$  and its transpose  $G^T$ , clearly have disjoint supports. This together with the antisymmetry of  $\Delta$  implies

$$G_R(x, y) = G_A(y, x). \quad (5.11)$$

We see that the antisymmetry of  $\Delta$  indeed *implies* the symmetry between advanced and retarded propagators. The equations of motion require that

$$\begin{aligned} \mathfrak{B}_x \Delta(x, y) &= \mathfrak{B}_x G_R(x, y) - \mathfrak{B}_x G_A(x, y) = 0 \\ \mathfrak{B}_y \Delta(x, y) &= \mathfrak{B}_y G_R(x, y) - \mathfrak{B}_y G_A(x, y) = 0. \end{aligned} \quad (5.12)$$

Together with (5.11) this implies that if any one propagator is a solution to Green's equation in one of its arguments, then it, as well as its counterpart, must be solutions in both arguments.

So let us assume that the latter holds. Consider the retarded propagator  $G_R(x, y)$ . For  $x \in \diamond\diamond$  the spurious source at the crotch singularity that appears when  $y \in \blacklozenge$  or  $y \in \blacklozenge$  can be cancelled by subtracting a linear combination of constant functions from the usual  $-\frac{1}{2}\chi(x \succ y)$ . Whence for  $x \in \diamond\diamond$  we may



propose a propagator of the form

$$G_R(x, y)|_{x \in \diamond \blacktriangleleft \blacktriangleright} = -\frac{1}{2} \left[ \chi(y \prec x) - a_1 \diamond \blacktriangleleft \blacktriangleright(y) - a_2 \blacktriangleleft \blacktriangleright \diamond(y) \right]. \quad (5.13)$$

In order for the contour integral  $\mathfrak{B}_y G_R(x, y) = 0$  to vanish we find that we must set  $a_1 + a_2 = 1$ . Similarly, for  $x \in \blacktriangleleft \blacktriangleright \diamond$  we can achieve  $\mathfrak{B}_y G_R(x, y) = 0$  if we set the propagator to

$$G_R(x, y)|_{x \in \blacktriangleleft \blacktriangleright \diamond} = -\frac{1}{2} \left[ \chi(y \prec x) - b_1 \blacktriangleleft \blacktriangleright \diamond(y) - b_2 \blacktriangleleft \blacktriangleright \diamond(y) \right]. \quad (5.14)$$

with  $b_1 + b_2 = 1$ . See Figure 5.5 for a visualisation of propagator (5.14). This leaves us with a two-parameter family of retarded propagators in the trousers (parameters  $a := a_1 = 1 - a_2$  and  $b := b_1 = 1 - b_2$ ). However, from  $\mathfrak{B}_x G_R(x, y) = 0$  we now obtain two additional constraints: to satisfy the equation for  $y \in \blacktriangleleft \blacktriangleright \diamond$ , we need  $a_1 + b_1 = 1$ , and to satisfy it for  $y \in \diamond \blacktriangleleft \blacktriangleright$ , we need  $a_2 + b_2 = 1$ . This illustrates the decoupling of the equations of motion with respect to the first and second arguments referred to above (5.8): none of the two equations (supplemented with boundary conditions) specifies a unique solution (as it would in a globally hyperbolic spacetime) — instead, the two equations impose independent constraints on the solution.

We are thus left with a one-parameter family of retarded and advanced propagators  $G_{R,p}(x, y) = G_{A,p}(y, x)$  parametrised by  $p := a_1 = b_2 = 1 - a_2 = 1 - b_1$ . For completeness we also show the propagator  $G_A(x, y) = G_R(y, x)$  for fixed  $x$  in the past of the crotch in Figure 5.6.

The case  $p = \frac{1}{2}$  corresponds to the symmetric case in which the added negative source propagates with equal strength into and out of the two legs (see Figures 5.5 and 5.6, respectively). The cases  $p = 0$  and  $p = 1$  correspond to the two opposite extremes in which the source either only propagates into (and out of) the left leg, or into (and out of) the right leg. It is worth emphasising that these additional sources in the retarded and advanced propagators do *not* in themselves yet constitute a “burst in energy”. They do of course influence the propagation of the field past the singularity, and the effect of the added sources on the propagation might well translate into divergences in the stress-energy tensor. However, in order reach such conclusions, one first has to obtain the quantum state (through the Wightman function, or, equivalently, a complete set of positive frequency modes) and compute the expectation value of physical observables therein.

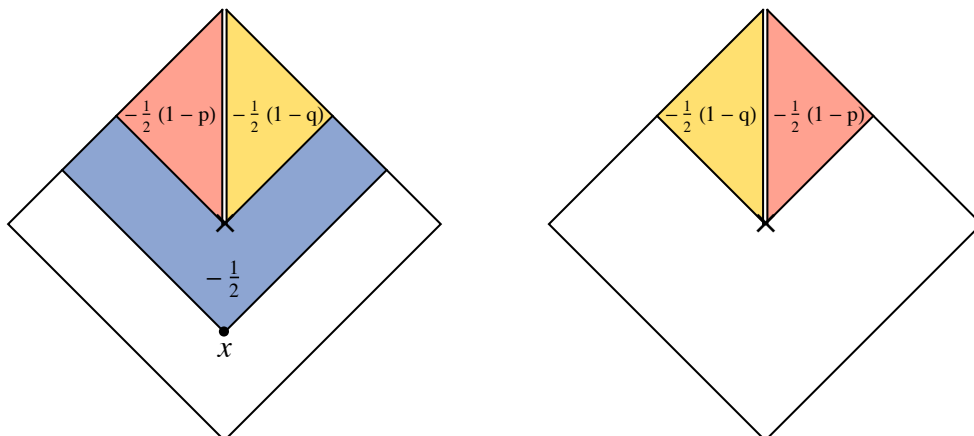


Figure 5.6.: The modified propagator  $G_{A,p}(x, y) = G_{R,p}(y, x)$  for fixed  $x$  in  $\diamond \diamond$ . Here  $q = 1 - p$ .

## 5.4. Propagation of plane waves past the singularity

What type of propagation law do the propagators defined in the previous section entail? To understand this let us consider modes in the trunk and propagate them forward past the singularity using the retarded propagator. This can be done explicitly using Stokes' theorem (or its special case known as Green's second identity). We recall the usual evolution procedure of initial data with a retarded propagator. Given a solution  $f(x)$  of the field equations (and its derivative) on a spacelike hypersurface  $\Sigma$  and a retarded Green function  $G_R(x, y)$  of the wave equation, one obtains the forward-propagated solution at a point  $x$  in the future domain of dependence of the hypersurface  $D^+(\Sigma)$  via an integral involving  $G_R(x, y)$  and  $f(x)$  over the section  $J^-(x) \cap \Sigma$  of the hypersurface (where  $J^-(x) = \{y : y \prec x\}$ ):

$$f(x) = \int_{J^-(x) \cap \Sigma} d\Sigma_y^\mu [f(y) \nabla_\mu^y G_R(x, y) - G_R(x, y) \nabla_\mu^y f(y)]. \quad (5.15)$$

Now we know that for  $G_R(x, y) = -\frac{1}{2}\chi(x \succ y)$ , plane waves  $u_k(x) = e^{-iku}$  (or  $v_k(x) = e^{-ikv}$ ) will propagate forward to themselves, i.e. if  $x$  is in the future domain of dependence of a hypersurface on which the solution is a plane wave, then (5.15) will yield the same plane wave evaluated at  $x$ .

Consider now the evolution generated by the modified retarded propagator  $G_{R,p}$  on the pair of diamonds. Intuitively it is clear that a right-moving (left-moving)

plane wave will just propagate freely along a diagonal  $u = \text{const.}$  ( $v = \text{const.}$ ) line and it will be oblivious to the singularity until it enters its future lightcone. What happens there? To find out, let us denote by  $u_k^1(x)$  initial data corresponding to a right-moving plane wave in the trunk region of diamond 1 which is zero in the trunk region of diamond 2, i.e.  $u_k^1(x) = e^{-iku} \blacklozenge \blacklozenge(x)$ . Using the evolution equation we find that the wave evolves to  $e^{-iku} - p$  for  $x \in \blacklozenge \blacklozenge$  (i.e. in the left leg) and to  $+p$  for  $x \in \blacklozenge \blacklozenge$  (i.e. in the right leg). The constant terms in fact appear in the form  $pe^{-iku_c}$  but since  $u_c = 0$  in our coordinates this reduces to  $p$ . The complete forward-propagated solutions for initial data corresponding to right- and left-movers in the trunk regions of diamonds 1 and 2 are given by:

$$\begin{aligned} u_k^1(x) &= e^{-iku} \blacklozenge \blacklozenge(x) + p \left[ \blacklozenge \blacklozenge(x) - \blacklozenge \blacklozenge(x) \right] \\ u_k^2(x) &= e^{-iku} \blacklozenge \blacklozenge(x) + p \left[ \blacklozenge \blacklozenge(x) - \blacklozenge \blacklozenge(x) \right] \end{aligned} \quad (5.16)$$

and

$$\begin{aligned} v_k^1(x) &= e^{-ikv} \blacklozenge \blacklozenge(x) + (1-p) \left[ \blacklozenge \blacklozenge(x) - \blacklozenge \blacklozenge(x) \right] \\ v_k^2(x) &= e^{-ikv} \blacklozenge \blacklozenge(x) + (1-p) \left[ \blacklozenge \blacklozenge(x) - \blacklozenge \blacklozenge(x) \right]. \end{aligned} \quad (5.17)$$

To find the evolution of plane waves in the *whole* trunk it suffices to take linear combinations of the above modes. Due to the periodicity on the actual trousers, the modes on the pair of diamonds corresponding to the natural “right-moving plane waves in the trunk” with periodic boundary conditions take the form  $u_k^1(x) + (-1)^n u_k^2(x)$  with  $k = \sqrt{2}n\pi/\lambda$  in our conventions (the factor of  $\sqrt{2}$  here comes from the factor of  $\sqrt{2}$  in our definition of the lightcone coordinates). For even  $n$ , the constant terms in (5.16) cancel. For odd  $n$ , they add up, leading to opposite constant terms  $\pm 2p$  in the causal futures of the singularity pertaining to the left/right legs. Similar statements apply to left-moving incoming modes. Interestingly, this corresponds precisely to the one-parameter family of propagation laws found in [89], which the authors arrived at by demanding the conservation of inner products under the evolution past the singularity (our parameter  $p$  is related to their parameter  $A$  via  $p = \frac{1}{2}(1 + A)$ ).

## 5.5. Eigenmodes of the Pauli-Jordan function

The one-parameter family of propagators derived in the previous section provides us with a one-parameter family of Pauli-Jordan functions  $\Delta_p = G_{R,p} - G_{A,p}$ . It is

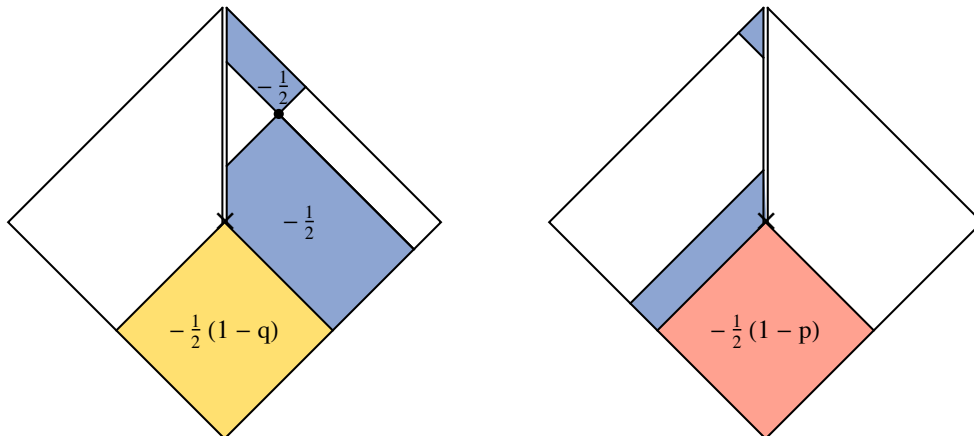


Figure 5.7.: The Pauli-Jordan function  $\Delta_p(x, y)$  in the trousers as a function of  $y$ , with the first argument  $x$  fixed (at the dot) in the causal future of the crotch singularity. Here  $q = 1 - p$ .

not very illuminating to write down its functional form; for an example in pictorial form see Figure 5.7. When both arguments are outside the domain of influence of the crotch,  $\Delta$  takes on its usual Minkowski form. Our aim is now to find the positive eigenfunctions of  $i\Delta$  that satisfy  $i\Delta(f) = \lambda f$  for  $\lambda > 0$ .

### 5.5.1. Counting eigenmodes

Recall from (2.54) that if  $i\Delta(x, y)$  is a Hilbert-Schmidt integral kernel on  $L^2(M \times M)$  with eigenvalues  $\lambda_k$  then

$$\int_M dx \int_M dy |i\Delta(x, y)|^2 = \sum_k \lambda_k^2. \quad (5.18)$$

Let us evaluate the left hand side for  $i\Delta_p(x, y)$  on the pair of diamonds. The integral over  $y \in \blacklozenge\blacklozenge$  yields

$$\int_{\blacklozenge\blacklozenge} dy |\Delta(x, y)|^2 = \frac{1}{2}(L^2 + uv) - \frac{1}{2}p(1-p)L^2\blacklozenge\blacklozenge(x) \quad (5.19)$$

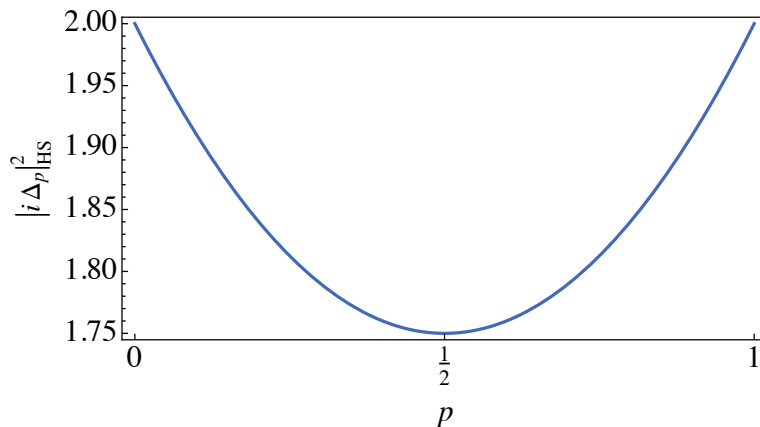


Figure 5.8.:  $L^2(M \times M)$ -norm of  $i\Delta_p(x, y)$  on the pair of diamonds as a function of  $p$ .

where  $x = (u, v)$ . Further integrating this expression over  $x \in \blacklozenge\blacklozenge$  we obtain

$$\int_{\blacklozenge\blacklozenge} dx \int_{\blacklozenge\blacklozenge} dy |i\Delta(x, y)|^2 = 2L^4 [2 - p(1 - p)]. \quad (5.20)$$

Compare this to the single flat diamond, on which the norm of  $i\Delta$  evaluates to  $2L^4$ . The relation (5.20) is useful because it allows us to check if a given set of eigenfunctions of  $i\Delta$  is the full set. If the eigenvalues (with multiplicities) sum to less than  $2L^4 [2 - p(1 - p)]$ , we know that we are missing eigenfunctions. It is also interesting to note that the value depends on  $p$ . This means that the eigenvalues must depend on  $p$ .

### 5.5.2. Ordinary plane waves

Since we know the SJ modes for the ordinary causal diamond from Chapter 3, we can use them as a first guide to guess what eigenmodes might look like on the pair of diamonds. Recall that on the causal diamond of “side-length”  $2L$  (i.e. volume  $4L^2$ ) in Minkowski space the Pauli-Jordan function is given by  $\Delta(x, y) = -\frac{1}{2} [\chi(x \prec y) - \chi(y \prec x)]$  and its eigenmodes are linear combinations of positive frequency plane waves and a constant (3.20)

$$\begin{aligned} f_k(u, v) &:= e^{-iku} - e^{-ikv}, & \text{with } k = \frac{n\pi}{L}, n = 1, 2, \dots \\ g_k(u, v) &:= e^{-iku} + e^{-ikv} - 2 \cos(kL), & \text{with } k \in \mathcal{K} \end{aligned}$$

with  $\mathcal{K} = \{k \in \mathbb{R} \mid \tan(kL) = 2kL \text{ and } k > 0\}$ . Evaluating the action of  $i\Delta_p$  on these modes involves rather long calculations on different parts of the pair of diamonds, so it will be helpful to first consider plane waves that are defined on smaller subregions of the diamond (i.e. that have smaller support).

### 5.5.3. Restricted plane waves

The simplest functions to start with are “in” and “out” plane waves, which correspond to plane waves that propagate from the trunk into the legs (or from one of the legs into the trunk). Left- and right- propagating plane waves will respectively be functions of  $v$  and  $u$  only, and therefore it is natural to restrict them to diagonal subregions of the pair of diamonds. We thus consider plane waves  $e^{-iku}$  and  $e^{-ikv}$ . Let us define four types of right-moving plane waves

$$U_k^R(x) = e^{-iku} R(x) \quad (5.21)$$

for regions  $R = \blacklozenge\blacklozenge, \blacklozenge\blacklozenge, \blacklozenge\lozenge, \lozenge\blacklozenge$  and four types of left-moving plane waves


$$V_k^L(x) = e^{-ikv} L(x) \quad (5.22)$$






for regions  $L = \blacklozenge\blacklozenge, \blacklozenge\blacklozenge, \blacklozenge\lozenge, \lozenge\blacklozenge$ . (Recall that we are using  $x = (u, v)$  as a spacetime coordinate.) These functions all solve the wave equation since they are functions of either  $u$  or  $v$  only (involving only exponentials and step functions in either  $u$  or  $v$  respectively).


To find the action of  $i\Delta_p$  on these functions we need to convolve them with the second argument of  $i\Delta_p$  over the pair of diamonds. There is of course perfect symmetry under an exchange of the two diamonds, so it suffices to consider the four modes defined with respect to  $D_1$  (i.e. the right-movers on  $\blacklozenge\blacklozenge$  and  $\blacklozenge\lozenge$  and the left-movers on  $\blacklozenge\blacklozenge$  and  $\blacklozenge\lozenge$ ). The actual calculation needs to be done for each subregion of the diamonds separately — for instance the integral






$$i\Delta_p U_k^R(x) = \int_{\blacklozenge\blacklozenge} \sqrt{-g(y)} dy i\Delta_p(x, y) U_k^R(y) \quad (5.23)$$

will look different depending on which subregion of the pair of diamonds  $x$  lies in due to the functional form of  $i\Delta_p$  (see Figure 5.7). For the right-moving plane wave






in the upper left diagonal region  we find

$$\begin{aligned}
 \frac{k}{L} i\Delta_p U_k \text{} (x) &= \text{} (x) \left[ e^{-iku} + \left(1 - \frac{v}{L}\right) \epsilon(kL) - 1 \right] \\
 &+ \text{} (x) \left(1 - p - \frac{v}{L}\right) \epsilon(kL) \\
 &+ \text{} (x) \left(1 - \frac{v}{L}\right) \epsilon(kL) \\
 &+ \text{} (x) p \epsilon(kL)
 \end{aligned} \tag{5.24}$$

where  $\epsilon(kL) = \frac{1}{2} (1 - e^{-ikL})$ . Given the mirror symmetry of the setup (symmetry under a simultaneous reflection in both diamonds about their vertical axes of symmetry), the expression for the action of  $i\Delta_p$  on left-movers in the upper right diagonal region  $i\Delta_p V_k \text{} (x)$  can be obtained from (5.24) by reflecting the regions in each of the two diamonds along the verticals  $x_1 = x_2 = 0$  and interchanging  $u \leftrightarrow v$  and  $p \leftrightarrow 1 - p$ . This leads to:

$$\begin{aligned}
 \frac{k}{L} i\Delta_p V_k \text{} (x) &= \text{} (x) \left[ e^{-ikv} + \left(1 - \frac{u}{L}\right) \epsilon(kL) - 1 \right] \\
 &+ \text{} (x) \left(p - \frac{u}{L}\right) \epsilon(kL) \\
 &+ \text{} (x) \left(1 - \frac{u}{L}\right) \epsilon(kL) \\
 &+ \text{} (x) (1 - p) \epsilon(kL).
 \end{aligned} \tag{5.25}$$

Analogous expressions can be derived for the lower diagonal right-movers

$$\begin{aligned}
 \frac{k}{L} i\Delta_p U_k \text{} (x) &= \text{} (x) \left[ e^{-iku} + \left(1 + \frac{v}{L}\right) \bar{\epsilon}(kL) - 1 \right] \\
 &+ \text{} (x) (1 - p) \bar{\epsilon}(kL) \\
 &+ \text{} (x) \left(p + \frac{v}{L}\right) \bar{\epsilon}(kL) \\
 &+ \text{} (x) \left(1 + \frac{v}{L}\right) \bar{\epsilon}(kL)
 \end{aligned} \tag{5.26}$$

where  $\bar{\epsilon}(kL) = \epsilon(-kL) = \frac{1}{2}(1 - e^{ikL})$ . For the lower diagonal left-movers we obtain

$$\begin{aligned}
 \frac{k}{L} i\Delta_p V_k^{\blacklozenge\blacklozenge}(x) &= \blacklozenge\blacklozenge(x) \left[ e^{-ikv} + \left(1 + \frac{u}{L}\right) \bar{\epsilon}(kL) - 1 \right] \\
 &+ \blacklozenge\blacklozenge(x) p \bar{\epsilon}(kL) \\
 &+ \blacklozenge\blacklozenge(x) \left(1 - p + \frac{u}{L}\right) \bar{\epsilon}(kL) \\
 &+ \blacklozenge\blacklozenge(x) \left(1 + \frac{u}{L}\right) \bar{\epsilon}(kL).
 \end{aligned} \tag{5.27}$$

We can see that in general, convolution with  $i\Delta$  spreads the support of a restricted plane wave onto other regions of the pair of diamonds. A special case is  $\epsilon(kL) = 0$ , which corresponds to  $kL = 2n\pi$  ( $n \in \mathbb{N}$ ), for which all but the first lines in the equations above vanish. However, for any single mode there is still an extra constant term on the right hand side and so no single mode will be an eigenfunction of  $i\Delta$ .

#### 5.5.4. Ordinary plane waves revisited

Given the above results it is easy to find the action of  $i\Delta$  on ordinary plane waves via linear combinations of the form  $u_k(x) = u_k^1(x) + u_k^2(x) = U_k^{\blacklozenge\blacklozenge}(x) + U_k^{\blacklozenge\blacklozenge}(x) + U_k^{\blacklozenge\blacklozenge}(x) + U_k^{\blacklozenge\blacklozenge}(x)$ . We find that the action of  $i\Delta$  on these ordinary plane waves is precisely the same as that for the single diamond if the length scale  $L$  on the single diamond is replaced by its direct counterpart  $L$  on the pair of diamonds — the dependence on  $p$  drops out. Hence, despite the modified form of the Pauli-Jordan function  $i\Delta_p$  on the pair of diamonds it turns out that these modes — when extended onto both diamonds — are eigenmodes of  $i\Delta_p$ , for any value of  $p$ . Notice that for even  $n$ , these modes can be viewed as forward-propagated modes on the full trousers (with  $L$  equal to  $\lambda$ ), but for odd  $n$ , they do *not* correspond to such modes. Now, we know from our analysis of the single diamond that the eigenvalues of these modes sum to  $2L^4$ ! Hence we are short by an amount  $2L^4[1 - p(1 - p)]$  from the total derived in (5.20). We must keep looking.

#### 5.5.5. Restricted constant functions

One of the problems with the general solutions above is that  $i\Delta$  acting on a restricted plane wave gives rise to terms that are constant or linear in  $u$  or  $v$ , on regions outside the support of the original function. Perhaps we may hope to find eigenmodes by including constant functions defined on subregions of the pair of diamonds. After all,



the single diamond SJ modes included a constant part as well. Note that constant functions can be denoted as multiples of the indicator function. We obtain for  $\blacklozenge\blacklozenge$ :

$$\begin{aligned} (i\Delta_p \blacklozenge\blacklozenge)(x) &= -\frac{i}{2}L(L+u+v)\blacklozenge\blacklozenge(x) \\ &\quad -\frac{i}{2}L^2p\blacklozenge\blacklozenge(x) - \frac{i}{2}L^2(1-p)\blacklozenge\blacklozenge(x) \\ &\quad -\frac{i}{2}L(L+v)\blacklozenge\blacklozenge(x) - \frac{i}{2}L(L+u)\blacklozenge\blacklozenge(x) \end{aligned} \quad (5.28)$$

for  $\blacklozenge\blacklozenge$  and  $\blacklozenge\blacklozenge$ :

$$\begin{aligned} (i\Delta_p \blacklozenge\blacklozenge)(x) &= -\frac{i}{2}L(u+v)\blacklozenge\blacklozenge(x) - \frac{i}{2}Lu\blacklozenge\blacklozenge(x) - \frac{i}{2}Lv\blacklozenge\blacklozenge(x) \\ (i\Delta_p \blacklozenge\blacklozenge)(x) &= -\frac{i}{2}L(u+v)\blacklozenge\blacklozenge(x) - \frac{i}{2}Lv\blacklozenge\blacklozenge(x) - \frac{i}{2}Lu\blacklozenge\blacklozenge(x) \end{aligned} \quad (5.29)$$

and for  $\blacklozenge\blacklozenge$  and  $\blacklozenge\blacklozenge$ :

$$\begin{aligned} (i\Delta_p \blacklozenge\blacklozenge)(x) &= \frac{i}{2}L(L-u-v)\blacklozenge\blacklozenge(x) + \frac{i}{2}L^2p\blacklozenge\blacklozenge(x) + \frac{i}{2}L^2(1-p)\blacklozenge\blacklozenge(x) \\ &\quad + \frac{i}{2}L(L-u)\blacklozenge\blacklozenge(x) + \frac{i}{2}L(L-v)\blacklozenge\blacklozenge(x) \\ (i\Delta_p \blacklozenge\blacklozenge)(x) &= \frac{i}{2}L(L-u-v)\blacklozenge\blacklozenge(x) + \frac{i}{2}L^2p\blacklozenge\blacklozenge(x) + \frac{i}{2}L^2(1-p)\blacklozenge\blacklozenge(x) \\ &\quad + \frac{i}{2}L(L-v)\blacklozenge\blacklozenge(x) + \frac{i}{2}L(L-u)\blacklozenge\blacklozenge(x) \end{aligned} \quad (5.30)$$

Unfortunately, we have not so far been able to find combinations of the functions listed in these sections that are eigenfunctions of  $i\Delta_p$ .

## 5.6. Outlook

In this chapter we have presented the current state of affairs of some initial investigations of the SJ formalism on the trousers spacetime. There are some clear open ends to be tied up, which include, in particular: (i) a derivation of the remaining eigenmodes of  $i\Delta$ , (ii) an analysis of time-reversibility and of backward-propagated modes, and (iii) a more careful study of the space  $L^2(M)$  on the pair of diamonds (and of its complete bases). These points are of course all intertwined and in addressing any one of them we may hope to gain new insight into the others. It is clear that the singularity associated with the topology-change makes the analysis of

eigenfunctions more complicated (as, for example, compared to the single diamond). This suggests that one may also try the approach taken in Chapter 4, i.e. starting with a complete set of modes and finding the SJ modes by solving for the Bogoliubov coefficients.

We have also found that the one-parameter family of evolution laws obtained by requiring  $\Delta$  to solve the wave equation in the sense of being annihilated by  $\mathfrak{B}$  seems to agree exactly with the family derived in [89]. The approach here has been rather different, but it is not surprising to find that conditions on the regularity of the classical propagators on one hand, and conditions on the conservation of the inner product on the other, lead to the same result.

In their conclusion, Copeland et. al. mention “one more possibility to be considered before accepting the conclusions [on the unphysical nature of the trousers topology-change] of Anderson and DeWitt”. This relates to the fact that in the field expansions used by both Anderson and DeWitt and Copeland et.al., some modes have been “overlooked”, namely the restricted constant functions of Section 5.5.5. These functions indeed come out naturally when using the one-parameter family of evolution laws compatible with the field equations to propagate plane waves past the singularity (see Section 5.4 above and the Appendix of [89]). In the canonical approach, it is not a priori *necessary* to include these functions in the field expansion, and indeed their inclusion requires the treatment of fundamentally discontinuous modes and their derivatives. In the SJ formalism, however, there seems to be no way to avoid them! Given the comments in the introduction to this chapter, this is not to say that one should expect such issues to cure the pathology of the trousers spacetime — still, it does raise interesting questions, which we will hopefully be able to answer better in the future.

## 6. For Future Investigation

We have made some steps toward a better understanding of the SJ formalism in the continuum and on causal sets, but many of the most interesting questions remain to be answered.

Are the contradictions we encountered in Chapter 3 tied to the sickness of the massless theory in two dimensions? To answer this question, it would be interesting to compute the SJ state either for a massless field in higher dimensions, or for a massive field in two dimensions (or, more ambitiously, for a massive field in higher dimensions!). The obstacle is that the Pauli-Jordan function in all these situations becomes more complicated and therefore it is harder to find its spectrum. Here causal set simulations may offer some insight, since it is much easier to sprinkle into a spacetime and compute the discrete SJ two-point function than going through the analytic calculation in the continuum. The more difficult part of the task is then to extract conclusions from the results of the numerical simulations.

Another question raised in the course of our analysis is: what is the meaning of the failure of the SJ state to satisfy the Hadamard condition, and what conclusions should we draw from it? A partial answer to the first question has been given in Chapter 4, and is highlighted by the modified (“smoothened”) versions of the SJ state analysed in [73], which do satisfy the condition at the cost of being non-unique. The latter development is certainly of interest in itself, since concrete examples of Hadamard states are notoriously difficult to construct despite the fact that they are known to be abundant [94]. Still, if one hopes to find a candidate for *the* physical ground state of a quantum field in spacetime, the failure of the Hadamard criterion for the SJ state in general spacetimes does deserve some attention, especially given that the Hadamard criterion is so far the only one to have stood the test of time in providing viable states for linear quantized fields in rigorous QFT. For some, the failure of the Hadamard criterion all but disqualifies the SJ state (as it currently stands) from being physically viable [95]. That said, it is possible to consider an alternative point of view on the matter altogether. Ultimately, the divergences in quantum field theory, including those in the stress-energy tensor, are tied to the

---

continuum spacetime manifold on which the theory is defined. Those of us who expect that the deep structure of spacetime is discrete might speculate that the underlying discreteness itself will produce the necessary “regularisation” of such divergences. Indeed, the SJ formalism was originally conceived as a model for quantum field theory on causal sets, where the procedure is free of the troubles it suffers in the continuum (even without postulating a fundamental spacetime discreteness, the discrete formalism can be seen as simply a Lorentz-invariant discretisation of the continuum formalism). Such a discretisation provides a natural “cut-off”. In the meantime, if one is interested in phenomenological applications for the SJ state that concern long wavelength phenomena, the short-distance behaviour of the two-point function appears less relevant.

This leads us to the most interesting question: can the SJ state have observable effects? One possible approach to this question would be to calculate the response rate of a moving Unruh-DeWitt detector when the field is in the SJ state. Another, more ambitious project, would be to study the renormalised stress-energy tensor and its back-reaction on the background geometry. Some first steps in this direction were made in [10]. In the case of de Sitter space, our calculations in Chapter 4 show that some of these questions reduce to the phenomenology of  $\alpha$ -vacua. These have been studied rather extensively in the literature, although their physical status is debated [72, 96, 97]. In that context, we will also have to think carefully about the global (or “teleological”) nature of the SJ state and what this says about the way in which we should set up physically meaningful calculations.

## A. Corrections to the SJ two-point function

In evaluating the second sum (3.25) of the continuum SJ two-point function (3.22), we made the approximation  $\mathcal{K} \rightarrow \mathcal{K}_0$ . For a given pair of spacetime points, this will induce an error in the two-point function, which (see (3.27) and (3.22)) is given by

$$\begin{aligned} \epsilon(u, v; u', v') = \sum_{n=1}^{\infty} \left[ \frac{L}{k_n} \frac{1}{\|g_{k_n}\|^2} g_{k_n}(u, v) g_{k_n}^*(u', v') \right. \\ \left. - \frac{L}{k_{0,n}} \frac{1}{\|g_{k_{0,n}}\|^2} g_{k_{0,n}}(u, v) g_{k_{0,n}}^*(u', v') \right], \end{aligned} \quad (\text{A.1})$$

where  $k_n$  and  $k_{0,n}$  denote the  $n^{\text{th}}$  terms in  $\mathcal{K}$  and  $\mathcal{K}_0$ , respectively. The contributions to the right hand side come mostly from long wavelength (small  $n$ ) terms, since the approximation  $\mathcal{K} \rightarrow \mathcal{K}_0$  becomes increasingly accurate for large  $n$  (see Figure 3.3). This means that we should expect  $\epsilon$  to be constant over small subregions of the diamond. We will first test this expectation numerically, restricting ourselves for simplicity to timelike related pairs of points

To estimate the mean and the variation of  $\epsilon(u, v; u', v')$  over different pairs of spacetime points in a subregion associated with the centre (i) or corner (ii) of the diamond, we evaluated  $\epsilon(u, v; u', v')$  on a random sample  $P$  of pairs of timelike related points within that region. We evaluated (A.1) by truncating the sums on the right hand side at a stage large enough for the sum to have converged sufficiently. We then calculated the mean value of  $\epsilon(u, v; u', v')$  and its standard deviation on the sample  $P$ . We present the results for the real part of  $\epsilon(u, v; u', v')$  below, since we are mainly interested in the real part of the Wightman function  $W$ . (The imaginary part of  $W$  is proportional to  $\Delta$  and therefore known exactly. Moreover, the imaginary part of  $\epsilon(u, v; u', v')$  was consistent with zero in all the regions we investigated numerically.)

Look at subregions in the centre and corner of the form depicted in Figure 3.4: a square in the centre, a triangle in the corner. Fix the linear dimension of the

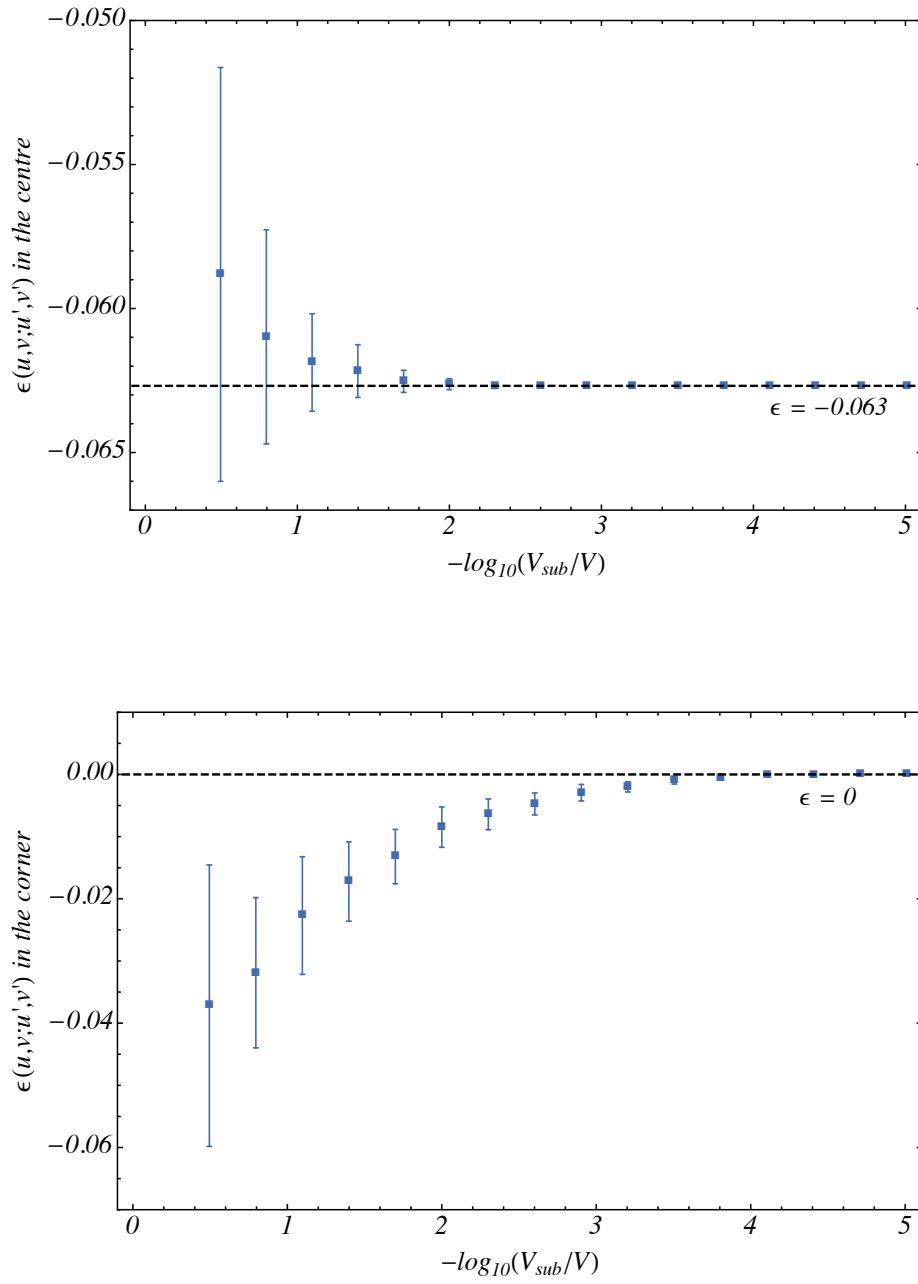


Figure A.1.: A plot of  $\epsilon(u, v; u', v')$  in the centre (top) and in the corner (bottom) against  $-\log_{10}(V_{sub}/V)$ .

---

subregion  $D \ll L$  and denote its spacetime volume by  $V_{\text{sub}}$ . Increase the size  $L$  of the full diamond while keeping  $D$  fixed, thereby decreasing the volume ratio  $V_{\text{sub}}/V$ . The mean and standard deviation of  $\epsilon(u, v; u', v')$  obtained in this way are shown in Figure A.1 for different values of  $V_{\text{sub}}/V$  ranging from  $\mathcal{O}(10^{-1})$  to  $\mathcal{O}(10^{-6})$ . These results were obtained by truncating the sum (A.1) at  $n = 50$ , which provides sufficient accuracy. We observe that the standard deviation in  $\epsilon(u, v; u', v')$  indeed quickly becomes negligible as  $V_{\text{sub}}/V$  is decreased. The mean of  $\epsilon(u, v; u', v')$  tends to a constant value in the centre given by  $\epsilon_{\text{centre}} = -0.0627$  and it vanishes in the corner:  $\epsilon_{\text{corner}} = 0$ . Notice that these results are unchanged under a simultaneous rescaling of  $L$  and  $D$ : the mean and standard deviation of  $\epsilon(u, v; u', v')$  depend only on the ratio  $V_{\text{sub}}/V$ .

It is worth noting that the asymptotic values for the mean of  $\epsilon$  seen at large  $L$  above agree with the values of  $\epsilon(u, v; u', v')$  that we obtain if we simply evaluate the infinite sum on a pair of coincident points in the centre of the diamond,  $(u, v) = (u', v') = (0, 0)$ , or in the corner  $(u, v) = (u', v') = (-L, L)$ . In the centre, the sum (A.1) reduces to

$$\epsilon(0, 0; 0, 0) = \sum_{n=1}^{\infty} \left[ \frac{\left(1 - \sqrt{4x_n^2 + 1}\right)^2}{2x_n(4x_n^2 - 1)} - \frac{1}{\pi(2n - 1)} \right], \quad (\text{A.2})$$

where  $x_n$  is the  $n^{\text{th}}$  positive solution to  $\tan(x) = 2x$ . This sum can be evaluated to arbitrary precision using numerical solutions for  $x_n$ , and it tends to  $\epsilon(0, 0; 0, 0) = -0.0627$ , corresponding to the horizontal asymptote in the centre plot of Figure A.1. In the corner, both terms in (A.1) vanish because the  $g_k$  modes (3.20) are identically zero at  $(-L, L)$  for all  $k_n \in \mathcal{K}$  and  $k_{0,n} \in \mathcal{K}_0$ . It follows that  $\epsilon(-L, L; -L, L) = 0$ , corresponding to the horizontal asymptote in the corner plot of Figure A.1.

## B. Modes in $dS^D$ and $dS_P^D$

Here we review the Bunch-Davies modes on the Poincaré patch  $dS_P^D$  (with the conventions of [53]) and the Euclidean modes on the global patch  $dS^D$  (with the conventions of [51]). The two sets of modes define the same quantum state, which is referred to as the Euclidean or the BD state. Even though these modes are used extensively in the literature, we include self-contained derivations in this appendix, not least because they provide a good place to present some of the identities and subtleties that are important in the calculations of Chapter 4.

### B.1. Bunch-Davies modes on $dS_P^D$

In cosmological coordinates, the de Sitter metric is given by (4.9)

$$ds^2 = \frac{\ell^2}{\eta^2} (-d\eta^2 + d\mathbf{x}^2), \quad (\text{B.1})$$

where  $d\mathbf{x}^2 = \sum_{i=1}^d (dx^i)^2$ ,  $\eta \in (-\infty, 0)$ , and  $x_i \in (-\infty, +\infty)$ . The Klein-Gordon equation is

$$[\partial_\eta^2 - \partial_i^2 + \ell^2 m^2 \eta^{-2}] \phi(\eta, \mathbf{x}) = 0. \quad (\text{B.2})$$

#### Klein-Gordon modes:

Consider the functions

$$u_{\mathbf{k}}(\eta, \mathbf{x}) = \frac{e^{i\mathbf{k}\cdot\mathbf{x}}}{(2\pi)^{d/2}} \chi_k(\eta), \quad \chi_k(\eta) = n_{\mathbf{k}} (-\eta)^{d/2} \psi_k(\eta), \quad (\text{B.3})$$

where  $n_{\mathbf{k}}$  is a normalisation constant and  $k := |\mathbf{k}|$ . These modes satisfy the Klein-Gordon equation if  $\psi_k(\eta)$  satisfies Bessel's differential equation:

$$z^2 \frac{d^2 \psi_k}{dz^2} + z \frac{d\psi_k}{dz} + (z^2 - \nu^2) \psi_k = 0, \quad (\text{B.4})$$



where

$$z = -k\eta, \quad \nu^2 = \frac{d^2}{4} - m^2\ell^2. \quad (\text{B.5})$$

The BD positive-frequency modes are taken to be  $\psi_k^{BD}(\eta) = H_\nu^{(1)}(-k\eta)$ , where  $H_\nu^{(1)}$  is the Hankel function of the first kind. These modes minimise the Hamiltonian associated with  $\frac{d}{d\eta}$  on the spatial slice at  $\eta \rightarrow -\infty$  (the diagonal in the Penrose diagram in Figure 4.1).

**Absolute value of the normalisation constant  $n_{\mathbf{k}}$ :**

In order to fix the normalisation  $n_{\mathbf{k}}$ , we use the fact that these modes should be orthonormal with respect to the Klein-Gordon inner-product:

$$\begin{aligned} (u_{\mathbf{k}}^{BD}, u_{\mathbf{q}}^{BD}) &= -(\bar{u}_{\mathbf{k}}^{BD}, \bar{u}_{\mathbf{q}}^{BD}) = \delta^{(d)}(\mathbf{k} - \mathbf{q}) \\ (u_{\mathbf{k}}^{BD}, \bar{u}_{\mathbf{q}}^{BD}) &= 0. \end{aligned} \quad (\text{B.6})$$

These conditions require the norm of  $n_{\mathbf{k}}$  to be  $|n_{\mathbf{k}}| = \sqrt{\frac{\pi}{4}}\ell^{-\frac{d+1}{2}}e^{-\pi\text{Im}(\nu)/2}$ , while leaving its phase unconstrained. To see this, note that in this foliation  $n^\mu = (-\eta/l, \mathbf{0})$  and  $d\Sigma = (-\ell/\eta)^d d^d x$ . Then

$$\begin{aligned} (u_{\mathbf{k}}^{BD}, u_{\mathbf{q}}^{BD}) &= i \int \frac{e^{i(\mathbf{q}-\mathbf{k})\cdot\mathbf{x}}}{(2\pi)^d} (-\ell/\eta)^{d-1} [\bar{\chi}_k \partial_\eta \chi_q - \bar{\chi}_q \partial_\eta \chi_k] d^d x \\ &= i |n_{\mathbf{k}}|^2 \ell^{d-1} \int \frac{e^{i(\mathbf{q}-\mathbf{k})\cdot\mathbf{x}}}{(2\pi)^d} (-\eta) \left[ \bar{H}_\nu^{(1)}(-k\eta) \partial_\eta H_\nu^{(1)}(-q\eta) \right. \\ &\quad \left. - H_\nu^{(1)}(-q\eta) \partial_\eta \bar{H}_\nu^{(1)}(-k\eta) \right] d^d x. \end{aligned} \quad (\text{B.7})$$

This inner product is conserved with time, so it suffices to evaluate it for  $\eta \rightarrow -\infty$ , where the Hankel function has the simple asymptotic form [57, Eq. 10.2.5]

$$H_\nu(-k\eta) \rightarrow \sqrt{\frac{-2}{\pi k\eta}} e^{-i(k\eta + \frac{\pi\nu}{2} + \frac{\pi}{4})}. \quad (\text{B.8})$$

Plugging this back into the above expression, we find

$$(u_{\mathbf{k}}^{BD}, u_{\mathbf{q}}^{BD}) = \ell^{d-1} \frac{4}{\pi} e^{\pi\text{Im}(\nu)} |n_{\mathbf{k}}|^2 \delta^{(d)}(\mathbf{k} - \mathbf{q}). \quad (\text{B.9})$$

The desired result now follows by requiring (B.6).

### Phase of the normalisation constant $n_{\mathbf{k}}$ :

We choose the phase of  $n_{\mathbf{k}}$  such that the mode functions satisfy the useful property

$$\bar{u}_{\mathbf{k}}(x_P) = u_{-\mathbf{k}}(x_P^A), \quad (\text{B.10})$$

where  $x_P^A$  is the antipode of  $x_P$ . The function  $\chi_k(\eta)$  has a branch cut that can be placed on the negative real axis, so the more precise statement is that we require

$$\bar{u}_{\mathbf{k}}(\eta, \mathbf{x}) = u_{-\mathbf{k}}(-\eta - i\epsilon, \mathbf{x}). \quad (\text{B.11})$$

Now when  $\nu$  is either purely real or purely imaginary, we have that

$$\bar{H}_{\nu}^{(1)}(x) = -e^{i\pi\text{Re}(\nu)} H_{\nu}^{(1)}(-x + i\epsilon) \quad (\text{B.12})$$

for real  $x > 0$  and small positive  $\epsilon$ .<sup>1</sup> Using this fact, we find that (B.11) will be satisfied if the phase of  $n_{\mathbf{k}}$  is  $e^{i\pi\left(\frac{\text{Re}(\nu)}{2} - \frac{d+2}{4}\right)}$  and so

$$n_{\mathbf{k}} = |n_{\mathbf{k}}| e^{i\pi\left(\frac{\text{Re}(\nu)}{2} + \frac{d}{4}\right)} = \sqrt{\frac{\pi}{4}} \ell^{-\frac{d+1}{2}} e^{i\pi\left(\frac{\nu}{2} - \frac{d+2}{4}\right)}. \quad (\text{B.13})$$

### Summary:

Collecting our results, the positive-frequency modes that define the BD vacuum  $|BD\rangle$  take the form

$$u_{\mathbf{k}}^{BD}(\eta, \mathbf{x}) = \frac{e^{i\mathbf{k}\cdot\mathbf{x}}}{(2\pi)^{d/2}} \chi_k(\eta), \quad \chi_k(\eta) = \sqrt{\frac{\pi\ell}{4}} e^{i\pi\left(\frac{\nu}{2} - \frac{d+2}{4}\right)} \left(\frac{-\eta}{\ell}\right)^{d/2} H_{\nu}^{(1)}(-k\eta). \quad (\text{B.14})$$

## B.2. Euclidean modes on $dS^D$

Our introduction of the Euclidean modes will follow that of [51], with some relevant additional details spelt out. In global coordinates, the de Sitter metric is given by (4.7)

$$ds^2 = -dt^2 + \ell^2 \cosh^2(t/\ell) d\Omega_d^2, \quad (\text{B.15})$$

---

<sup>1</sup> To see this, note that  $H_{\nu}^{(1)}(-z) = -e^{-i\pi\nu} \bar{H}_{\nu}^{(1)}(\bar{z})$  [57, Eqs. 10.11.5 & 10.11.9]. Letting  $z = x - i\epsilon$ , we find  $\bar{H}_{\nu}^{(1)}(x) = -e^{-i\pi\nu} H_{\nu}^{(1)}(-x + i\epsilon)$ . For real  $\nu$ , the desired relation then follows. For purely imaginary  $\nu$ , we get the same result by using  $H_{-\nu}^{(1)}(z) = e^{i\pi\nu} H_{\nu}^{(1)}(z)$  [57, Eq. 10.4.6].

where  $d\Omega_d^2$  is the line element on the  $d$ -sphere  $S^d$  and  $t \in (-\infty, +\infty)$ . The Klein-Gordon equation is

$$\ell^{-2} [-\partial_t^2 - d \tanh t \partial_t + (\cosh t)^{-2} \Delta_{S^d}] \phi(t, \boldsymbol{\theta}) = 0 \quad (\text{B.16})$$

where  $\Delta_{S^d}$  is the Laplacian on the  $d$ -sphere.

### Klein-Gordon modes

We introduce spherical harmonics  $Y_{Lj}(\boldsymbol{\theta})$ , which form a complete and orthonormal eigenbasis of  $\Delta_{S^d}$ . That is, they are eigenfunctions of  $\Delta_{S^d}$ :

$$\Delta_{S^d} Y_{Lj} = -L(L + d - 1) Y_{Lj}, \quad (\text{B.17})$$

and they satisfy the orthonormality relations

$$\int Y_{Lj}(\boldsymbol{\theta}) \bar{Y}_{Lj'}(\boldsymbol{\theta}) d\Omega_d = \delta_{LL'} \delta_{jj'} \quad (\text{B.18})$$

as well as the completeness relation

$$\sum_{Lj} Y_{Lj}(\boldsymbol{\theta}) \bar{Y}_{Lj}(\boldsymbol{\theta}') = \frac{\delta^{(d)}(\boldsymbol{\theta}, \boldsymbol{\theta}')}{\sqrt{h(\boldsymbol{\theta})}} \quad (\text{B.19})$$

where  $h(\boldsymbol{\theta})$  is the determinant of the metric and  $d\Omega_d = \sqrt{h(\boldsymbol{\theta})} d\boldsymbol{\theta}$  the volume element on  $S^d$ . Here  $L \in \{0, 1, 2, \dots\}$  and  $j$  is a collective index for  $j_1, j_2, \dots, j_{d-1}$ , which run over values  $|j_{d-1}| \leq j_{d-2} \leq \dots \leq j_1 \leq L$ . We work with a particular choice of harmonics  $Y_{Lj}(\boldsymbol{\theta})$  that enjoys the useful property

$$\bar{Y}_{Lj}(\boldsymbol{\theta}) = (-1)^L Y_{Lj}(\boldsymbol{\theta}) = Y_{Lj}(\boldsymbol{\theta}^A), \quad (\text{B.20})$$

where  $\boldsymbol{\theta}^A$  is the antipodal point to  $\boldsymbol{\theta}$  on  $S^d$ . Consider then the mode functions

$$u_{Lj}(t, \boldsymbol{\theta}) = y_L(t) Y_{Lj}(\boldsymbol{\theta}) \quad (\text{B.21})$$

where

$$y_L(t) = n_L e^{(a+\nu)t/\ell} \cosh^L(t/\ell) v_L(t) \quad (\text{B.22})$$

and  $\nu^2 = \frac{d^2}{4} - m^2 \ell^2$  as in (B.5),  $a = L + d/2$  and  $n_L$  is a normalisation constant. These modes satisfy the Klein-Gordon equation if  $v_L(t)$  is a solution to the hypergeometric

differential equation

$$z(1-z)\frac{d^2v_L}{dz^2} + [c - (a+b+1)z]\frac{dv_L}{dz} - av_L = 0, \quad (\text{B.23})$$

with  $c = 2a$ ,  $b = a + \nu$  and

$$z = z(t) = 1 + e^{2t/\ell}. \quad (\text{B.24})$$

The modes that define the Euclidean vacuum are those corresponding to the particular solution

$$v_L(t) = F(a, a + \nu; 2a; z(t) - i\epsilon), \quad (\text{B.25})$$

where  $F$  is the hypergeometric function  ${}_2F_1$ . More precisely,  $F$  stands for the hypergeometric function obtained by introducing a branch cut from 1 to  $\infty$  on the real axis. This is exactly the range relevant to us and  $-i\epsilon$  determines the side of the branch cut on which the function should be evaluated.

### Absolute value of the normalisation constant $n_L$ :

The normalisation constant  $n_L$  is determined by requiring the modes to be orthonormal in the Klein-Gordon inner product:

$$\begin{aligned} (u_{Lj}, u_{L'j'}) &= -(\bar{u}_{Lj}, \bar{u}_{L'j'}) = \delta_{LL'}\delta_{jj'} \\ (\bar{u}_{Lj}, u_{L'j'}) &= 0, \end{aligned} \quad (\text{B.26})$$

which is equivalent to

$$\begin{aligned} i &= \ell^d \cosh^d(t/\ell) \left( y_L \frac{d\bar{y}_L}{dt} - \frac{dy_L}{dt} \bar{y}_L \right) \\ &= \frac{\ell^{d-1} |n_L|^2}{2^{2a-1}} z^{2a} (z-1)^{\text{Re}(\nu)} \left[ (z-1) \left( v_L \frac{d\bar{v}_L}{dz} - \bar{v}_L \frac{dv_L}{dz} \right) - i\text{Im}(\nu) v_L \bar{v}_L \right]. \end{aligned} \quad (\text{B.27})$$

Since the above expression is conserved in time, it suffices to look at the  $z \rightarrow \infty$  (i.e.  $t \rightarrow \infty$ ) limit. In that limit:

$$\begin{aligned} F(a, a + \nu; 2a; z(t) - i\epsilon) &\xrightarrow{z \rightarrow \infty} z^{-a} e^{-i\pi a} \left( \gamma + \xi e^{-\nu \ln z} e^{-i\pi \nu} \right) \\ \frac{d}{dz} F(a, a + \nu; 2a; z(t) - i\epsilon) &\xrightarrow{z \rightarrow \infty} z^{-a-1} e^{-i\pi(a+1)} \left( a\gamma + (a + \nu)\xi e^{-\nu \ln z} e^{-i\pi \nu} \right) \end{aligned} \quad (\text{B.28})$$

where all functions assume their principal values (if  $z$  and  $c$  are two complex numbers, then  $z^c = e^{c \text{Ln} z}$ , where  $\text{Ln} z = \ln |z| + i\vartheta$ , with  $z = |z|e^{i\vartheta}$  and  $-\pi < \vartheta \leq \pi$ ) and

$$\gamma = \frac{\Gamma(\nu)\Gamma(2a)}{\Gamma(a+\nu)\Gamma(a)}, \quad \xi = \frac{\Gamma(-\nu)\Gamma(2a)}{\Gamma(a-\nu)\Gamma(a)}. \quad (\text{B.29})$$

This expression is valid when  $\nu \neq 0, \pm 1, \pm 2, \dots$ ,  $a \neq \nu$ . To arrive at these expressions, we have used [57, Eqs. 15.1.1, 15.1.2, 15.8.2] to obtain

$$\begin{aligned} & \frac{\sin(\pi(b-a))}{\pi\Gamma(c)} F(a, b; c; z) = \\ & \frac{1}{\Gamma(b)\Gamma(c-a)\Gamma(a-b+1)} (-z)^{-a} F(a, a-c+1; a-b+1; 1/z) \\ & + \frac{1}{\Gamma(a)\Gamma(c-b)\Gamma(b-a+1)} (-z)^{-b} F(b, b-c+1; b-a+1; 1/z). \end{aligned} \quad (\text{B.30})$$

Here all functions assume their principal values and the relations are valid for  $|\text{ph}(-z)| < \pi$  and  $(b-a) \neq 0, \pm 1, \dots$ . Then using (4.38) to rewrite  $\sin(\pi(b-a))$  in terms of Gamma functions and (4.38) to get  $\Gamma(\pm(a-b)+1) = \pm(a-b)\Gamma(\pm(a-b))$ , we find

$$\begin{aligned} F(a, b; c; z) &= \frac{\Gamma(b-a)\Gamma(c)}{\Gamma(b)\Gamma(c-a)} (-z)^{-a} F(a, a-c+1; a-b+1; \frac{1}{z}) \\ &+ \frac{\Gamma(a-b)\Gamma(c)}{\Gamma(a)\Gamma(c-b)} (-z)^{-b} F(b, b-c+1; b-a+1; \frac{1}{z}). \end{aligned} \quad (\text{B.31})$$

We can also relate the derivative of  $F$  to another hypergeometric function using [57, Eq. 15.5.1]:

$$\frac{d}{dz} F(a, b; c; z) = \frac{ab}{c} F(a+1, b+1; c+1; z). \quad (\text{B.32})$$

Noting that for any complex number  $x_c$  and  $1 < z < \infty$  we have  $(z-i\epsilon)^c = e^{c \ln z} e^{i c \pi}$ , and also using the fact that  $F(a, b; c; 0) = 1$ , the desired expressions follow.

Note that because  $\Gamma(\bar{z}) = \bar{\Gamma}(z)$ , both  $\gamma$  and  $\xi$  are real when  $\nu$  is real, and  $\bar{\gamma} = \xi$  when  $\nu$  is purely imaginary. Using these facts, evaluating (B.27) in the limit  $z \rightarrow \infty$  constrains the norm of  $n_L$  to

$$|n_L|^2 = \frac{e^{-\pi \text{Im}(\nu)}}{2^{2a} \ell^{d-1}} \frac{\Gamma(a+\nu)\Gamma(a-\nu)}{\Gamma(a+\frac{1}{2})^2}, \quad (\text{B.33})$$

where we have used [57, Eq. 15.5.5] to rewrite  $\Gamma(2a) = \pi^{-1/2} 2^{2a-1} \Gamma(a)\Gamma(a+1/2)$ . Although the derivation of this result uses relations which are only valid for  $\nu \neq$

$0, 1, 2, \dots$  the final result is completely well-defined for such values. Therefore, we could imagine a limiting procedure in which we add a tiny amount  $\epsilon$  to an integer value of  $\nu$ , go through the same derivation, and then let  $\epsilon$  go to zero.

### Phase of the normalisation constant $n_L$ :

We use the freedom in the phase of  $n_L$  to endow the mode functions with the useful property

$$u_{Lj}(x_G^A) = \bar{u}_{Lj}(x_G). \quad (\text{B.34})$$

Given that we have chosen spherical harmonics with the property  $\bar{Y}_{Lj}(\boldsymbol{\theta}) = Y_{Lj}(\boldsymbol{\theta}^A)$ , this condition reduces to

$$y_L(-t) = \bar{y}_L(t), \quad (\text{B.35})$$

which can be achieved by setting

$$n_L = |n_L| e^{i\frac{\pi}{2}[a+\text{Re}(\nu)]}. \quad (\text{B.36})$$

To see this, let  $n_L = |n_L| e^{i\vartheta_L}$ . It follows from the definition of  $F$  (see [57, Eq. 15.2.1]) and  $\Gamma(\bar{z}) = \bar{\Gamma}(z)$  that

$$\bar{F}(a, a + \nu; 2a; z - i\epsilon) = \begin{cases} F(a, a + \nu; 2a; z + i\epsilon) & \nu \text{ real} \\ F(a, a - \nu; 2a; z + i\epsilon) & \nu \text{ imaginary.} \end{cases} \quad (\text{B.37})$$

Using [57, Eq. 15.8.1], it may be checked that

$$\begin{aligned} F(a, a + \nu; 2a; z(t) + i\epsilon) &= (1 - z(t) - i\epsilon)^{-a-\nu} F(a, a + \nu; 2a; \frac{z(t)}{z(t) - 1} - i\epsilon) \\ &= e^{-2(a+\nu)t/l} e^{i\pi(a+\nu)} F(a, a + \nu; 2a; z(-t) - i\epsilon). \end{aligned} \quad (\text{B.38})$$

Using the relations above when  $\nu$  is real, it follows from the definition of  $y_L(t)$  that  $y_L(-t) = e^{2i\vartheta_L} e^{-i\pi(a+\nu)} \bar{y}_L(t)$ . The same formula in [57] also guarantees

$$\begin{aligned} F(a, a - \nu; 2a; z(t) + i\epsilon) &= (1 - z(t) - i\epsilon)^{-a} F(a, a + \nu; 2a; z(t) / (z(t) - 1) - i\epsilon) \\ &= e^{-2at/l} e^{i\pi a} F(a, a + \nu; 2a; z(-t) - i\epsilon). \end{aligned} \quad (\text{B.39})$$

Using this expression and (B.37) when  $\nu$  is purely imaginary, it follows that  $y_L(-t) = e^{2i\vartheta_L} e^{-i\pi a} \bar{y}_L(t)$ . Combining these results we find  $\vartheta_L = \frac{\pi}{2} [a + \text{Re}(\nu)]$ .

**Summary:**

Collecting the results above, the Euclidean modes are

$$u_{Lj}^E(t, \boldsymbol{\theta}) = y_L^E(t) Y_{Lj}(\boldsymbol{\theta}) \quad (\text{B.40})$$

where

$$y_L^E(t) = n_L e^{(a+\nu)t/\ell} \cosh^L(t/\ell) F(a, a + \nu; 2a; z(t) - i\epsilon) \quad (\text{B.41})$$

and  $z(t) = 1 + e^{2t/\ell}$ ,  $a = L + d/2$  and

$$n_L = \frac{e^{i\frac{\pi}{2}(a+\nu)}}{2^a \ell^{\frac{d-1}{2}}} \frac{\sqrt{\Gamma(a + \nu)\Gamma(a - \nu)}}{\Gamma(a + \frac{1}{2})}. \quad (\text{B.42})$$

# Bibliography

- [1] N. Afshordi, M. Buck, F. Dowker, D. Rideout, R. D. Sorkin, and Y. K. Yazdi, *A Ground State for the Causal Diamond in 2 Dimensions*, *JHEP* **1210** (2012) 088, [[arXiv:1207.7101](https://arxiv.org/abs/1207.7101)].
- [2] S. Aslanbeigi and M. Buck, *A preferred ground state for the scalar field in de sitter space*, *Journal of High Energy Physics* **2013** (2013), no. 8.
- [3] S. W. Hawking, *Particle creation by black holes*, *Communications in mathematical physics* **43** (1975), no. 3 199–220.
- [4] S. A. Fulling, *Nonuniqueness of canonical field quantization in riemannian space-time*, *Physical Review D* **7** (1973), no. 10 2850.
- [5] P. C. Davies, *Scalar production in schwarzschild and rindler metrics*, *Journal of Physics A: Mathematical and General* **8** (1975), no. 4 609.
- [6] W. G. Unruh, *Notes on black-hole evaporation*, *Physical Review D* **14** (1976), no. 4 870.
- [7] V. Mukhanov, H. Feldman, and R. Brandenberger, *Theory of cosmological perturbations*, *Physics Reports* **215** (1992), no. 56 203 – 333.
- [8] R. M. Wald, *The Formulation of Quantum Field Theory in Curved Spacetime*, [arXiv:0907.0416](https://arxiv.org/abs/0907.0416).
- [9] R. M. Wald, *The formulation of quantum field theory in curved spacetime*, [arXiv:0907.0416](https://arxiv.org/abs/0907.0416).
- [10] N. Afshordi, S. Aslanbeigi, and R. D. Sorkin, *A Distinguished Vacuum State for a Quantum Field in a Curved Spacetime: Formalism, Features, and Cosmology*, [arXiv:1205.1296](https://arxiv.org/abs/1205.1296).
- [11] C. J. Fewster and R. Verch, *On a Recent Construction of 'Vacuum-like' Quantum Field States in Curved Spacetime*, [arXiv:1206.1562](https://arxiv.org/abs/1206.1562).



- 
- [12] P. Dirac, *The Lagrangian in Quantum Mechanics*, *Physikalische Zeitschrift der Sowjetunion* **3** (1933) 64–72.
- [13] R. D. Sorkin, *Scalar Field Theory on a Causal Set in Histories Form*, *J. Phys. Conf. Ser.* **306** (2011) 012017, [[arXiv:1107.0698](#)].
- [14] S. Johnston, *Feynman Propagator for a Free Scalar Field on a Causal Set*, *Phys.Rev.Lett.* **103** (2009) 180401, [[arXiv:0909.0944](#)].
- [15] R. D. Sorkin. Private communication, 2012.
- [16] S. Hawking and G. Ellis, *The large scale structure of space-time*, vol. 1. Cambridge Univ Pr, 1975.
- [17] R. Peierls, *The commutation laws of relativistic field theory*, *Proceedings of the Royal Society of London. Series A. Mathematical and Physical Sciences* **214** (1952), no. 1117 143–157.
- [18] G. Barnich, M. Henneaux, and C. Schomblond, *Covariant description of the canonical formalism*, *Phys. Rev. D* **44** (Aug, 1991) R939–R941.
- [19] L. Bombelli, J. Lee, D. Meyer, and R. Sorkin, *Space-Time as a Causal Set*, *Phys.Rev.Lett.* **59** (1987) 521–524.
- [20] R. D. Sorkin, *Causal sets: Discrete gravity (notes for the valdivia summer school)*, in *Lectures on Quantum Gravity, Proceedings of the Valdivia Summer School, Valdivia, Chile, January 2002* (A. Gomberoff and D. Marolf, eds.), Plenum, 2005. [gr-qc/0309009](#).
- [21] J. Henson, *The Causal set approach to quantum gravity*, in *Approaches to Quantum Gravity: Towards a New Understanding of Space and Time* (D. Oriti, ed.). Cambridge University Press, 2006. [gr-qc/0601121](#).
- [22] E. H. Kronheimer and R. Penrose, *On the structure of causal spaces*, *Mathematical Proceedings of the Cambridge Philosophical Society* **63** (4, 1967) 481–501.
- [23] S. W. Hawking, A. R. King, and P. J. McCarthy, *A new topology for curved spacetime which incorporates the causal, differential, and conformal structures*, *Journal of Mathematical Physics* **17** (1976), no. 2 174–181.

- 
- [24] D. B. Malament, *The class of continuous timelike curves determines the topology of spacetime*, *Journal of Mathematical Physics* **18** (1977), no. 7 1399–1404.
- [25] R. Ilie, G. Thompson, and D. Reid, *A numerical study of the correspondence between paths in a causal set and geodesics in the continuum*, *Classical and Quantum Gravity* **23** (2006) 3275.
- [26] S. P. Johnston, *Quantum Fields on Causal Sets*. PhD thesis, Imperial College, 2010. [arXiv:1010.5514](https://arxiv.org/abs/1010.5514).
- [27] M. Reed and B. Simon, *Methods of Modern Mathematical Physics — Volume 1: Functional Analysis*. Gulf Professional Publishing, 1980.
- [28] R. Wald, *Quantum field theory in curved spacetime and black hole thermodynamics*. University of Chicago Press, 1994.
- [29] C. J. Fewster and R. Verch, *On a Recent Construction of “Vacuum-like” Quantum Field States in Curved Spacetime*, [arXiv:1206.1562](https://arxiv.org/abs/1206.1562).
- [30] S. R. Coleman, *There are no Goldstone bosons in two dimensions*, *Commun.Math.Phys.* **31** (1973) 259–264.
- [31] E. Abdalla, M. Abdalla, and K. Rothe, *Non-perturbative methods in 2 dimensional quantum field theory*. World Scientific Pub Co Inc, 1991.
- [32] M. Faber and A. Ivanov, *On the ground state of a free massless (pseudo)scalar field in two dimensions*, [hep-th/0212226](https://arxiv.org/abs/hep-th/0212226).
- [33] W. Rindler, *Kruskal Space and the Uniformly Accelerated Frame*, *Am.J.Phys.* **34** (1966) 1174.
- [34] W. Rindler, *Relativity: special, general, and cosmological*. Oxford University Press, USA, 2006.
- [35] S. A. Fulling, *Nonuniqueness of canonical field quantization in Riemannian space-time*, *Phys.Rev.* **D7** (1973) 2850–2862.
- [36] P. Davies, *Scalar particle production in Schwarzschild and Rindler metrics*, *J.Phys.A* **A8** (1975) 609–616.
- [37] W. Unruh, *Notes on Black Hole Evaporation*, *Phys.Rev.* **D14** (1976) 870.

- 
- [38] M. Spiegel, *The summation of series involving roots of transcendental equations and related applications*, *Journal of Applied Physics* **24** (1953), no. 9 1103–1106.
- [39] N. Birrell and P. Davies, *Quantum fields in Curved Space*. Cambridge University Press, 1984.
- [40] P. Davies and S. Fulling, *Radiation from a moving mirror in two-dimensional space-time: conformal anomaly*, *Proc.Roy.Soc.Lond.* **A348** (1976) 393–414.
- [41] N. Aviln, A. F. Reyes-Lega, and B. C. da Cunha, *Coupling the Sorkin-Johnston State to Gravity*, [arXiv:1408.3446](https://arxiv.org/abs/1408.3446).
- [42] H.-J. Schmidt, *On the de Sitter Space-Time – The Geometric Foundation of Inflationary Cosmology*, *Fortschritte der Physik/Progress of Physics* **41** (1993), no. 3 179–199.
- [43] M. Spradlin, A. Strominger, and A. Volovich, *Les Houches lectures on de Sitter space*, [hep-th/0110007](https://arxiv.org/abs/hep-th/0110007).
- [44] E. Mottola, *Particle Creation in de Sitter Space*, *Phys.Rev.* **D31** (1985) 754.
- [45] B. Allen, *Vacuum states in de Sitter space*, *Physical Review D* **32** (1985), no. 12 3136.
- [46] C. Schomblond and P. Spindel, *Conditions d’unicité pour le propagateur  $\Delta^1(x, y)$  du champ scalaire dans l’univers de de Sitter*, *Ann. Inst. Henri Poincaré* **25** (1976) 67.
- [47] P. Candelas and D. Raine, *Feynman Propagator in Curved Space-Time*, *Phys.Rev.* **D15** (1977) 1494–1500.
- [48] J. Dowker and R. Critchley, *Scalar Effective Lagrangian in de Sitter Space*, *Phys.Rev.* **D13** (1976) 224.
- [49] M. B. Einhorn and F. Larsen, *Interacting quantum field theory in de Sitter vacua*, *Phys.Rev.* **D67** (2003) 024001, [[hep-th/0209159](https://arxiv.org/abs/hep-th/0209159)].
- [50] N. Birrell and P. Davies, *Quantum fields in curved space*. No. 7. Cambridge University Press, 1984.

- 
- [51] R. Bousso, A. Maloney, and A. Strominger, *Conformal vacua and entropy in de Sitter space*, *Phys.Rev.* **D65** (2002) 104039, [[hep-th/0112218](#)].
- [52] E. Tagirov, *Consequences of field quantization in de Sitter type cosmological models*, *Annals Phys.* **76** (1973) 561–579.
- [53] T. Bunch and P. Davies, *Quantum field theory in de sitter space: renormalization by point-splitting*, *Proceedings of the Royal Society of London. A. Mathematical and Physical Sciences* **360** (1978), no. 1700 117–134.
- [54] P. Candelas and D. Raine, *Quantum Field Theory in Incomplete Manifolds*, *J.Math.Phys.* **17** (1976) 2101–2112.
- [55] P. Lagogiannis, A. Maloney, and Y. Wang, *Odd-dimensional de Sitter Space is Transparent*, [arXiv:1106.2846](#).
- [56] K. Yagdjian, *Huygen’s principle for the Klein-Gordon equation in the de Sitter spacetime*, *J. Math. Phys.* **54** (2013), no. 9.
- [57] F. W. Olver, D. W. Lozier, R. F. Boisvert, and C. W. Clark, *NIST Handbook of Mathematical Functions*. Cambridge University Press, New York, NY, USA, 1st ed., 2010.
- [58] M. Bertola, V. Gorini, U. Moschella, and R. Schaeffer, *Correspondence between minkowski and de sitter quantum field theory*, *Physics Letters B* **462** (1999), no. 3-4 249–253.
- [59] J. de Boer and S. N. Solodukhin, *A holographic reduction of Minkowski space-time*, *Nucl. Phys.* **B665** (2003) 545–593, [[hep-th/0303006](#)].
- [60] M. Matsumoto and T. Nishimura, *Mersenne twister: a 623-dimensionally equidistributed uniform pseudo-random number generator*, *ACM Transactions on Modeling and Computer Simulation (TOMACS)* **8** (1998), no. 1 3–30.
- [61] B. Schmitzer, *Curvature And Topology On Causal Sets*, . M.Sci. Thesis. Supervisor: Fay Dowker.
- [62] J. P. Gazeau, *An introduction to quantum field theory in de Sitter space-time*, *AIP Conf.Proc.* **910** (2007) 218–269.
- [63] M. Fukuma, Y. Sakatani, and S. Sugishita, *On propagators in de Sitter space*, [arXiv:1301.7352](#).

- 
- [64] D. Marolf and I. A. Morrison, *The IR stability of de Sitter: Loop corrections to scalar propagators*, *Phys.Rev.* **D82** (2010) 105032, [[arXiv:1006.0035](#)].
- [65] D. P. Jatkar, L. Leblond, and A. Rajaraman, *On the Decay of Massive Fields in de Sitter*, *Phys.Rev.* **D85** (2012) 024047, [[arXiv:1107.3513](#)].
- [66] D. Marolf, I. A. Morrison, and M. Srednicki, *Perturbative S-matrix for massive scalar fields in global de Sitter space*, [arXiv:1209.6039](#).
- [67] J. Bros, H. Epstein, and U. Moschella, *Particle decays and stability on the de Sitter universe*, *Annales Henri Poincare* **11** (2010) 611–658, [[arXiv:0812.3513](#)].
- [68] J. Bros, H. Epstein, and U. Moschella, *Lifetime of a massive particle in a de Sitter universe*, *JCAP* **0802** (2008) 003, [[hep-th/0612184](#)].
- [69] R. Brunetti and K. Fredenhagen, *Microlocal Analysis and Interacting Quantum Field Theories: Renormalization on Physical Backgrounds*, *Communications in Mathematical Physics* **208** (2000) 623–661, [[math-ph/9](#)].
- [70] S. Hollands and R. M. Wald, *Local Wick polynomials and time ordered products of quantum fields in curved space-time*, *Commun.Math.Phys.* **223** (2001) 289–326, [[gr-qc/0103074](#)].
- [71] S. Hollands and R. M. Wald, *Existence of local covariant time ordered products of quantum fields in curved space-time*, *Commun.Math.Phys.* **231** (2002) 309–345, [[gr-qc/0111108](#)].
- [72] R. Brunetti, K. Fredenhagen, and S. Hollands, *A Remark on alpha vacua for quantum field theories on de Sitter space*, *JHEP* **0505** (2005) 063, [[hep-th/0503022](#)].
- [73] M. Brum and K. Fredenhagen, *Vacuum-like Hadamard states for quantum fields on curved spacetimes*, *Class.Quant.Grav.* **31** (2014) 025024, [[arXiv:1307.0482](#)].
- [74] S. Johnston, *Particle propagators on discrete spacetime*, *Class.Quant.Grav.* **25** (2008) 202001, [[arXiv:0806.3083](#)].
- [75] J. Leray, J. Leray, J. Leray, and J. Leray, *Hyperbolic differential equations*. Institute for advanced study Princeton, 1953.

- 
- [76] S. Avis, C. Isham, and D. Storey, *Quantum Field Theory in anti-De Sitter Space-Time*, *Phys.Rev.* **D18** (1978) 3565.
- [77] R. P. Geroch, *The domain of dependence*, *J.Math.Phys.* **11** (1970) 437–439.
- [78] R. P. Geroch, *Topology in general relativity*, *J.Math.Phys.* **8** (1967) 782–786.
- [79] R. D. Sorkin, *Forks in the road, on the way to quantum gravity*, *Int.J.Theor.Phys.* **36** (1997) 2759–2781, [[gr-qc/9706002](#)].
- [80] K. S. Thome, *Closed timelike curves*, in *General Relativity and Gravitation 1992, Proceedings of the Thirteenth INT Conference on General Relativity and Gravitation, held at Cordoba, Argentina, 28 June-July 4 1992*, p. 295, CRC Press, 1993.
- [81] R. D. Sorkin, *Consequences of Spacetime Topology*, .
- [82] T. Dray, C. Manogue, and R. Tucker, *Particle production from signature change*, *Gen.Rel.Grav.* **23** (1991) 967–971.
- [83] G. Gibbons, *Topology change in classical and quantum gravity*, [arXiv:1110.0611](#).
- [84] J. Wheeler, *On the nature of quantum geometrodynamics*, *Annals of Physics* **2** (1957), no. 6 604–614. cited By (since 1996)188.
- [85] J. A. Wheeler, *Geons*, *Physical Review* **97** (1955), no. 2 511.
- [86] R. Sorkin, *Introduction to topological geons*, in *Topological Properties and Global Structure of Space-Time* (P. Bergmann and V. De Sabbata, eds.), NATO ASI Series, pp. 249–270. Springer US, 1986.
- [87] R. D. Sorkin and S. Surya, *An Analysis of the representations of the mapping class group of a multi - geon three manifold*, *Int.J.Mod.Phys.* **A13** (1998) 3749–3790, [[gr-qc/9605050](#)].
- [88] A. Anderson and B. S. DeWitt, *Does the Topology of Space Fluctuate?*, *Found.Phys.* **16** (1986) 91–105.
- [89] C. Manogue, E. Copeland, and T. Dray, *The trousers problem revisited*, *Pramana* **30** (1988), no. 4 279–292.

- 
- [90] F. Dowker and S. Surya, *Topology change and causal continuity*, *Phys.Rev.* **D58** (1998) 124019, [[gr-qc/9711070](#)].
- [91] J. Louko and R. D. Sorkin, *Complex actions in two-dimensional topology change*, *Class.Quant.Grav.* **14** (1997) 179–204, [[gr-qc/9511023](#)].
- [92] R. D. Sorkin, “Notes on Stokes’ Theorem.”  
<https://www.perimeterinstitute.ca/personal/rsorkin/lecture.notes/stokes.theorem.ps>. Accessed: 2014-07-10.
- [93] E. Garcia-Rio and D. N. Kupeli, *Divergence theorem in semi-riemannian geometry*, in *Proceeding of the Workshop on Recent Topics in Differential Geometry, Santiago de Compostela (Spain) and Public. Depto. Geometria y Topologia, Univ. Santiago de Compostela*, no. 89, pp. 131–140, 1998.
- [94] S. A. Fulling, M. Sweeny, and R. M. Wald, *Singularity structure of the two-point function quantum field theory in curved spacetime*, *Communications in Mathematical Physics* **63** (1978), no. 3 257–264.
- [95] C. J. Fewster and R. Verch, *The Necessity of the Hadamard Condition*, *Class.Quant.Grav.* **30** (2013) 235027, [[arXiv:1307.5242](#)].
- [96] J. de Boer, V. Jejjala, and D. Minic, *Alpha-states in de Sitter space*, *Phys.Rev.* **D71** (2005) 044013, [[hep-th/0406217](#)].
- [97] H. Collins and R. Holman, *Taming the alpha vacuum*, *Phys.Rev.* **D70** (2004) 084019, [[hep-th/0312143](#)].